ISBN 978-82-326-7628-6 (printed ver.)
ISBN 978-82-326-7627-9 (electronic ver.)
ISSN 1503-8181 (printed ver.)
ISSN 2703-8084 (electronic ver.)

NTNU
Norwegian University of
Science and Technology

Doctoral theses at NTNU, 2024:13

Yang Bi

Energy efficient airflow distribution methods for surgical microenvironment control in operating rooms

NTNU
Norwegian University of
Science and Technology
Thesis for the degree of
Philosophiae Doctor
Faculty of Engineering
Department of Energy and Process Engineering

NTNU
Norwegian University of
Science and Technology

Doctoral thesis
Yang Bi
Doctoral theses at NTNU, 2024:13
NTNU

Yang Bi

Energy efficient airflow distribution methods for surgical microenvironment control in operating rooms

Thesis for the degree of Philosophiae Doctor

Trondheim, January, 2024

Norwegian University of Science and Technology
Faculty of Engineering
Department of Energy and Process Engineering

NTNU
Norwegian University of
Science and Technology

NTNU
Norwegian University of Science and Technology

Thesis for the degree of Philosophiae Doctor

Faculty of Engineering
Department of Energy and Process Engineering

ISBN 978-82-326-7628-6 (printed ver.)
ISBN 978-82-326-7627-9 (electronic ver.)
ISSN 1503-8181 (printed ver.)
ISSN 2703-8084 (electronic ver.)

Doctoral theses at NTNU, 2024:13

PRINTED IN NORWAY
NO - 1598

NORDIC SWAN ECOLABEL
Printed matter
2041 0731

Printed by Skipnes Kommunikasjon AS

PREFACE

This thesis is submitted to the Norwegian University of Science and Technology (NTNU) for partial fulfillment of the requirement for the degree of Doctor of Philosophy. The doctoral work was carried out between September 2020 and September 2023 at the Department of Energy and Process Engineering under the guidance of Professor Guangyu Cao.

ACKNOWLEDGEMENTS

I extend my profound gratitude to my supervisor, Prof. Guangyu Cao, for being a source of inspiration and guiding me with his exceptional expertise and profound knowledge. His constant encouragement, patience, and constructive feedback have been instrumental in shaping my research and personal growth.

I am equally indebted to my co-supervisors, Prof. Hans Martin Mathisen and Assoc. Prof. Gabriel Kiss, for their valuable contributions to my research. Their unique perspectives and insightful suggestions have significantly enriched the quality of my work.

My heartfelt thanks go to the FOR team at St. Olavs Hospital, especially Jan Gunnar Skogås, for their warm collaboration and unwavering support in facilitating the experimental studies conducted within the hospital premises. The smooth coordination and generous assistance provided by Liv Inger Stenstad have been indispensable in executing the experiments successfully.

I am truly grateful to fellow researchers and collaborators, Prof. Sasan Sadrizadeh, Parastoo Sadeghian, Nan Hu, Amar Aganovic, Jarek Kurnitski, and Pawel Wargocki, with whom I had the pleasure of working. Their expertise, cooperation, and enthusiasm have broadened my horizons and enhanced the impact of our collaborative research.

A special word of appreciation goes out to my esteemed colleagues within the research group, Tomáš Fečer, Xingji Yu, Behnam Rosti, Azimil Gani Alam, and Siyue Ren. Their camaraderie, lively discussions, and unwavering support have created a stimulating and nurturing environment for academic exploration.

I would also like to express my gratitude to my companions in Trondheim, Jiatong Jiang, Lei Zhang, Xuemei Zhang, Ding Peng, Zhishuo Zhang, Meng Jiang, Jie Hu, and Jianan Liu. Their friendship and companionship have added joy, laughter, and cherished memories to my life in Trondheim.

I extend my heartfelt thanks to all the individuals who have extended their helping hands and offered encouragement throughout my doctoral journey. Your support has been a constant motivation and source of strength.

Last but not least, my deepest appreciation goes to my parents, whose unconditional love, belief in my abilities, and unyielding support have been the cornerstone of my pursuit of knowledge. Their sacrifices and unwavering encouragement have made me who I am today.

ABSTRACT

With approximately 300 million surgeries performed worldwide each year, the operating room (OR) environment plays an important role in creating a satisfactory setting for all occupancies. However, there are currently several challenges within ORs, significantly affecting the well-being of the surgical team, patient safety, comfort, health, as well as the overall energy efficiency of the surgical environment.

Surgical site infections (SSI) pose a significant concern within healthcare settings, ranking as the third most common type of hospital-acquired infections (HAIs). The associated risk of infection varies from 2% to 13%, leading to substantial financial costs ranging from $400 to $3,000 per infection. The primary cause of SSI is the compromised immune response of the patient, making them vulnerable to invading microorganisms. The primary source of these microorganisms is believed to be bacteria-carrying particles (BCP) released by the surgical team and patient themselves. Ventilation systems play a crucial role in mitigating the presence of BCP, yet the absence of universally accepted standards for operating room (OR) ventilation parameters impedes effective measures to reduce patient exposure to BCP threats.

Airborne microbes released from infected patients represent a substantial hazard to the surgical team, particularly in cases involving infection diseases such as tuberculosis and severe acute respiratory syndrome (SARS-CoV-2). The risk of cross-infections has prompted the adoption of negative pressure operating rooms (ORs), a measure that has gained prominence, especially during the COVID-19 pandemic. Nevertheless, there exists a notable research gap in the assessment of the surgical team's exposure levels within these negative-pressure OR environments.

Inadvertent perioperative hypothermia (IPH), characterized by a core body temperature below 36 °C during surgery, is a prevalent issue with incidence rates ranging from 4% to as high as 90% in surgical cases. This condition of IPH can have severe consequences for patient health and recovery, including disruptions of using drug in metabolism, increased blood loss, coagulation problems, thermal discomfort, prolonged recovery times, and extended hospital stays. Furthermore, hypothermia elevates the risk of surgical site infections

by approximately 50%. Consequently, the challenge of reducing the incidence of IPH has emerged as a prominent topic in ongoing research within this field.

Comparing with traditional turbulent mixing ventilation (TMV), though laminar airflow (LAF) operating rooms have shown promising results in maintaining cleaner surgical microenvironments, the issue of high energy consumption in LAF OR remains apparent, with an average consumption 34% higher than traditional turbulent mixing ventilation operating rooms. To promote the sustainable aspect of hospital ventilation, there is an urgent need to develop new types of ventilation solutions that secure a cleaner OR environment with higher energy efficiency.

This thesis extensively investigates the most influencing factors for safe and sufficient environment within operating rooms, where either negative pressure or positive pressure may be applied according to the property of diseases. The research scope of this thesis is mainly in the field of ventilation engineering and indoor environment. This encompasses an examination of exposure levels exposed by the surgical team to airborne microbes in negative pressure operating rooms (NPOR). This thesis also evaluates the impact of ambient air temperatures on the colony forming unit (CFU) level of surgical microenvironment in one OR with turbulent mixing ventilation. Furthermore, a human body heat transfer model has been developed to predict patients' core body temperatures to reduce the incidence of perioperative hypothermia. On the basis of traditional laminar airflow, a novel laminar airflow distribution solution is developed to minimize energy consumption while maintaining an ultra-clean surgical microenvironment.

The results of this thesis demonstrate that higher pressure difference in negative pressure TMV OR reduces the impact of the thermal plume above the patient's incision, thereby minimizing healthcare professionals' exposure to airborne viruses like COVID-19. In TMV OR, room air temperature significantly influences the development of thermal plume in surgical microenvironment. Lower air temperatures may lead to stronger thermal plume flow which may prevent deposition of particulate matter. However, higher temperatures may result in reduced shedding of skin scales (diameter larger than 5 μm) from the surgical team. This may contribute to fewer detected CFUs, which are the primary cause of surgical site infection. In addition, this thesis also demonstrates that the developed model for patient core

temperature prediction may calculate core temperature. This model may be used as a valuable tool for preventing hypothermia in patients during surgeries.

Moreover, the novel airflow distribution method for ORs demonstrates substantial energy savings of up to 10% while maintaining high local air quality in the surgical microenvironment. This method provides an example for further development of operating room ventilation strategies, which may contribute to energy efficient ORs in the future.

In conclusion, this thesis offers key insights into influencing parameters and energy-efficient ventilation strategies for maintaining safe operating room environments. The findings underscore the impact of ventilation parameters on indoor air quality of ORs, which is crucial for future OR ventilation design. Additionally, the patient core temperature prediction model is proposed to enhance patient safety by predicting the adverse effect of the OR environment on hypothermia. The results of this thesis may contribute to future developments in new ventilation solutions for ORs.

TABLE OF CONTENTS

ABBREVIATIONS

ACH	Air Change per Hour
ASHRAE	The American Society of Heating, Refrigerating and Air-Conditioning Engineers
AUC	Area Under Curve
BCP	Bacteria-Carrying Particles
BMI	Body Mass Index
CDC	The Center for Disease Control and Prevention
CFD	Computational Fluid Dynamics
CFU	Colony Forming Units
HAI	Hospital Acquired Infection
HCW	Healthcare Worker
HEPA	High Efficiency Particulate air
HTM	Health technical memoranda
HVAC	Heating Ventilation Air Conditioning
IPH	Inadvertent perioperative hypothermia
LAF	Laminar Airflow
LMICs	low- and middle-income countries
OR	Operating room
PPE	Personal Protective Equipment
SSI	Surgical Site Infection
TMV	Turbulent Mixing Ventilation

LIST OF SYMBOLS

C_{he}	Circumstance of the head, m
F_{12}	Angle factor from plate one to plate two
h	Convective heat transfer coefficient, W/m^2·℃
h_{pa}	Height of the patient, m
m	The amount of sweat the body produces, g
$\dot{M}$	Metabolic rate, W
S	Souse term, W
t	Time, second
T	Temperature, ℃
T_{sk}	Skin temperature, ℃
T_{am}	Ambient temperature, ℃
T_w	Wall temperature, ℃
Th_{ch}	The thickness of patient chest, m
$\dot{V}_{O_2}$	The difference in the flowrate of O_2 inhaled and exhaled, L/min
$\dot{V}_{CO_2}$	The difference in the flowrate of CO_2inhaled and exhaled, L/min
$\dot{m}_{N_2}$	The amount of nitrogen element excreted by the human body, g/day
α	Thermal diffusivity, m^2/s
ρ	Density, kg/m^3
σ_r	Stefan-Boltzmann constant, 5.670374419×10^{-8} W/(m^2·K^4)
ε	Thermal emissivity
F_{12}	Angle factor from plate one to plate two

LIST OF FIGURES

LIST OF TABLES

Chapter 1: Introduction

1.1 Background and motivation

It is estimated that the global annual surgical volume exceeds 300 million procedures and is trending upward [1-4]. In less developed regions, an additional 143 million surgeries are needed in middle-income countries, according to the Lancet Commission on Global Surgery [5], They propose six global targets to be achieved by 2030, including a surgical volume of 5,000 procedures per 100 000 population per year (400 million/year), as shown in Figure 1.1. The high and increasing volume of surgery highlights the paramount importance of ensuring patient safety and comfort during surgeries.

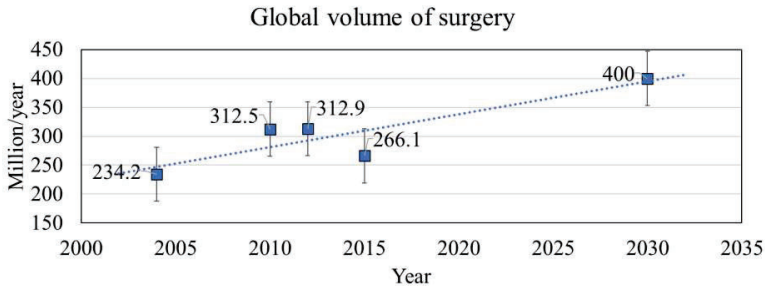

Figure 1.1 The trend of annual surgical volume

Surgical site infection (SSI) poses a great risk to patients, resulting in an average additional cost of $3,500 per patient and an average extra hospital stay of 9.7 days. According to the World Health Organization (WHO), the overall SSI rate ranges from 1.2% to 23.6% in low- and middle-income countries(LMICs) [6]. Factors contributing to SSI primarily include external environmental contamination and compromised patient immune response. Various measures have been implemented to reduce contamination of the environment, including preoperative disinfection, antibiotic prophylaxis, clean air provided near the surgical site through high-efficiency filters, and the use of more efficient ventilation systems to maximize air cleanliness in the vicinity of the surgical site. The effect of room air temperature on the cleaning degree of the surgical site is very complex, including the aspect of airflow distribution and human physiological desquamation. However, there is a lack of real operating room (OR) studies on the effect of turbulent mixing ventilation (TMV) OR ambient temperature on the cleanliness of the surgical microenvironment. Therefore, it is necessary to carry out related studies to elucidate the mechanism of the influence of room air temperature on the cleanliness of the surgical microenvironment.

Inadvertent perioperative hypothermia(IPH), the main cause of immunosuppression in perioperative patients, is a common occurrence during surgery, and it is defined as a core body temperature of less than 36 °C [7]. The incidence of the IPH can vary in the range of 4%-90% [8-11] of all surgery cases. One of the negative consequences of IPH is the significant increase in the occurrence of SSI due to reduced patient immunity. Therefore, preventing the occurrence of perioperative hypothermia can effectively reduce the occurrence of SSI.

Ventilation is an important means to ensure the air quality of the surgical microenvironment in the OR. Generally, there are two commonly used types of ventilation systems in OR based on the principles of dilution and local displacement: TMV and laminar airflow (LAF). TMV has the advantage of lower operational costs but lower air quality, making it suitable for procedures with lower requirements of air quality such as endoscopy, plastic surgery, hysteroscopy, and vaginal examinations. LAF is more suitable for larger and longer procedures requiring higher cleanliness, such as cardiac surgery, brain surgery, and joint replacement. Here, it is crucial for the author to clarify that while the terms laminar flow and mixed flow are widely employed in the field of operating room ventilation, it does not imply that the laminar flow environment in the operating room is entirely laminar. Even when the cold air flows from the ceiling diffuser in operation rooms, there is some turbulence; for instance, the turbulence intensity measured with a velocity sensor will be at least 10%. Additionally, in rooms with highly mixed airflow, there exist laminar and transitional flow regimes near surfaces. Therefore, using laminar and turbulent flow to describe unidirectional and mixing flow in the space is technically inaccurate. The more precise terms would be unidirectional flow and mixed flow. Nevertheless, this doctoral thesis adopts the broader usage of Laminar Airflow (LAF) and Turbulent Mixing Ventilation (TMV) and clarifies this point here.

Although the air quality in LAF OR is cleaner compared to TMV OR, it does come at the cost of increased energy consumption. LAF systems are designed to provide a highly controlled and sterile environment in sensitive areas such as OR. These systems utilize high-efficiency particulate air (HEPA) filters to remove airborne microbes and maintain a unidirectional flow of clean air. This helps reduce the concentration of airborne microbes in the OR. However, maintaining LAF requires powerful air handling systems, including fans and filters, to continuously circulate and condition large volumes of air. These systems consume significant amounts of energy to operate effectively. The energy consumption is

influenced by factors such as the size of the room, the desired airflow rate, and the efficiency of the filtration system. The cost-effectiveness of LAF systems is also an important factor as they are expensive to install and maintain and have significant energy requirements [12]. The installation cost ranged from $60,000 to $90,000 [13] and required a 34% increase in annual operating costs compared to a conventional TMV [14].

Besides the patient, the surgical team is increasingly threatened by the cross-infection of airborne transmission diseases in the OR, especially during the COVID-19 pandemic. Some countries recommend performing the surgery in the negative pressure operating room (NPOR) for the patient who is infected by serious diseases such as tuberculosis (TB) and COVID-19. Different from the positive pressure OR, the pressure difference in the NPOR has an influence on the airflow in the surgical microenvironment [15]. However, there is no consensus on the appropriate negative pressure value in national operating room ventilation standards. The safety of the surgical team in the NPOR has not been widely concerned. Few studies focus on the exposure level of the surgical team to airborne transmission diseases under different pressure differences.

1.2 Objective and scope of the thesis

The research scope of this thesis focuses on addressing indoor environment issues in ORs from the perspective of ventilation engineering, including patients' and surgical teams' safety as well as energy consumption. The objective of this thesis is to enhance the efficiency of airflow distribution methods in the OR to provide a safe surgical microenvironment for both the patient and surgical team. To achieve the objectives of this thesis, the following four questions are formulated through a detailed review of the state of the art of airflow distribution systems in TMV and LAF OR. See also Figure 1.2.

Research question one. Does the pressure difference influence the exposure level of the surgical team to airborne microbes in the negative pressure TMV OR?

Research question two: How does ambient air temperature influence the cleanliness of the surgical microenvironment in the TMV OR?

Research question three: How to maintain the core temperature of the patient to reduce the risk of hypothermia in ORs with different ventilation solutions?

Research question four: Could the cleanliness of the surgical microenvironment be maintained with energy energy-efficient airflow distribution method?

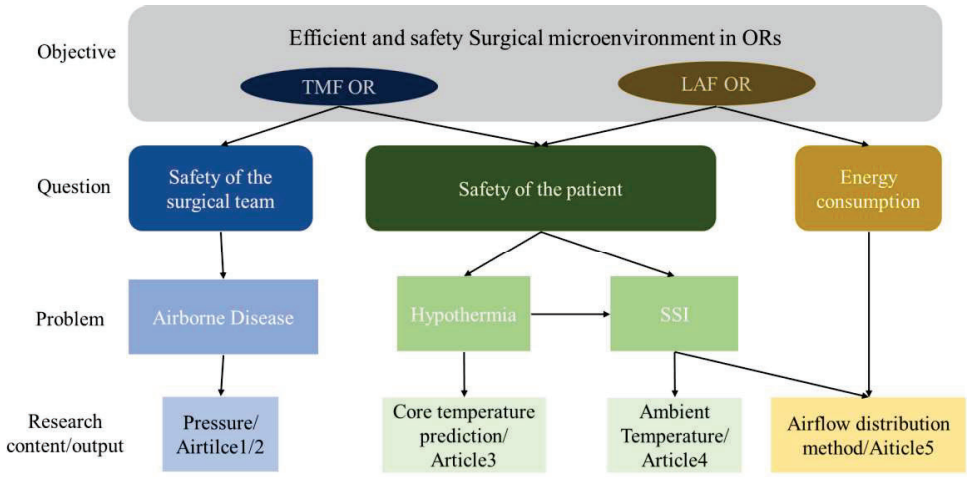

Figure 1.2 The layout of the research content of this thesis

The thesis is based on work presented in the following research papers (Table 1.1)

Table 1.1 List of research papers

Paper 1	**Y. Bi**, A. Aganovic, H.M. Mathisen, G. Cao, Experimental study on the exposure level of surgical staff to SARS-CoV-2 in operating rooms with mixing ventilation under negative pressure, Building and Environment 217 (2022) 109091.
Paper 2	Sadeghian, P., **Bi, Y.**, Cao, G. et al. Reducing the risk of viral contamination during the coronavirus pandemic by using a protective curtain in the operating room. Patient Saf Surg 16, 26 (2022).
Paper 3	**Yang Bi,** Tomáš Fečer, Hans Martin Mathisen; Liv Inger Stenstad, Jan Gunnar Skogås, Gabriel Kiss, Guangyu Cao. Modeling of body temperature for perioperative patients in the operating room. (Submitted to *Building and Environment)*
Paper 4	**Yang Bi,** Tomas Facer, Hans Martin Mathisen; Sara Edvardsen, Liv Inger Stenstad, Jan Gunnar Skogås, Guangyu Cao. Influence of the room air temperature on the airborne particles of the surgical microenvironment in an operating room with mixing ventilation (Submitted to *BMC Infectious Diseases*)
Paper 5	**Yang Bi,** Nan Hu, Parastoo Sadeghian, Sasan Sadrizadeh, Marina Asuero Von Munthe Af Morgenstierne, Hans Martin Mathisen, Elyas Larkermani, Laurent Georges1, Guangyu Cao. Numerical study on an improved protective operating room laminar flow ventilation system. (Submitted to *Energy and Buildings*)

The paper's contribution to research questions posed in the thesis is presented in Table 1.2

Table 1.2 Article and the correlated research questions

Article No.	Research question one	Research question two	Research question three	Research question four
1	×			
2	×			
3		×		
4			×	
5				×

1.3 Future impact

This doctoral thesis focuses on characterizing human exposure and efficient airflow distribution methods in the surgical microenvironment in ORs with different ventilation systems. Through this research, improved ventilation parameters for TMV OR were identified. These findings will aid the design of OR ventilation systems, thereby providing a safer surgical environment for both surgical teams and patients. In addition, the results of this study will help reduce the incidence of perioperative hypothermia and thus reduce SSI rate. The proposed enhanced LAF system shows a new direction for the development of future OR, aiming to achieve desired operating environments that are more comfortable, energy-efficient and safer for surgical procedures.

Chapter 2: Literature review

2.1 Transport of airborne microbes in the OR

Airborne transmission stands as the primary route through which numerous diseases spread, including tuberculosis, severe acute respiratory syndrome (SARS), influenza [16], smallpox [17], and SARS-CoV-2 [18, 19]. The distinguishing characteristic of airborne transmission lies in the ability of microorganisms to travel within air currents, thus enabling them to infect individuals even at considerable distances. These infectious agents are released through various means, encompassing physical contact and human respiratory activities [20]. The size of the particles carrying these microorganisms varies, resulting in distinct movement patterns [21]. Particles larger than 10 μm in diameter, referred to as microbial droplets, may rapidly settle due to gravity [22]. In contrast, microbial aerosols measuring less than 10 μm in diameter evaporate and transform into droplet nuclei, further diminishing their size. These minute microbial aerosols can navigate indoor air currents and endure for extended periods [23]. They disperse through the air around individuals and enter their upper respiratory tracts along with their inhalation, ultimately finding their place in the trachea or bronchus [24]. In some cases, microorganism aerosols with exceedingly small diameters can directly deposit within the alveoli of the human body's lungs. Consequently, the accumulation rather than effective elimination of microbes indoors can pose risks to the well-being of occupants [25].

Since the outbreak of the coronavirus disease COVID-19 pandemic in 2019, healthcare workers in hospitals have been at high risk of being infected by severe acute respiratory syndrome coronavirus 2 (SARS-CoV-2) [26-29]. The OR is a setting where both patients and surgical staff may stay for a long time, which increases the infection risk for surgical staff. The average duration of the majority of operation types is beyond 2 hours [30]. Therefore, ORs have also received great attention, and researchers have continuously proposed measures to prevent surgical staff from infecting ORs, including the utilization of personal protective equipment (PPE) [31-33], aerosol boxes [34], and stricter infection control methods [33]. In addition, some hospitals shared their experience in the prevention of infection control in OR [28, 35].

Many studies have suggested transforming ventilation in the OR from positive to negative pressure to treat COVID-19 patients [28, 36-40]. Compared with positive pressure ventilation, the air outside ORs flows into ORs by penetrating through the cracks of doors and windows

of the NPOR, which prevents SARS-CoV-2 from spreading out of the OR. In contrast, the pressure difference of positive pressure ventilation has no significant effect because there is little air penetrating the room to disturb the airflow distribution in a positive pressure room. At present, there is very little experimental research on the exposure risk of airborne transmission of COVID-19 in the NPOR, except in a few studies using simulation [41, 42]. Different countries have different recommendations and requirements regarding the value of the pressure difference of the NPOR. For example, the technical specification of surgical cleaning units in China clearly states that patients infected with airborne diseases should be operated on in an NPOR, but the specification does not indicate a specific pressure value [43]. British ventilation guidelines suggest that the pressure in an NPOR should be at least -5 Pa [44]. Both Canadian and CDC guidelines suggest a pressure difference of -2.5 Pa in an NPOR [45, 46].

Equipping PPE has been recommended since the COVID-19 pandemic to prevent surgical staff from being infected in the OR by aerosol viruses released by patients [31, 47]. PPE, including respirators, can effectively reduce the wearer's exposure to airborne microbes. In some cases, nurses, who usually stay far from the patient during operations, should also wear PPE during surgery. However, more than half of OR surgical staff reported a decrease in overall comfort with PPE, and more than 80% of respondents reported increased fatigue [48]. In addition, this combination of PPE can lead to increased respiratory work, reduced vision, reduced touch, and heat stress [49-51]. However, the air change rate in the OR is higher than 20 air changes per hour (ACH), and surgical staff away from the operating table may not be exposed to high concentrations of airborne microbes. This makes it difficult for surgical staff to choose protection equipment that may result in different safety and comfort levels. Therefore, revealing the contaminated exposure level of the breathing zone of surgical staff in the OR is an important indicator to help the medical staff determine whether PPE should be worn.

To date, there have been few studies on the exposure levels of surgical staff to airborne microorganisms in OR. Some of these studies statistically analyze the existing infection cases of surgical staff. In addition to some investigation studies, some experimental and simulation studies were also carried out. Loth Andreas G et al. [52], conducted an experimental study of aerosol exposure levels in patients during tracheotomy and found that 4.8 ± 3.4% of aerosols were in contact with the surgeons in laminar OR, compared with 10 times as much in nonlaminar OR (47.9 ± 10.8%). Alex Murr et al. [53] used an optical particle sizer to measure

aerosol concentrations during endoscopic nasal surgery. Aerosol concentrations at the surgeon's position were significantly increased with the drilling and microdebrider. Ban C.H. Sui et al. [54] used a nebulizer to simulate aerosol exposure during intubation and compared aerosol concentrations in the OR and isolation room, and the results showed that aerosol exposure levels in both rooms were similar. Marc Garbey et al. [55] conducted experimental and simulated studies on the diffusion of surgical smoke in the OR. The results suggest that opening doors during surgery and inefficient actions by medical personnel can increase indoor airborne microbes' concentrations. However, none of the earlier studies have investigated the effect of different negative pressure conditions on the exposure level of surgical staff to airborne microorganisms in the OR with TMV.

Based on the above literature review, there is a need to propose appropriate measures to reduce the level of airborne microbial exposure that surgical teams face during surgery in the NPOR.

2.2 Safety of the perioperative patient

SSI arise from the accumulation of bacteria at the surgical wound, often leading to incomplete clearance by the body's immune system [56]. The incidence of SSI depends on two pivotal causes: the quantitative load of pathogenic microorganisms introduced into the surgical milieu and the robustness of the patient's immunological response. This underscores the imperative of maintaining aseptic conditions within the surgical environment while simultaneously shielding the patient's immune competence from potential compromise, such as the advent of perioperative hypothermia [57].

Advances in both prophylactic and therapeutic antibiotic modalities for surgical patient management have led to reductions in SSI incidence. The use of high-efficiency particulate air (HEPA) filtration systems has been validated to be a pragmatic solution to reduce SSI because the operating theater is enriched with cleaner air [58, 59]. Additionally, making sure medical staff are well-sterilized before surgery, giving antibiotics wisely, closely supervising the surgical process, and evaluating a patient's specific physical conditions to predict the risk of infection are important aspects of this topic. However, it's important to mention that discussing these details, while relevant, is not the focus of this thesis. So, this section won't go into a detailed discussion of these topics.

2.2.1 Indoor Environment and SSI

SSIs are infections that occur at or near surgical incision within 30 days of operation or one year [60]. It is the third commonly reported nosocomial infection accounting for 10 to 40% of all nosocomial infections [61, 62]. Globally, SSI rates are from 2.5% to 41.9% [61, 63, 64]. In many studies, the CFU level has been proven to positively correlate with the probability of SSI. Therefore, the CFU level has been considered an important indicator of OR design in different countries [65, 66]. The main source of bacteria-carrying particles (BCPs) in the OR is believed to be the skin scales of the surgical teams and the patient [67]. Researchers are increasingly discovering that the concentration of BCPs released by humans at rest is much lower than that released during mild activity [68].

The surgical microenvironment is defined as the area in close vicinity to the surgical wound [69]. An efficient airflow distribution in this area is crucial to control the local air quality, which may contribute to the reduction of airborne bacterial levels that may cause SSI [70, 71]. The airflow distribution in this area is influenced by multiple factors, including ACH [72, 73], pressure difference, medical equipment [74], and surgical lamps [75, 76]. There have been some studies on OR ambient temperature, but most of these studies focus on the relationship between low ambient temperature and the probability of hypothermia [77, 78]. Few studies have examined the relationship between ambient temperature and surgical site air cleanliness. Earlier studies have investigated the effect of ambient temperature on the CFU level in the OR microenvironment, but few studies consider the influencing factor of surgical lamp radiation which may increase the wound surface temperature and generate the thermal plume then disturb the airflow above the wound [79, 80]. Recent research indicates that surgical lamp radiation can result in elevated temperatures on the surface of wounds. Due to convection, the hot surface of the wound may generate thermal plumes above the wound, which play a dominant role in the airflow dynamics of the surgical microenvironment and may prevent particle deposition [81]. Other studies have demonstrated that ambient temperature has an important effect on the intensity of the human thermal plume [82, 83]. This suggests that low temperatures may lead to lower CFU levels at the surgical site, as stronger thermal plumes prevent the deposition of BCPs. Moreover, other studies indicated that increased indoor relative humidity would reduce the rate of BCP release from the human body [84]. Therefore, the variation in the amount of BCP at the surgical site within the operating room with changing room air temperature should be clarified.

During the normal surgery procedure, patients are covered with a drape at the time of surgery and will have little or no movement, and they are not considered the primary source of BCPs

in the OR [67]. Most previous studies also did not consider BCPs released by patients themselves. Still, the WHO recommends that surgical patients need to bathe before surgical procedures [6]. The answer to the question of whether patients are the source of their SSI during surgery is unknown.

2.2.2 Hypothermia and temperature control

Inadvertent perioperative hypothermia(IPH) is a common occurrence during surgery, and it is defined as a core body temperature of less than 36 °C [7]. The incidence of IPH can be from 4-90% [8-11] of all surgery cases, and it can have negative consequences for the patient's health and recovery, such as disturbed drug metabolism [85], SSIs [86], blood loss and coagulopathy [87], postoperative ileus [88], thermal discomfort [87], prolonged recovery and prolonged duration of hospitalization [89, 90]. The fundamental cause of IPH is that anesthesia drugs affect the patient's thermoregulatory center. In a low-temperature environment of the OR, the patient's metabolic heat production is less than the heat loss from the body, resulting in a decrease in core temperature drop 1.6 °C after a prolonged surgery [91]. Common measures to prevent hypothermia include raising the temperature in the OR, using appropriate anesthesia, heating blankets, and employing the Bair Hugger forced-air convection heating device. However, these measures do not immediately increase the patient's body temperature. Therefore, it is more effective to get the trend of the patient's core temperature in advance.

Previous studies have proposed numerous hypothermia prediction models, which can be roughly classified into two categories based on their computational principles. The first category is data driven. This type of model collects parameters that may affect the probability of hypothermia, such as patient height, weight, age, and gender, as well as surgical type and duration, and uses statistical methods such as regression analysis or machine learning to establish a model of the relationship between these parameters and the probability of hypothermia occurrence [90, 92-95]. The first type of model is usually more convenient, but it can only provide limited information and is dependent on the quality of the training data. The second category is based on the body's thermal balance. Such models were first developed by Stolwijk to assess the biological response of space crews to the dynamic surrounding environment [96]. It was, improved by Fiala et al. to calculate human body temperature regulation under different environmental conditions [97]. It was widely applied to human body temperature prediction under different scenarios, the establishment of a heat balance model evaluation of thermal comfort, etc. [98-103]. This type of method simplifies the human body model, establishes the thermal balance relationship of the human body, and predicts the relationship between core temperature and time through numerical heat transfer or empirical equations. The second type of

method can usually provide more detailed information. Table 2.1 shows the literature review of these models and their features.

Table 2.1 Literature review of the human heat balance model

Study ID	Model Method	Input	Output
Rincon 2008	Logistic regression	Personal and surgery information (age, weight, duration, type of surgery...)	Risk level (low, middle, high, and very high)
Kim 2014	Logistic regression	Gender, age, ASA class, disease, weight, and height tympanic membrane CBT, heart rate, and SBP	/
Yi 2017	Logistic regression	Magnitude surgery, intravenous fluid, duration anesthesia, mode of patient warming, ambient temperature	The risk that the body temperature falls below 35.5 °C during surgery
Wallisch 2021	Liner regression	Gender, age, weight, ASA class, Urgency, Surgery type, Type of anesthesia and drug use, vital signs, and medical history	The risk that the body temperature falls below 35.5 °C during surgery
Severens 2007	Fiala model	Weight, height, fat percentage, Bypass flow, the fluid–blood gradient, mattress temperature, surrounding temperature	Tissue temperature changes over time
Severens 2008	Fiala model	Weight, height, fat percentage, Bypass flow, the fluid–blood gradient, mattress temperature, surrounding temperature	Tissue temperature changes over time
M.J. Tindall 2008	Three-compartment mode (the core organs, a rectal region, and peripheral parts)	The initial temperature of these three compartments	The temperature of these three compartments
Brauer 2011	ThermoSim software	Gender, age, weight, height, duration of the induction of anesthesia, duration of the operation, thermal management during the procedure	Core temperature
Romadhon 2017	Fiala model	Ambient temperature	Temperature distribution
Duh 2022	Fiala model	Thermal imbalances due to sedation and anesthesia, increased metabolic rates induced by inflammatory processes, and various external cooling techniques	Temperature distribution

Developing a heat transfer model for predicting core body temperature poses several challenges. One of the critical factors is to simplify the physical model of the human body and incorporate appropriate boundary conditions. The accuracy of the numerical heat transfer

model depends heavily on the physical model and boundary conditions employed. A reasonable simplification of the physical model and boundary conditions may not significantly impact the results, while an unreasonable one can led to substantial deviations. Another challenge involves collecting data to accurately define a boundary condition. To ensure the model's accuracy, a considerable amount of body temperature distribution data is required for verification. However, obtaining temperature data from within a patient's body is challenging. For example, it is extremely difficult to measure the temperature distribution inside a patient's body during surgery due to the need for a sterile environment.

2.3 Role of ventilation system in creating a safe environment in ORs

Ventilation in surgical operating rooms plays a crucial role in maintaining a safe and sterile environment during surgeries. Efficient ventilation systems are essential to reduce the risk of SSIs, which not only harm patients but also strain healthcare budgets. Throughout history, using Laminar Airflow (LAF) systems has significantly lowered SSI rates [104]. It's worth noting that different countries have different regulations regarding surgical operating room ventilation. Even though LAF systems are widely used, there are still some ongoing debates and uncertainties [105].

In this section, an investigation was conducted into the application and research of various ventilation systems in operating rooms. This encompasses commonly utilized systems such as mixed ventilation and laminar airflow, both of which have defined ventilation parameters specified in regulations across different countries. Additionally, other ventilation systems like temperature-controlled ventilation and displacement ventilation were also examined.

2.3.1 TMV in OR

TMV in OR is based on the principle of dilution to reduce airborne microbes [106]. High-speed and high-turbulence clean air is supplied through diffusers, rapidly mixing with the indoor air, and reaching appropriate room air temperature and humidity levels. The airborne microbes in the indoor air are diluted during this process. Due to the high air exchange rate in the OR, indoor dilution is rapid, resulting in lower temperature gradients, humidity gradients, and concentration gradients [107]. Ideally, the well-mixed air is extracted through the exhaust outlets.

Table 2.2 outlines the ventilation parameter requirements for TMV in different countries' ventilation standards. While there may be slight variations in the recommended surgical types

for TMV OR across countries, common procedures such as endoscopic and laparoscopic surgeries can typically be performed in TMV OR, except for certain surgeries with exceptionally high cleanliness requirements, such as joint replacement surgeries, cardiac surgeries, brain surgeries, and organ transplant surgeries.

Table 2.2 Review of standard of ventilation in TMV OR from different countries

Country	Standards	Temperature (°C)	Relative humidity (%)	The pressure difference between the operating room and adjacent rooms (Pa)	Minimum air change rate (ACH)	Applicable OR types
Brazil [108]	NBR 7256	20-24	<60	5	25 /15	Class1/Class2
China [109]	GB 50333	21–25	30–60	5–20	12/18/24	Class IV/III/II,
France [110]	NF S 90-351	19–26	45-65	10–25	25–30/15-20	Class 3/Class2
Germany [111]	DIN 1946/4	19–24	30–50	–	30-60	Class Ib
Japan [112]	HEAS-02-2004	22-26	50-55	–	>15	–
Norway [113]	–	–	–	5–10	20 ACH	–
Russian [114]	GOST R 52539-2006	18-24	>30	–	12-20	–
Spain [115]	UNE100713	22–26	45–55	5–20	20 ACH	Type A/B
Sweden [116]	SIS-TR 39	18-26	20-65	–	>20	
The U.K. [117]	HTM 03-01	18–25	35–60	20	25 ACH	General/UCV
The U.S. [118]	ASHRAE 170	20–24	20–60	4	20 ACH	Class B/C

Although the importance of creating an indoor environment through ventilation systems in operating rooms to mitigate SSI has been elucidated in Section 2.2.1, there remains a lack of globally standardized ventilation parameters and a consensus. Certain ventilation parameters, such as air change rates and the positioning of exhaust outlets, have been summarized in previous research. However, the influence and mechanistic role of room air temperature on

the surgical microenvironment's indoor environment in operating rooms is yet to be definitively understood.

2.3.2 LAF in OR

The principle of LAF in OR involves using low-turbulence ventilation to swipe airborne microbes away. The supply air diffusers are typically located on the ceiling, covering an area of 8-10 m², with supply velocities ranging from 0.2-0.4 m/s. Due to the low supply velocity and resulting low turbulence, the airflow in the OR is relatively straight and unidirectional. The movement of airborne microbes follows the direction of the unidirectional airflow, resulting in lower levels of contamination in LAF OR compared to TMV OR [119]. Table 2.3 summarizes some countries' ventilation standards for LAF OR. Due to their high air quality characteristics, LAF OR are recommended for surgeries that require a high level of cleanliness or surgeries where SSIs could be life-threatening, such as joint replacement surgeries, cardiac surgeries, and organ transplant surgeries. However, in recent years, there has been controversy regarding the suitability of LAF OR for joint replacement surgeries. The WHO's 2018 guidelines also provide a recommendation against performing joint replacement surgeries in LAF OR [6]. The specific principle for this phenomenon has not been definitively determined to date.

Table 2.3 Review of standard of ventilation in LAF OR from different countries

Country	Temperature (°C)	Relative humidity (%)	Pressure difference (Pa)	Minimum Supply velocity	LAF area	Require maximum bacterial load (CFU/m^2)
Brazil [108]	20-24	<60	5	-	-	-
China [109]	21–25	30–60	5–20	0.20-0.25(0.8m above floor)	-	5
France [110]	19–26	45-65	10–25	0.25-0.35	-	10
Germany [111]	19–24	30–50	-	>0.23	>3.2×3.2	4-10
Japan [112]	22-26	50-55	-	0.35-0.45	-	-
Norway [113]	-	-	5–10	0.25-0.28	-	10
Russian [114]	18-24	>30	-	0.24-0.3	-	-
Spain [115]	22–26	45–55	5–20	-	-	-
Sweden [116]	18-26	20-65	-	-	-	-

Country	Temperature (°C)	Relative humidity (%)	Pressure difference (Pa)	Minimum Supply velocity	LAF area	Require maximum bacterial load (CFU/m^2)
The U.K. [117]	18–25	35–60	20	0.38	>2.8×2.8	10
The U.S. [118]	20–24	20–60	4	0.13-0.18	-	-

Since the last century, the utilization of LAF to mitigate SSI has led to the establishment of numerous laminar flow operating rooms in various countries worldwide. However, in recent years, an increasing body of research has employed statistical analysis to compare laminar flow ventilation with TMV for knee arthroplasty surgeries, revealing that laminar flow ventilation does not confer any advantage in reducing SSI [120]. Consequently, the guidelines provided by the WHO do not recommend the use of LAF operating rooms for knee arthroplasty procedures. Furthermore, the installation costs and operational energy consumption of LAF operating rooms significantly exceed those of TMV, necessitating more efficient ventilation strategies against the backdrop of global energy crises. It is imperative to seek a ventilation solution that not only ensures a safe surgical microenvironment but also reduces ventilation-related energy consumption.

2.3.3 Temperature controlled airflow methods in OR

Temperature-controlled airflow systems have emerged as innovative solutions that combine multiple ventilation principles, aiming to optimize system effectiveness while minimizing operational expenses. An illustrative instance is the recent development of a system commonly referred to as temperature-controlled airflow (TCF) [121, 122]. TCF amalgamates the attributes of both LAF and TMV, whereby HEPA-filtered air is directed toward the surgical region at a slightly lower temperature (1.5-3 °C) than the ambient room air temperature [122]. This subtle thermal contrast effectively segregates the Operating Room (OR) into two discrete zones.

Warmer air is dispersed from surrounding air showers, which prevents the emergence of stagnant regions along the periphery of the room and upholds the temperature gradient needed for forcing the central vertical downward flow of cooled air. Diverging from the LAF and TMV paradigms, the TCF configuration exhibits notable resistance to impediments and thermal plumes [123], while demanding comparatively less voluminous airflow and energy expenditure, as compared to its counterparts LAF and TMV [121, 124]. An instructive

clinical investigation conducted in 2019 scrutinized a cohort of 1000 primary total joint arthroplasties, both pre-and post-TCF implementation, and verified a substantial reduction in infectious complications, diminishing from 3.3% to 1.1% [125].

2.3.4 Displacement Ventilation System in OR

Displacement ventilation (DV) systems are predicated on the introduction of a controlled, low-velocity stream of cold and uncontaminated air at ground level, facilitating the displacement of tainted air towards the upper regions of the OR ceiling [126]. In the operational context, when the cold air encounters heat sources within the surgical microenvironment, a resultant temperature differential and buoyant forces create an upward movement of warmed and polluted air toward the ceiling. Subsequently, this air is expelled from the room. A prominent drawback inherent in DV systems, especially within hospital spaces like OR, is the phenomenon termed "lock-up." Notably, prior investigations have shown that airborne microbes can become trapped or immobilized at the breathing height under specific thermal conditions, due to temperature stratification [127].

A clinical inquiry conducted by Andersson et al. [128] conducted a comparative assessment between LAF and DV systems within the context of both planned and acute orthopedic implant surgeries. This research disclosed that LAF systems offer superior air quality, characterized by diminished CFUs, in contrast to DV systems. Additionally, it is worth noting that prevailing national standards for OR ventilation systems lack comprehensive stipulations regarding the requisite characteristics of DV systems [108-118].

The diagram of different ventilation forms in the operating room is shown in Figure 2.1.

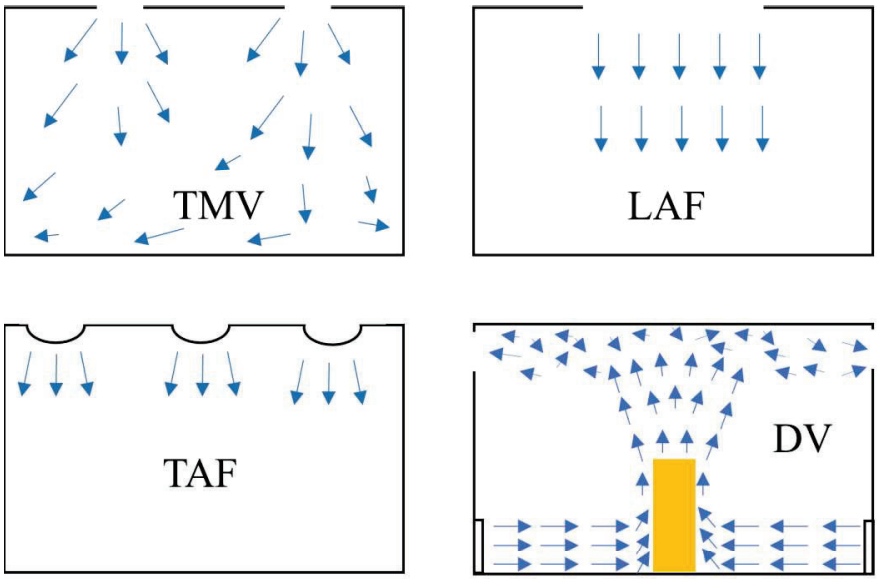

Figure 2.1 Illustration of different ventilation solutions in ORs

Chapter 3: Methods

3.1 Introduction

This thesis employs a combination of experimental and numerical simulation methods. Three OR facilities were used to carried experimental measurements to achieve the goal of this thesis. The experimental measurements were performed in:

1) An airflow laboratory equipped with a TMV system at the Department of Energy and Process Engineering, NTNU.
2) An OR equipped with a TMV system at St. Olavs Hospital in Trondheim.
3) An OR equipped with an LAF system at St. Olavs Hospital in Trondheim.

The experimental research and numerical simulation completed in this doctoral could be grouped in four, answering the research questions:

1) According to **research question one**, experimental measurement using tracer gas in the OR laboratory and CFD simulation to investigate the influence of the pressure difference between operating room and adjacent room validate the performance of physical barriers to reduce the exposure level of airborne microbes. This part includes the following tasks:

   a) Assessment of the exposure levels of the surgical team under different pressure differences to airborne microbes using tracer gas (presented in **Article number one**).

   b) CFD simulations to study the effectiveness of physical barriers in protecting healthcare personnel from exposure (presented in **Article number two**).

2) Perform mock-up surgeries in the TMV OR concerning **research question two**. To collect data to build a numerical heat transfer model to predict the patient's core temperature. This part includes the following tasks:
   a) Performing a series of mockup surgeries with the patient (sedated pig), collecting the indoor environment and the body parameters of the pig during the mockup surgery. (Presented in **Article number three**).
   b) Establishing a model according to the collected data of mockup surgery, and the real core temperature data of patients in the OR was collected to verify the reliability of the model. (Presented in **Article number three**).

3) According to **research question three**, performing one mockup surgery with simulated animal patients and two mockup surgeries with simulated human patients under different ambient temperatures in a TMV OR. This part includes the following tasks:
   a) Measuring and analyzing the air quality parameters such as CFU level and particle concentration, at the surgical site. (Presented in **Article number four**).
   b) The data characteristics were analyzed by statistical methods and the possible reasons were discussed in combination with the literature. (Presented in **Article number four**).
4) In relation to **research question four**, a mockup surgery was conducted in a LAF OR, this part includes the following tasks:
   a) Investigation of the velocity distribution characteristics of the thermal plume above the patient in the LAF OR (presented in **Article number five**).
   b) CFD simulations of the CFU levels in critical areas in LAF and Advanced Protective Laminar airflow (PLAF) OR (presented in **Article number five**).

3.2 Experimental measurement

3.2.1 The OR Laboratory at NTNU

The OR lab is equipped with a TMV system with four supply air diffusers (0.55 m× 0.55 m), as shown in Figure 3.1, four lower-level exhaust outlets (0.175 m × 0.575 m), and four higher-level exhaust outlets (0.55 m × 0.55 m), as shown in Figure 3.1(c). Each lower exhaust grill is connected to a 0.6 m × 0.2 m × 0.315 m plenum box, and each upper exhaust is connected to a 0.315 m × 0.4 m plenum box. The plenum box is equipped with a balancing damper and pressure outlets so that the airflow rate can be measured and controlled. The distribution of exhausted air between the higher and lower exhaust grills for each of the vertical exhaust modules is 1/3 and 2/3, respectively.

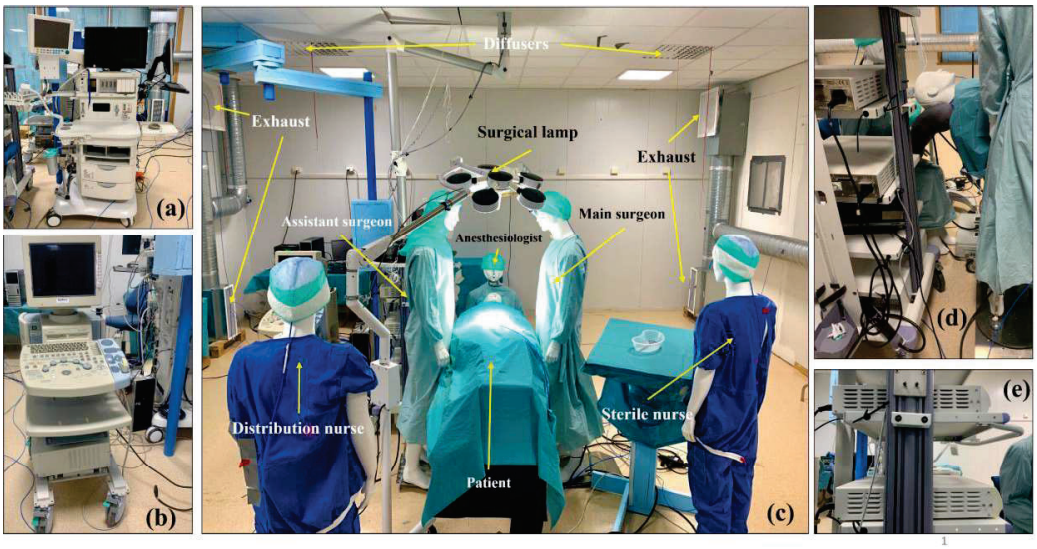

Figure 3.1 Medical equipment and layout in the OR. (a) Anesthesia machine; (b) Ultrasonic imager; (c) the layout of the OR laboratory; (d) Endoscope imager; (e) The cooling fan of the endoscope imager

3.2.1.1 *OR lab facilities and thermal manikins*

The OR lab is equipped with several real medical equipment for OR, as shown in Figure 3.1. For some of the other medical devices that do not produce heat, six thermal manikins were used to mimic surgical staff in an OR, including one patient, two surgeons, two nurses, and an anesthesiologist. The surface temperature of the anesthesiologist and the patient can be controlled by the temperature control device. The patient's head, arms, and body were set at 33°C, 30°C, and 31°C, respectively. The head, arms, body, and legs of the anesthesiologist were set at 33°C, 30°C, 31°C and 30°C, respectively. The heat power data of other facilities can be found in Table 3.1.

Table 3.1 The heat power of all heat sources in the OR laboratory

Equipment	Heating power (W)
Surgical lamp 1	61
Surgical lamp 2	74
Supersonic cleaner	45
Endoscope imager	232
Anesthesia machine	136
Main surgeon	150
Assistant Surgeon	150
Sterile nurse	140
Distribution nurse	140

3.2.1.2 Experiment setup

A study by Bivolarova et al. [129] found a strong linear relation ($r^2 > 0.9$) between the mean concentrations of microparticles sized 0.7 and 3.5 μm and a tracer gas nitrous oxide (N_2O) in

an indoor ventilated environment. In this thesis, N_2O tracer gas was used to simulate coronaviruses released from the breath and wound of a surgical patient. Commonly used tracer gases include SF_6(146.06 g/mol), which has a molecular weight slightly heavier than N_2O (44.01 g/mol) and air (28.97 g/mol) and is relatively more expensive compared to N_2O. The objective of this study includes experimental study on ventilation performance, where the selected tracer gas will represent the dispersion of indoor air. It is preferable to choose a gas with a density as close to air as possible. Previous studies have also indicated differences in the diffusion rates of these two tracer gases when simulating indoor air dispersion [130]. Considering all factors, N_2O was chosen as the tracer gas for this experiment. Studies have shown that aerosolized blood droplets may carry airborne microbes during laparoscopic surgery to release intra-abdominal pressure [131]. This thesis will use two surgical lights throughout all measurements. The tracer gas was released from the nose and wound of the patient separately in each case.

A constant air supply volume of 20 ACHs and a constant room air temperature of 22±1 °C was used in this thesis according to most standards [109, 132-134]. Three negative values were used: -5 Pa, -15 Pa, and -25 Pa. The change in pressure difference in the OR lab was achieved by regulating the air extract rate. In total, three cases were investigated with tracer gas under conditions with or without a ventilation system, different heights of surgical lamps, and different indoor heat intensities. The measurement conditions for each case can be found in Table 3.2. The supply airflow rate of all cases is 4000 m^3/h.

Table 3.2 Illustration of the case set up for the study on Research question one

Case	Tracer gas source	Pressure difference	Air extract rate
1.	Nose	-5 Pa	4140 (m^3/h)
2.		-15 Pa	4242 (m^3/h)
3.		-25 Pa	4316 (m^3/h)
4.	wound	-5 Pa	4140 (m^3/h)
5.		-15 Pa	4242 (m^3/h)
6.		-25 Pa	4316 (m^3/h)

Besides, the airflow distribution measurement was conducted to validate the CFD result. AirDistSys5000 was used to measure the air velocity (with an accuracy of 0.2 m/s), and temperature (with an accuracy of 0.2 °C) distributions. Overall, there were 66 measurement points, as presented in Figure 3.2.

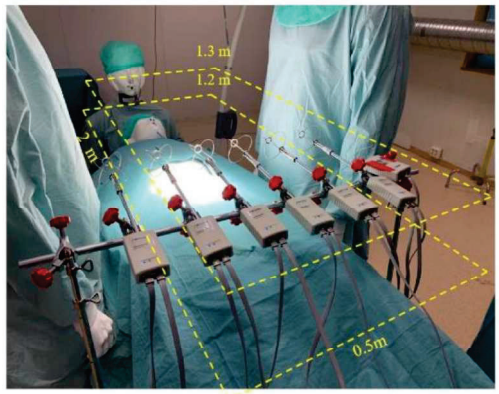

Figure 3.2 Experiment setup in TMV OR

3.2.1.3 Measurement procedure and data processing

The N_2O flow rate was kept at 0.18 m^3/h (3 L/min) in all cases of this thesis. The sampled tracer gas was then sent continuously to a Innova 1303 multigas sampler and dozer (Brüel & Kjær, Ballerup, Denmark) coupled with an Innova 1302 photoacoustic monitor. There were six tracer gas measurement points, including exhaust (Point (1)), breathing zone of distribution nurse (Point (2)), anesthetist (Point (3)), sterile nurse (Point (4)), main surgeon (Point (5)), and assistant surgeon (Point (6)). Each measurement lasts for over five hours, with 50 data collected at each location.

Before each experiment, the OR lab was ventilated for two hours in advance, the tracer gas was turned on after the indoor temperature was stable and the wall temperature remained unchanged. The sampling time of the Innova 1302 photoacoustic monitor was approximately 60 s/channel, and six channels were measured in sequence, giving 6 min between each measurement at the same location.

Descriptive statistics were used for the analysis of the sampled N_2O levels at six measurement points. Skewness and kurtosis statistics were used to test the assumption of normality for the N_2O levels. Levene's test for equality of variances was used to test the assumption of homogeneity of the variance. One-way analysis of variance (ANOVA) and Kruskal–Wallis methods were used to assess whether the mean N_2O levels were significantly different between the same measurement points for different cases. The significance was defined as $p < 0.05$.

Air change efficiency and local air change index category indicators were used to interpret the measured results in this thesis [135, 136]. The air change efficiency, ε, is defined as the ratio between the shortest possible air change time for the air in the room, the nominal time constant, τ_n,

and the actual air change time, $\bar{\tau}_e$. For the measurement of the local air index, each measurement session lasts for 5 minutes. Gas release begins at the start of the session and continues until stability is achieved. The measurement concludes once stability is reached after the initial gas release.

3.2.2 TMV OR in St. Olavs hospital

3.2.2.1 OR layout

To achieve the objective of the study on Research questions one and two, an OR with a TMV system in the St. Olavs hospital was used to carry out experimental measurements. In total, six animal (sedated pig) tests and six mockup surgeries were performed in this OR, as shown in Figure 3.3. The OR has an area of 53 m^2 and a height of 2.9 m. The OR is equipped with four radial air diffusers and four exhaust grills. The total supply airflow rate was 3680 m^3/h, and the average airflow rate in the exhaust was 2933 m^3/h. The air change rate of the OR was 23.9 ACH. The pressure difference between the OR and the adjacent room is 12 Pa.

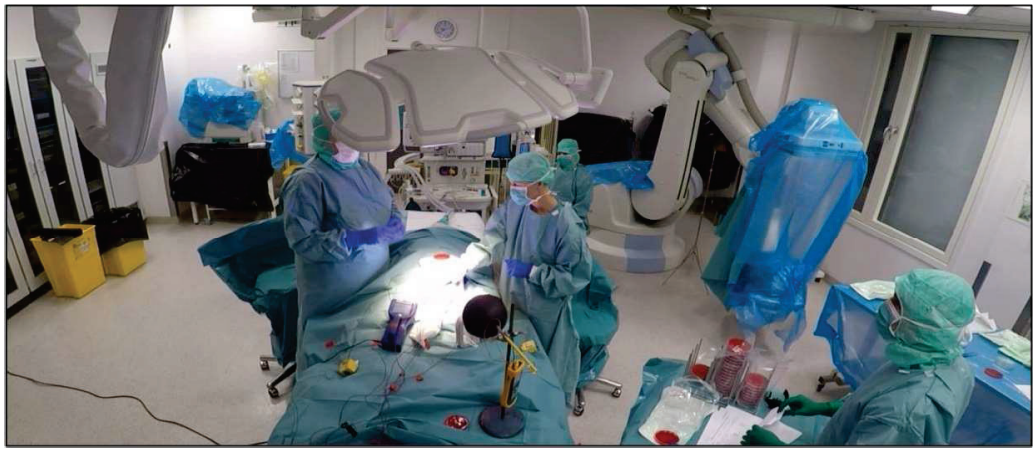

Figure 3.3 The layout of the mock surgery experimental setup(a)scenario. (b)measurement instrument (c)animal patient(d) blood agar plate

3.2.2.2 Experiment setup

In this thesis, 21℃, 23℃, and 25℃ are set in the OR for the animal test and mock-up surgery. These measurement conditions are shown in Table 3.3.

Two animal tests were performed on two pigs under anesthesia, and the mockup surgeries were performed with simulated patients which were considered as heat and pollutant sources. The surgical team consisted of a main surgeon, an assistant surgeon, an anesthesiologist, a sterile nurse, and a distribution nurse.

All mock surgeries were performed with the same procedure and lasted approximately 42-44 mins. For the first 20 mins, everyone remained in a static state to allow the ventilation to

reduce indoor particulate concentrations caused by preoperative activities. This was followed by a 10-min active period. During this stage of the animal surgery, the surgeon's activity included making the incision, cutting a piece of tissue, and suturing the wound. Before incising a wound, chlorhexidine is applied as a disinfectant and preservative. Its molecular formula is $C_{22}H_{30}Cl_2N_{10}$. However, in the mock surgeries, the surgeons performed a similar activity but did not make real incisions, which is the only difference between the animal surgery and the mock surgeries. Everyone remained still for the final 10 mins to allow the particulate levels to fall again after the surgeon's activity. CFU and particulate matter concentrations near the wound were measured simultaneously starting at the initiation of the surgery.

The measurement results of Cases 1-9 were used to evaluate the effect of ambient temperature on CFU levels, while Cases 1-3 and 10-12 were used to develop a heat balance model. During animal tests, surface, and deep wound (0.03-m deep) temperatures were measured using thermal couples, while the animal patient's core temperature was measured by an anesthesia machine.

Table 3.3 Illustration of the cases setup for Research question three

Surgery type	Case	Temperature (°C)
Mock-up surgery 1 (animal patient)	1	21
	2	23
	3	25
Mock-up surgery 2 (simulated patient)	4	21
	5	23
	6	25
Mock-up surgery 3 (simulated patient)	7	21
	8	23
	9	25
Mock-up surgery 4 (animal patient)	10	21
	11	23
	12	25

3.2.3 LAF OR at St. Olavs hospital

To achieve the objective of study on Research question four, an OR with a LAF system in the St. Olavs hospital in Trondheim was used to carry out experimental measurements as shown in Figure 3.4. The OR has a floor area of 56.58 m^2 with a room height of 3 m. The area of the protected zone under the cover of the LAF system is 11 m^2 (3.12m x 3.12m). The ventilation system in the OR consists of a vertical LAF system as shown in Figure 3.4. The OR is also equipped with six exhausts. The laminar flow area is surrounded by a canopy, and its inner

edge is considered to be the boundary between sterile and unsterile areas. During the experimental measurements, the ventilation system was operated at full load, and the room air temperature was set to 22 °C. The designed supply airflow in the LAF OR was 10500 m^3/h, comprising 4300 m^3/h of outdoor air and 6200 m^3/h of recirculated air.

The experiment in the laminar flow OR is mainly to validate the CFD simulation. The velocity of five lines with seven points on each line on the plane above the surgical site were measured, as shown in Figure 3.4 (b)(c)(d).

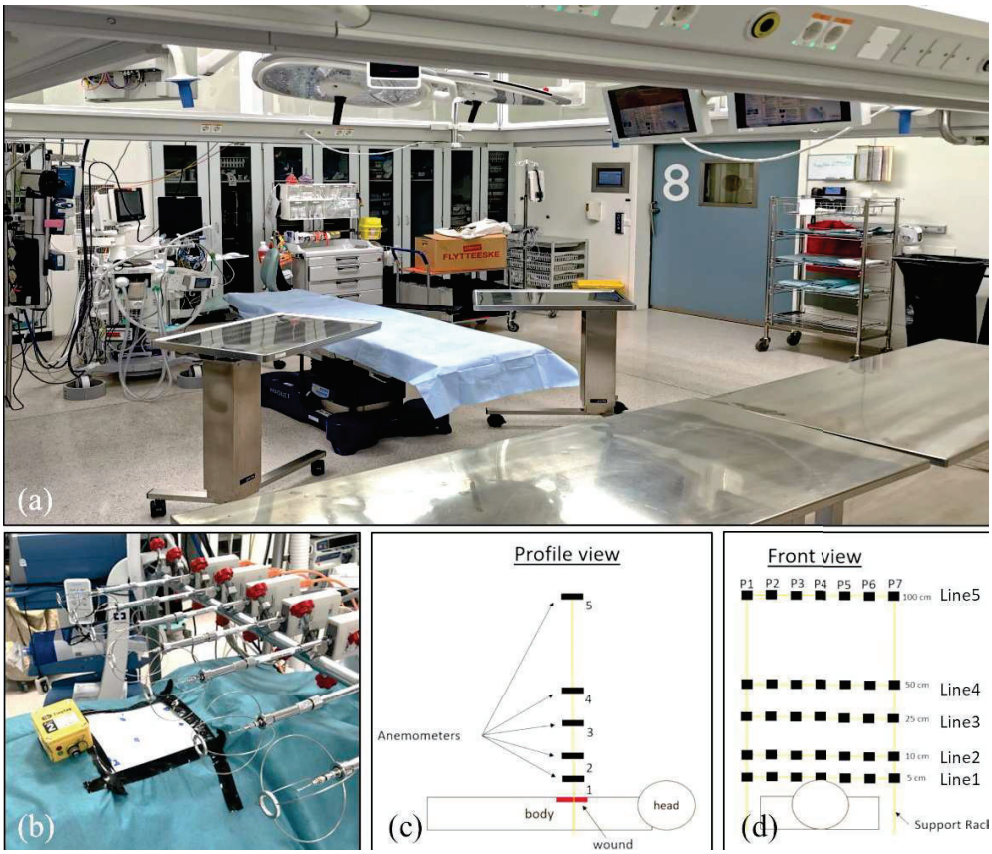

Figure 3.4 Picture of the LAF OR and measurement points in St. Olavs hospital

3.2.4 Instruments

In the experimental measurement, different experimental instruments were used to measure various parameters, including velocity, temperature, humidity, pressure difference, particle concentration, CFU, tracer gas concentration, etc. Figure 3.5 shows the pictures of these instruments and Table 3.4 lists detailed parameters of these instruments.

The tracer gas N_2O, which was placed outside of the OR lab, was continually released through a plastic tube (ϕ33 mm). The flow rate of N_2O is controlled by a gas rotameter connected to the tank. The N_2O flow rate was kept at 0.18 m^3/h (3 L/min) in all cases. The sampled tracer gas was then sent continuously to a precalibrated Innova 1303 multigas sampler and doser (Brüel & Kjær, Ballerup, Denmark) coupled to an Innova 1302 photoacoustic monitor, which is shown in Figure. 3.5(a). According to the manufacturer, the repeatability of the Innova 1302 measurements is ±1% under standard conditions. All standard deviations of the measured results performed under conditions without medical equipment were calculated to be under 5% of the mean value. An active CFU sampler, as shown in Figure 3.5(c), and a passive sampler, which is a blood agar plate as shown in Figure 1(d), were used to measure the CFU levels. The blood agar used in the mock surgeries consisted of 5-7% bovine blood in Petri dishes measuring 90 mm in diameter. The active air sampler used was the AirIdeal 3P model from Biomérieux, which consists of 3 main components: the machine, a filter, and blood agar plates. The active air sampler works by drawing in the surrounding air at a constant suctioning volume of 100 L/min, causing the particles in the air to collide with a blood agar plate at a velocity of less than 20 m/s. The TSI 9306 particle counter, as shown in Figure 3.5(c), measures the particle concentration. The device facilitates particle measurement across six distinct size ranges, 0.3-0.5 μm, 0.5-1 μm, 1-3 μm, 3-5 μm, 5-10 μm, and 10-25 μm. This particle size spectrum effectively covers the majority of BCP ranging from 10-20 μm. AirDistSys5000 anemometers were used to measure air temperature and airspeed at 5×7=35 points in the OR lab, as shown in Figure. 3.5(f). The lowest measurement points were 0.10 m higher than those of the patient.

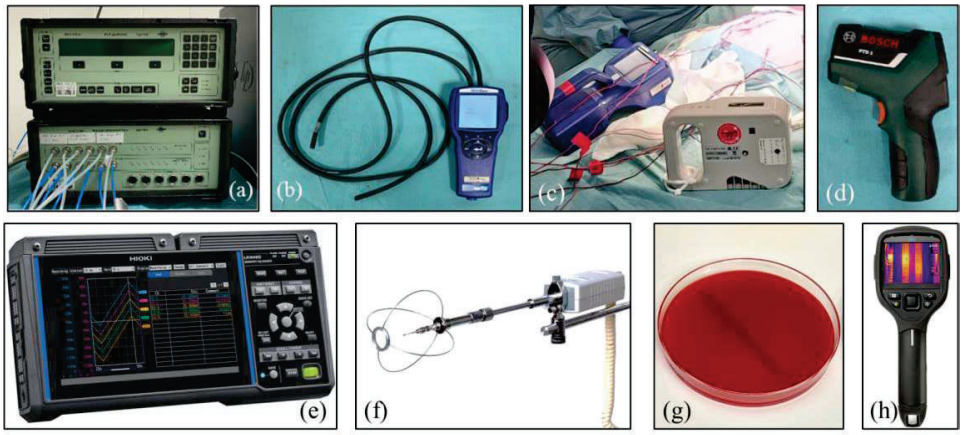

Figure 3.5 Picture of instruments(a) Tracer gas (b) VelociCalc 9565-p (c) TSI 9306 and active air sampler (d)Bosch infrared meter (e) HIOKI LR8450 T type (f) AirDistSys5000 (g) Bloody ager (h) FLIR E60

Table 3.4 lists some of the instruments that were used in this thesis.

Table 3.4 List of instruments used in this thesis

Instrument	Type	Parameter	accuracy
Thermal couple	HIOKI LR8450 T type	Temperature	±0.05% of reading and ±0.1% of range,
Infrared camera	FLIR E60	Surface temperature	±2 °C
Anemometer	AirDistSys5000	Air velocity	± 0.02 m/s
Tracer gas	Innova 1302	Concentration	±1%
Particle counter	TSI 9306	Particle concentration	±5%
Ventilation Meter	VelociCalc 9565-p	Pressure difference	±1 Pa

3.3 Numerical methods

3.3.1 Modeling of wound and core temperature

The model of heat transfer of the human body was established according to the following assumptions.

1) The heat generation in the human body due to cell metabolism, which is constant and stable during the operation.

2) Heat is transferred from the core of the body to the skin surface by two mechanisms, one is the thermal conduction of human tissues, and the other is the convective heat transfer through blood flow. The convective heat transfer is simplified by expressing it as an equivalent thermal conductivity efficiency and superimpose it on the conduction process.

3) Regarding heat exchange with room air, the convective heat transfer coefficient of different parts of the human body is the same.

4) The time taken for blood vessels to constrict or dilate has been ignored.

3.3.1.1. Physical models of patients

Physical models used in this thesis were simplified and used for all patients. Figure 3.6 shows how to simplify the physical model and divide the nodes. Relevant data from previous studies is used to describe the size of the human body, by using height and weight as input parameters, the size of other parts can be calculated as well.

Bushy et.al [137] presents the relationship between height and head size,

$$C_{he} = 42.2 + 0.08673 \times h_{pa} \quad (1)$$

The relationship between body size and Body Mass Index (BMI) can be found below [138]

$$W_{ch} = 0.0015 \times (BMI - 21.75) \quad (2)$$

With the use of the above parameters, the distance and dimensions between all nodes and the body dimensions can be calculated.

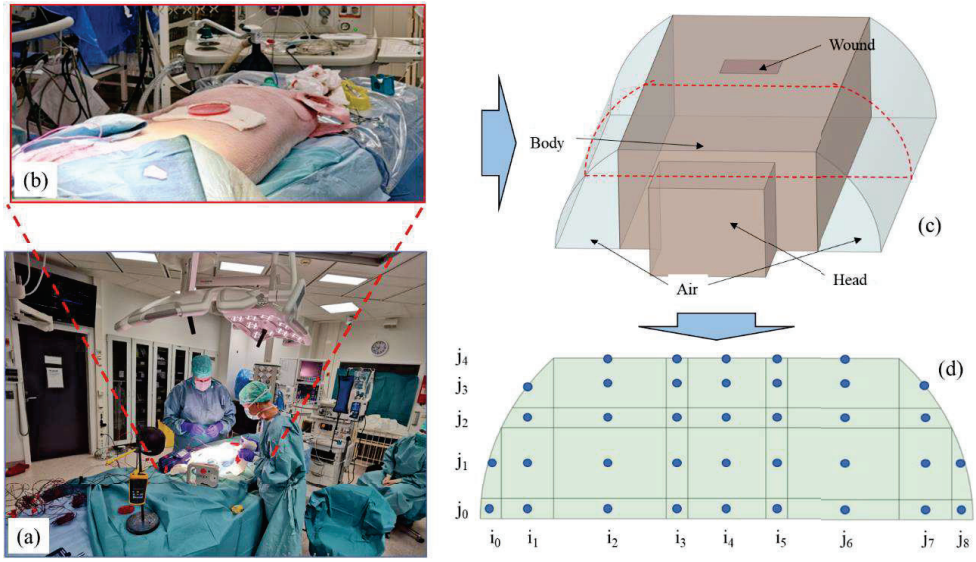

Figure 3.6 Modelling process (a) simulated surgery (b) pig patient (c) Simplified model of pig patient (d) division of control volume

3.3.1.2 Heat balance

The body's heat balance can be established between heat input and heat output. The heat input is the heat produced by the metabolism of the cells of the body. In the OR environment, the light from the surgical lamp is an input, which may warm up the surgical wound. The heat output is convection heat transfer from the body to the room air, sweat, and respiration. These are all boundary conditions for the body, and the heat conduction taken place inside the body.

The differential form of the three-dimensional thermal conductivity equation can be expressed in a rectangular coordinate system as follows:

$$\rho c \frac{\partial T}{\partial t} = \lambda \frac{\partial^2 T}{\partial x^2} + \lambda \frac{\partial^2 T}{\partial y^2} + \lambda \frac{\partial^2 T}{\partial z^2} + S \quad (3)$$

The human thermal conductivity coefficient, λ, is an important parameter in the equation. In practice, heat is transferred from the core to the skin in two ways: by conduction through the tissues, for which previously researched data were referenced [99, 101], and by convection heat transfer through the blood vessels, which is driven by the heart's pumping action and transferred to surrounding tissues through the vessel walls. In this thesis, both convection and

conduction of heat transfer are treated in a similar way, using the analogous equation and thermal conductivity coefficient to calculate the convective heat transfer. In this simulation, measurements from both human and pig subjects were used to calculate the equivalent thermal conductivity coefficient.

The heat conduction in this model requires discretization to convert higher-order partial differential equations into numerical equations. To discretize the equation, the control volume method was employed, and the internal node method was used to divide the nodes. To ensure the stability of the calculation, full implicit iterations were conducted. The detailed derivation and numerical solution process can be found in the Article number three [139].

3.3.1.3. Source term and boundary condition

Regarding the processing of boundary conditions, the additional source term method was used to handle different types of boundary conditions. For boundary conditions with constant temperature, the temperature in the specific direction is set as a fixed value without participating in the iteration. For boundaries with constant heat flux, heat flux was used to eliminate the temperature term in the equation. A detailed derivation process can be found in the Article number three [139].

Metabolic rate

Indirect calorimetry is the reference standard and clinically recommended means to measure energy expenditure. Notwithstanding the limitations of the assumptions, indirect calorimetry has been found to be consistent and in close agreement with direct calorimetry [140]. The principle of the indirect is that human breathing. The basis of the caloric method is that the oxygen consumed by respiration participates in the metabolism of fats, proteins, and carbohydrates in the body and produces carbon dioxide exhaled from the body. Metabolic rate can be estimated by measuring respiration, carbon dioxide difference, and oxygen difference.

$$\dot{M} = 3.941 \times \dot{V}_{O_2} + 1.106 \times \dot{V}_{CO_2} - 2.17 \times \dot{V}_{N_2} \quad (4)$$

Where $\dot{M}$ is the metabolic rate, kcal/min; $\dot{V}_{O_2}$ and $\dot{V}_{CO_2}$ is the O_2 and CO_2 intake and exhalation, L/ min; $\dot{V}_{N_2}$ is the daily urine nitrogen emissions, g/day.

Convective heat transfer

The additional source term method needs to calculate the heat flux at the boundary, for convective heat transfer, according to Fourier's law,

$$q_B = h(T_{sk} - T_{am}) \tag{5}$$

$$h_{c,mix} = \sqrt{a_{net}\sqrt{T_{sk} - T_{\mathrm{am}}} + a_{frc}v_{a,eff} + a_{mix}} \tag{6}$$

Where, a_{net}, a_{frc} and a_{mix} are regression coefficients and $v_{a,eff}$ is the effective relative air speed, which is measured in the TMV OR. For the LAF OR, the value $v_{a,eff}$ is different. In the article number three, the values for the regression coefficient are given.

Radiation heat transfer

To consider the radiative heat transfer between the outermost grid and the external environment, the additional source term method was employed, which is explained in article number three. Specifically, the grid located near the wound was designed to incorporate the radiation input from the operating lamp. Conversely, the grids that were exposed to air, except for the layers that were next to the bed, were configured to consider only the radiation output which was known to vary with surface temperature.

The radiation heat transfer equation of the body node is,

$$q = \frac{\sigma_r\left({T_{sk}}^4 - T_w^4\right)}{\frac{1-\varepsilon_1}{\varepsilon_1 A_1} + \frac{1}{A_1 F_{12}} + \frac{1-\varepsilon_2}{\varepsilon_2 A_2}} \tag{7}$$

Where, ε_1 is the Thermal emissivity, F_{12} is the angle factor from plate one to plate two; T_{sk} is the skin temperature, °C; T_w is the wall temperature, °C.

Sweating

Sweating is a natural thermoregulatory behavior of the human body. When the temperature is too high, the central nervous system prompts the sweat glands to secrete sweat, which evaporates and removes heat from the body, thereby reducing the body temperature. This relationship has already been established [141].

$$m = 16.2\dot{M} + 92.6T_{sk} - 3117.16 \tag{8}$$

Where, m is the amount of sweat the body produces, g; $\dot{M}$ is the metabolic rate, W.

Breathing

The human breath carries away part of the heat from the body. The air inhaled is heated in the lungs to about 31 °C. The heat needed can be expressed in terms of the ambient temperature T_{amb} and the exhalation temperature T_{br} and the amount of breath, as explained in Eq. (9). At the same time, the inhaled air of respiration is accompanied by an increase in humidity,

which increases to around 80%. Therefore, the sensible and latent heat of water vapor can be calculated directly.

$$Q_{br} = V_{br}\rho_a C_{pa}(T_{br} - T_{amb}) \quad (9)$$

Where, Q_{br} is the sensible heat loss from the breathing, W/s; V_{br} is the breathing rate, m^3/s; ρ_a is the density of the air, kg/m^3; C_{pa} is the heat capacity of the air, W/kg·°C.

3.3.1.4. Conductivity change

The determination of the heat transfer coefficient is based on different factors. Since the heat transfer in the human body is very complicated, the heat transfer process inside the human body model is simplified. Essentially, this means that even though the two heat transfer processes differ, they ultimately result in the same amount of heat moving from the inside to the outside. The thermal conductivity of the whole process is equal to the sum of the thermal conductivity of the two-heat conduction.

When the brain detects the body's temperature is too low, it initiates a series of measures to alter the amount of heat the body loses. For example, the brain controls blood vessel constriction, chills, etc. And when it is hot, the brain controls blood vessel dilation, sweating, etc. This degree of vasodilation is not thought to be linear with temperature, and this mode of regulation is turned on when the body temperature reaches a certain point, this mode of regulation is dependent on the anesthetic and dose used.

3.3.1.5. Initialization

When performing unsteady simulations, proper initialization is crucial to obtaining accurate and reliable results. To ensure proper initialization, we first conduct a longer simulation period with the model to obtain temperature distributions at different locations. Then divide the simulated temperature into several intervals and correlate the temperature within each interval with the corresponding ambient temperature, core temperature, and skin temperature. This temperature correlation equation is then incorporated into the initialization process to ensure that the initial simulation does not fluctuate due to an unrealistic temperature distribution. By utilizing this method, the model can achieve a more stable and accurate simulation.

3.3.1.6. Flow of simulation process

Figure 3.7 illustrates the computational procedure using the entire model, which is written in the C++ programming language. Firstly, all boundary conditions are provided at time t_0,

including the patient's height, weight, oxygen consumption, carbon dioxide production, current core temperature, and ambient air temperature. Subsequently, based on the input values, the patient size, metabolic heat generation, convective heat transfer from the skin surface, radiative heat exchange with the environment, and skin temperature based on core temperature and ambient air temperature can be calculated. These values are then assigned to each control volume as initial conditions for the model. Next, the temperatures of all control volumes at time t_{+1} are computed using the discretized equations and iterated until the residuals of temperature calculations for all control volumes are less than 10^{-6}. Once the residuals reach 10^{-6}, the temperatures of nodes at time t_{+2} are calculated. A time step of 0.5s and a maximum of 14400 steps, equivalent to 2 hours was used. After each time step, the radiative heat exchange between the human body and the environment is recalculated, and the core temperature is checked against a threshold value. Every time the threshold of core temperature is reached, adjustments are made to the heat conductivity, the value is provided in Article number three. The computational model shown in Figure 3.7 is for a pig, with the main differences in the core temperature threshold and the adjustments to the heat conductivity for the human body. While the governing equations, boundary conditions, and calculation flow are the same.

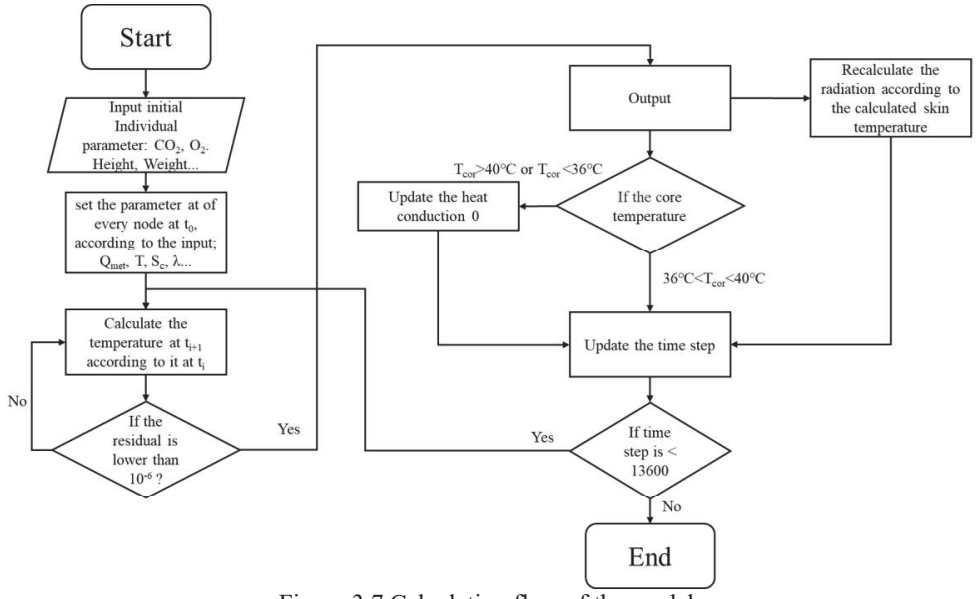

Figure 3.7 Calculation flow of the model

3.3.2 Computational fluid dynamic simulation

3.3.2.1 Computational domain

The simulated physical model presented in this section is based on the laminar flow OR at Health St. Olavs Hospital. A simplified illustration of the LAF and an improved LAF system, the Protective Laminar Airflow (PLAF) system can be seen in Figure 3.8. In this simulation, the geometry of the anesthesiology machine was simplified to a box and neglected OR lockers. The layout of the OR with surgical staff and instrument tables are the same as that of the real OR.

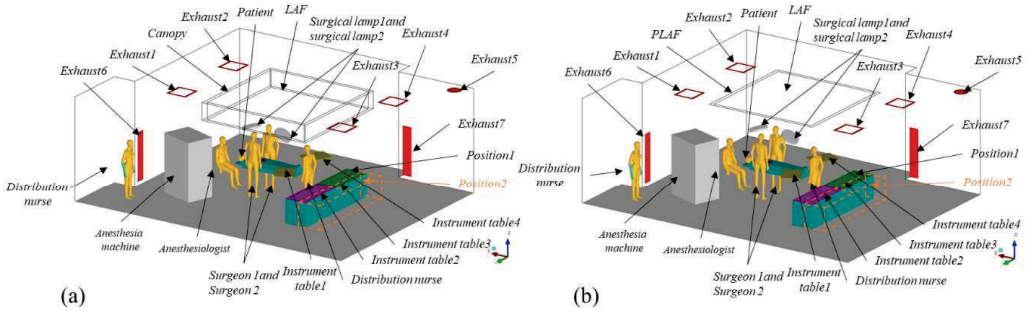

Figure 3.8 Illustration of the OR model for CFD simulation using LAF and PLAF (a) LAF (b) PLAF

Figure 3.9 shows an OR model with TMV, which is based on a TMV OR laboratory in EPT. The medical instruments in the model are simplified into rectangles but retain some of the details of the human body. Its layout, the calorific value of the human body, and medical devices are the same as that of the laboratory. The boundary conditions are adiabatic, but the body and the medical device are set to constant temperature based on the measurements.

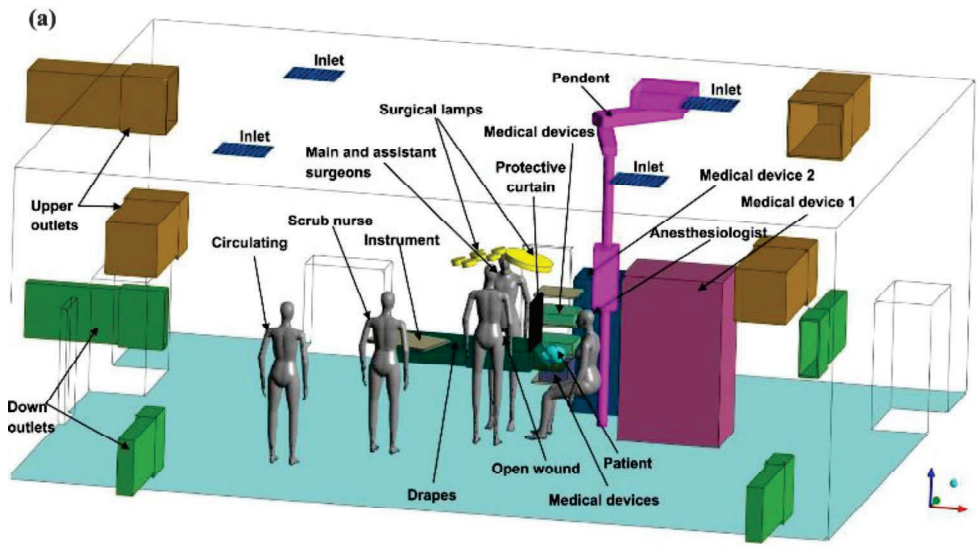

Figure 3.9 Illustration of the OR model for CFD simulation using TMV

3.3.2.2 Turbulent airflow model

Due to the intricacies of indoor airflow dynamics, an accurate simulation of turbulent airflow indoors relies heavily on a proper turbulence model. The two-equation k-ε model is the most employed turbulent model for indoor airflow simulations. In the study on Research questions one and four, the Realizable model, a recently developed approach, was used. The formulation of this model adheres to specific mathematical constraints associated with Reynolds stress, thus ensuring its alignment with the physical characteristics of turbulence. Notably, prior scholarly endeavors [122, 142] have demonstrated the utility of the Realizable k-ε model, particularly in the context of intricate simulations within complex indoor environments [143]. In a broader conceptual framework, the governing equations encompassing continuity, momentum, energy, and turbulence quantities find expression in a generalized transport equation format [144]

$$\frac{\partial(\rho\phi)}{\partial t} + \nabla \cdot \left(\rho\phi\vec{V}\right) = \nabla \cdot \left(\Gamma_\phi \nabla_\phi\right) + S_\phi \tag{10}$$

where ρ is the air density, $\vec{V}$ is the air velocity vector, ϕ denotes the transported quantity, Γ_ϕ is the (effective) diffusion coefficient of ϕ, and S_ϕ is the source term. Given the consideration of exclusively steady-state conditions, the transient term was omitted from the formulation. Notably, a second-order upwind scheme was employed to discretize the convective terms, while the diffusion terms underwent discretization through the implementation of a central difference scheme. The detailed setting of boundary conditions can be found in Article number five. The basis for setting parameters can be found in the literature [145].

3.3.2.3 A numerical model for particle transport

Lagrangian particle tracking was employed in the present study to model the BCPs transport, in which the motion of an inert particle in a viscous flow was described by an ordinary differential equation,

$$\frac{d\vec{u}_p}{dt} = F_D\left(\vec{u} - \vec{u}_p\right) + \frac{\vec{g}\left(\rho_p - \rho\right)}{\rho_p} + \vec{F} \tag{11}$$

where $\vec{u}$ is the velocity, ρ is the density, and $\vec{g}$ is the gravitational acceleration, and the subscript p denotes particle related variables whereas unsubscribed symbols refer to airflow quantities. The ultimate term encompassed within Equation (11) serves to account for supplementary forces exerted upon the particle. Given the particularities of the airflow conditions and particle dimensions under scrutiny within this thesis, it is prudent to solely

consider Saffman's lift force. This selective focus arises from the negligible impact of alternative supplementary forces when juxtaposed with the dominant drag force [146]. More detailed setting of boundary conditions for particle tracking models and the basis for setting them can be found in Article number five. The basis for setting parameters can be found in the literatures [147-150].

Assuming that particle sizes conform to a Rosin-Rammler two-parameter distribution, the particle size distribution within the operating room is determined by data from previous studies. The diameters corresponding to the 25%, 50%, and 75% percentiles are 7×10^{-6}, 12.8×10^{-6}, and 18×10^{-6}, respectively. By employing the Rosin-Rammler distribution function to fit this data, the resulting distribution functions are derived. In total, there are ten sets of particle size distributions.

$$Y = e^{-\left(\frac{d}{\overline{d}}\right)^n} \tag{12}$$

Where, Y is the probability that the particle size is larger than d; $\overline{d}$ is the average diameter of particulate matter, in this thesis is 12.5×10^{-6}, and the n is 3.41 in this thesis.

3.3.2.4 Verification and validation of the model

In this thesis, the simulation is verified firstly by doing the grid independence tests. Besides, simulation results were compared with experimental data to ensure the accuracy of the applied CFD program in predicting airflow behavior within the TMV operating room. Before validation, measurements of the surgical microenvironment's airflow distribution were conducted in a TMV OR laboratory and a OR with LAF at St. Olavs Hospital.

The measured data were then compared with the simulated data, revealing a relative error of less than 10% between experimental and simulated results. This suggests that the selection of the turbulence model, the configuration of boundary conditions, and the simplification of the physical model in this simulation are reasonable. See Appendix -Article five for details.

3.3.2.5 Cases setup

The TMV OR CFD study setup is for study the comparison of implementing the protective curtain behind the patient's face to reduce the exposure level of the surgeon to airborne microbes. Therefore, only the two conditions were compared, with and without protective curtains, which are Case 7 and Case 8 in the study on Research question one. For modeling the spread of airborne microbes, the SF_6 gas was released from the patient's mouth and nose.

Due to the higher relative molecular weight of SF_6 compared to N_2O, it is more suitable for simulating the diffusion of particles, especially those with a larger diameter, taking into account gravitational effects. Although many studies have compared the performance of these two gases in predicting the movement of different particles and found that both tracer gases can accurately predict particle motion [129, 151, 152], considering the comprehensive aspects, this study primarily focuses on simulating particles of a certain micron size, SF_6 was chosen as the tracer gas in the simulation.

This simulation was accomplished by solving the gas transport model and equations. All the equations for the simulation of BCPs and airborne disperse were solved using commercial CFD code Fluent 19.2. Moreover, a novel approach, locating a protective shield curtain between the patient's head and lower body, was introduced to moderate the airborne disperse.

In a simulation of using an OR with LAF, to find the effect of different parameters on the performance of PLAF, different angles, different downward plate jet diffusor lengths, and different downward plate jet velocity were compared. The compared parameters are shown in Table 3.5.

Table 3.5 Case study setting up for study on Research question four

Case No.	Ventilation form	downward plate jet angel	Slot width	Downward plate jet velocity	LAF velocity(m/s)	Airflow rate(m^3/h)
1	LAF	/			0.25	8760
2					0.30	10513
3	PLAF	Downward	0.01 m	1.5 m/s	0.25	9098
4					0.30	10850
5		Downward	0.01 m	2.0 m/s	0.25	9210
6					0.30	10963
7		Downward	0.02 m	1.5 m/s	0.25	9437
8					0.30	11189
9		23°(inward)	0.01 m	1.5 m/s	0.25	9098
10					0.30	10850
11		23(outward)	0.02 m	1.5 m/s	0.25	9437
12					0.30	11189

Chapter 4: Results and Discussions

This chapter presents the main results of the doctoral thesis. Section 4.1 showcases a study on tracer gas research, conducted in the operating room laboratory, focusing on exposure risks of medical staff when patients act as pollution sources under different pressure differentials. Additionally, it includes a CFD simulation study on the effectiveness of using plate to reduce staff exposure, corresponding to Research question one. Section 4.2 demonstrates the comparison between our established predictive model for perioperative patient temperature and experimental results, as well as the collection of patient outcomes, corresponding to Research question two. Section 4.3 displays the results of the impact of ambient temperature on CFU levels in the surgical site within the operating room, as well as the relationship between CFU levels and particle concentration, corresponding to Research question three. Section 4.4 presents the comparative results of CFU levels on surgical site and instrument tables under different ventilation conditions for PLAF and LAF systems, corresponding to Research question four.

4.1 Research question one: Influence of pressure difference and protective curtain on the exposure level of surgical team to the airborne microorganism in the TMV OR

4.1.1 Measurement results of tracer gas concentration with pollutant released from the patient nose (Cases 1-3)

Figure 4.1 shows a boxplot of the measured concentration results in Cases 1 to 3 when the tracer gas is released through the patient's nose under three different pressure values. Due to the large difference in data at different points, the y-axis is displayed as a logarithmic axis. This figure shows that the highest concentration appears at point (6), the breathing zone of the assistant surgeon, under three different pressure conditions. This was followed by point (5), at the breathing zone of the main surgeon. The lowest concentration results were found at point (2), the breathing zone of the distribution nurse, which is lower than the exhaust concentration. The concentration at point (3), the breathing zone of the anesthesiologist, was slightly higher than that in the exhaust at between 103% (35.8 ppm) and 114% (42.5 ppm). Considering the effect of pressure change on concentration, except for the distribution nurse, the mean value of concentration at all points decreases with increasing pressure. Despite this,

except for two surgeons, the concentrations in the breathing area of other surgical staff were not significantly different from those of the exhaust.

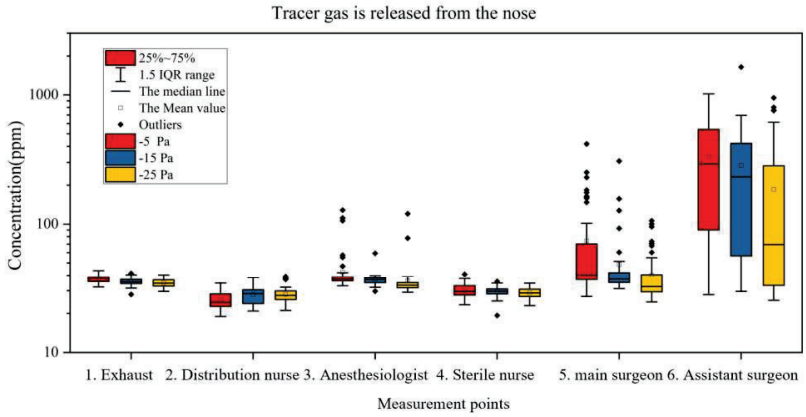

Figure 4.1 Boxplot of concentration results when tracer gas is released from the patient's nose.

4.1.2 Measurement results of tracer gas concentration with pollutant released from the patient wound (Cases 4-6)

Figure 4.2 shows the boxplot of concentration results at each point in Case 4-Case 6 as tracer gas is released from the wound of the patient. The highest mean concentrations were found at point (6), all of which were more than 12 times the mean value of the concentration at point (1), the exhaust. This was followed by concentration point (5). The mean concentrations of other measurement points were close to the mean concentration at the exhaust, point (4). Considering the influence of the pressure difference on the concentration, with increasing pressure difference, the concentration of all the measuring points decreased except the concentration at point (2), which shows a similar trend as Case 1 to Case 3. The difference comparing the first three cases is that the concentration at point (6) does not change drastically with the change in the pressure difference.

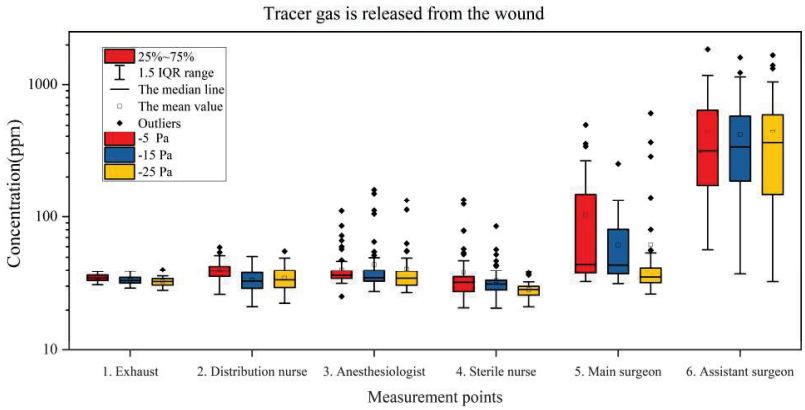

Figure 4.2 Boxplot of concentration results when tracer gas is released from patient's wound

From Figure 4.1 and Figure 4.2, it is noticed that the data did not follow a normal distribution. Air pollutant concentrations are inherently random variables because of their dependence on the fluctuations of a variety of meteorological and emission variables [153]. According to the random dilution theory, when the pollutants are still in the dilution stage rather than the complete mixing stage, the measured pollutant concentration data show a two-parameter lognormal distribution [154, 155]. This kind of distribution of tracer gas concentration in the breathing areas of surgical staff near the surgical microenvironment, including an anesthesiologist, assistant surgeon, and main surgeon is also observed in this thesis, which suggests that tracer gas is still in the intermediate stage of dilution when moving to these areas rather than being completely mixed with air. The results may indicate that surgical staff who work in proximity to an airborne-infected patient may be exposed to a higher airborne microbes' concentration than those who work further from the patient in the OR with TMV under negative pressure.

4.1.3 Air change efficiency and local air change index

The air change efficiency and local air change index were used to evaluate the performance of airflow distribution at these measurement points. Air change efficiency represents the performance of the air distribution of the ventilation system in the room. The calculated value of the air change efficiency of the OR is 49.24%, 49.91%, and 50.18% at -5 Pa, -15 Pa, and -25 Pa, respectively.

Figure 4.3 shows the local air change index from point (2) to point (6) by using the measurement results. The ideal value in a TMV room is 100%. If the index at a point is less than 100%, it means that the air reaches this point slower than the air reaches the exhaust, and

vice versa. From the figure, the local air change index of points (2), (3), and (4) is like the trend of pressure; that is, the increase in pressure will increase the local air change index of these points. Among them, point (3) has the largest variation range, which increases from 75.26%, which is the lowest value, at -5 Pa to 108.56% at -25 Pa. However, this value is the lowest among the three points at -5 Pa and -15 Pa.

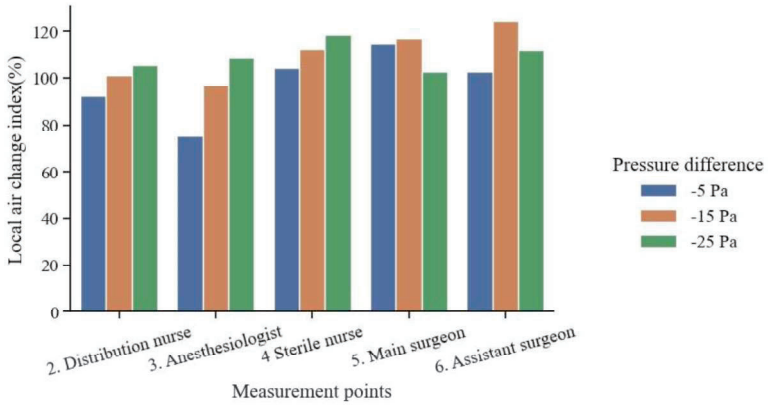

Figure 4.3 Local air change index of each surgical staff breathing area.

Table 4.1 shows the results of the intergroup posttest, indicating whether there was a statistically significant difference between the two groups. Points (1) and (2), regardless of whether the pollutant is released from the nose or the wound, show similar characteristics. This is easy to understand since both sites are far away from the patient. When the pressure difference changes from -5 Pa to -15 Pa, there is a significant difference between the two groups of data, but when the pressure difference changes from -15 Pa to -25 Pa, there is no significant difference between the two groups of data. According to the actual measured exhaust air volume, there is a small difference in the actual ventilation volume with different pressure differences. The ventilation volume differences between -5 Pa and -15 Pa and between -15 Pa and -25 Pa are 102 m^3/h and 74 m^3/h, respectively. This difference is due to the relationship between the pressure difference and ventilation volume determined by the following equation:

$$\Delta p^{0.5} \delta = Q \tag{13}$$

where Δp is the pressure difference, Pa; Q is the flow rate, m^3/h; and δ is a coefficient. For this experiment, the relationship between the flow rate and pressure difference can be fitted as $63.58\,\Delta p^{0.5} = Q$ (R=0.99). Therefore, the primary factor causing the concentration differences at points (1) and (2) under different pressure differentials is the variation in ventilation rate.

Table 4.1 Data analysis of whether the variation of pressure difference in different positions has a significant effect on the concentration data.

Measurement point	Case #-#					
	1-2	2-3	1-3	4-5	5-6	4-6
1. Exhaust	p=0.001	p=0.180	p<0.001	p=0.001	p=0.371	p<0.001
2. Circulation nurse	p=0.003	p=1.000	p=0.006	p<0.001	p=0.823	p<0.001
3. Anesthesiologist	p=0.126	p<0.001	p<0.001	p=0.758	p=0.848	p=0.998
4. Sterile nurse	p=0.807	p=0.098	p=0.127	p=0.538	p=0.001	p<0.001
5. Main surgeon	p=0.039	p=0.008	p<0.001	p=0.301	p<0.001	p<0.001
6. Assistant surgeon	p=0.268	p=0.005	p<0.001	P=0.767	p=0.649	p=0.989

At point (3), there is a significant difference only between the Case 2 and Case 3 data, while at point (4), there is a significant difference only between the Case 5 and Case 6 data. From the concentration results, such a difference is very small and may be caused by changes in ventilation volume.

On the other hand, according to the results of the local air change index at each point combined with the results of the concentration, with the increase of the pressure difference, the local air change index at point (2) to point (4) increases, and the concentration at each point decreases accordingly. The concentration data can be related to the local air change index. That is, the greater the local air index is, the smaller the concentration. This can explain the influencing factors of indoor concentration at each point, including the actual ventilation volume and air distribution.

When the pressure difference changes from -15 Pa to -25 Pa, the concentration data at point (5) differs significantly regardless of where the tracer gas is released. It can be seen from the thermal plume results that the change of pressure difference can significantly change the characteristics of the patient's thermal plume, which may be due to the influence of airflow infiltration into the gap of the room envelope, and this influence is more intense for point (5) than the change of ventilation rate and the change of the same fraction efficiency. When tracer gas was released from the wound, the concentration data of point (6) did not differ significantly under different pressure differences. This may be due to the Coanda effect on the chest of the assistant surgeon after the thermal plume from the patient's wound is diverted to the assistant surgeon. This effect will not be affected by external airflow.

4.1.4 CFD simulation results of velocity

The CFD simulation was conducted to evaluate the performance of using a physical curtain in front of the patient to reduce the exposure level of the surgical team to the airborne microbes. The CFD simulation results are shown in Figure 4.4 that the air temperature above the

surgical site was higher than in other areas. The maximum air temperature was 25°C above the surgical site at the height of 1.2 m and 23.5°C at 1.3 m above the floor. However, the air temperature was around 21°C, further from the wound in the surgical microenvironment. A careful analysis of the measurement data confirmed this temperature variation in the surgical microenvironment. Furthermore, the surface temperature of the wound area increased from 20°C to 40°C during the experimental study.

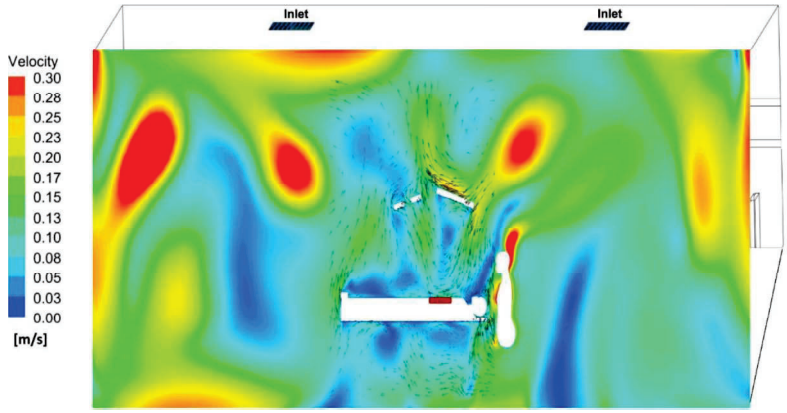

Figure 4.4 CFD velocity contour results

4.1.5 CFD simulation results of pollutant concentration

In the simulation, SF_6 was released from the nose of the patient during an ongoing surgery to evaluate the exposure level of the surgical team. Overall, two different scenarios, with and without the curtain, were numerically simulated to investigate the spread of airborne infectious diseases from the patient. The distribution of pollutant from the contaminated patient is presented for all cases in Figure 4.5, in which SF_6 tracer gas represents the airborne infectious particles.

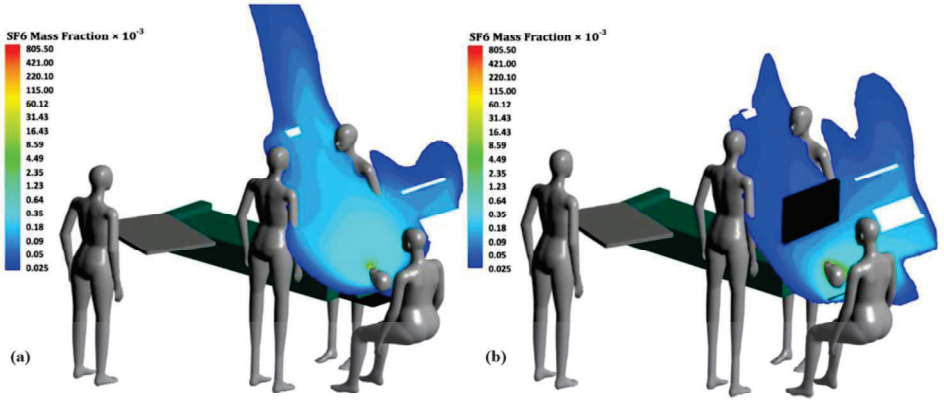

Figure 4.5 CFD SF_6 concentration results(a)without protective curtain, (b) with protective curtain

The results showed that in Case 7, the infectious airborne particles reached the maximum mass fraction of 0.18×10^{-3} at the breathing zone of the surgeon, and the assistant surgeon who was located around the operating table. Using a protective curtain in Case 8 resulted in a 0.025×10^{-3} particle mass fraction in the surgeons' breathing zone. In both cases, with and without a protective curtain, the microbes were not obtained in the breathing zone of scrub and circulating nurses. However, the microbes were detected close to the anesthesiologist nurse in all studied cases.

4.1.6 The performance of the application of the protective curtain

Since the outbreak of COVID-19, the safety of the surgical team has become a priority. Various strategies have been proposed to increase the protection level of health care workers in hospitals. Hill et al. [16] suggested a novel concept entitled "Corona Curtain" that implemented plastic drape roles for making an intubation tent for a COVID-19 patient. Although their proposed concept was successful, the Corona Curtain was designed for hospital wards. In this regard, the current study evaluated the exposure level of the surgical team while using a protective curtain located between the upper and lower patient's body in the OR. The CFD simulations showed that using this protective curtain reduced the exposure level by up to 75% in the breathing area of the surgeons. Since using a protective curtain between the anesthesiologist nurse and patient might affect the performance of this nurse, using a high-protection mask rather than a surgical mask is highly recommended. Thus, using the proposed protective curtain reduces the spread of airborne infectious diseases from the patient and improves the safety of the surgeons.

4.2 Research question two: Predictive modelling of patient's core temperature

4.2.1 Core body temperature of the pig patient

Experimental measurement results were used to evaluate the performance of the developed model for predicting core body temperature using general anesthesia.

Figure 4.6 shows the comparison of simulated and experimental results of core temperature. It shows a good agreement between the predicted core temperature and measured values with an R^2 coefficient of over 0.97. The difference in temperature between predicted and measured values was within 0.2 °C even after one hour.

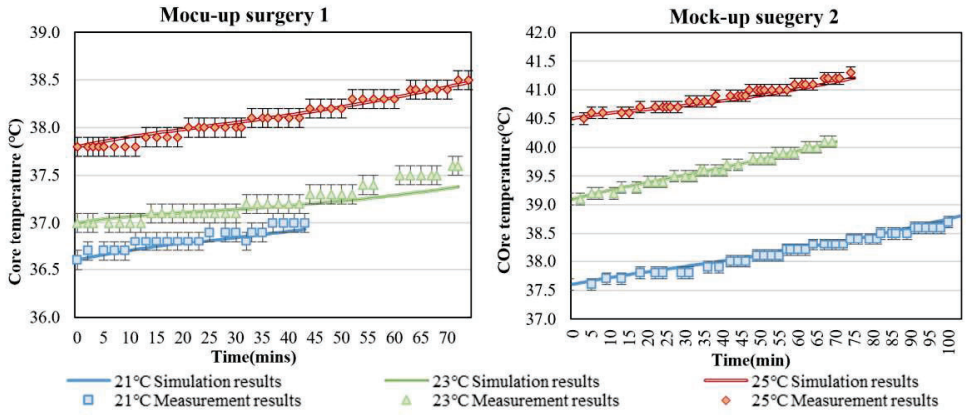

Figure 4.6 Comparison of simulated and experimental results of core temperature

4.2.2 Deep wound temperature of the pig patient

To evaluate the performance of this model in predicting tissue temperature at the surgical site, thermocouples was used to measure the tissue temperature 0.03 m underneath the wound and compared the results with the predicted values from this model, as shown in Figure 4.7.

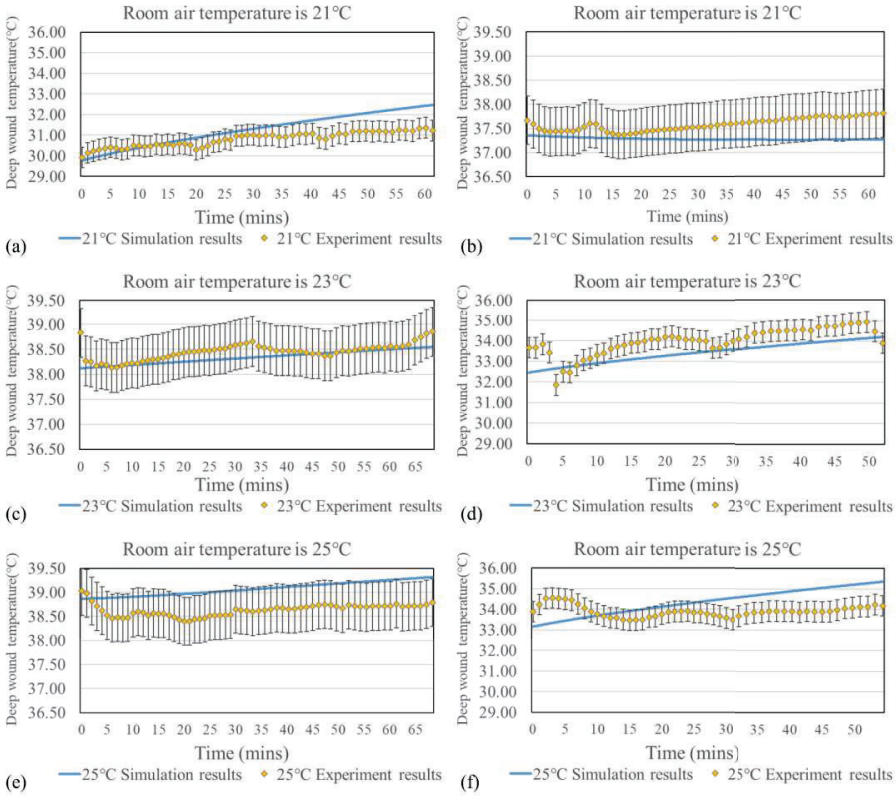

Figure 4.7 Comparison of simulated and experimental results of 0.03-m deep wound temperature, (a)(c)(e) mockup surgery 1: Case 1-3, (b)(d)(f) mockup surgery 2: Case 10-12.

The results demonstrate that this model accurately predicted tissue temperature at the surgical site for most cases, with most of the temperature measurements falling within the error bars of the predicted values. The accuracy of the predictions was especially notable for Cases 1-3 and Cases 10 and 11, where the temperature measurements were within 0.5 °C of the predicted values. However, in Case 12, the measured temperature was consistently lower than the predicted values, with the difference reaching up to 1 °C at some points during the surgery.

4.2.3 Skin surface temperature of the pig patient

Thermal images were taken using an infrared camera to measure the surface temperature of the surgical patient during surgery, and the measurement results are shown in Figure 4.8. The figure on the right shows simulation results. Case 3 was selected for comparison, and the temperature of the surgical site exceeded 37 °C due to the illumination of the surgical lamp. In addition, the temperature of the upper part of the patient's body was higher than that of the sides, with the upper part being about 30 °C and the sides about 25 °C. Simulation results in this thesis also was discovered this phenomenon because the sides of the patient's body as an air layer was set, which is consistent with the actual situation.

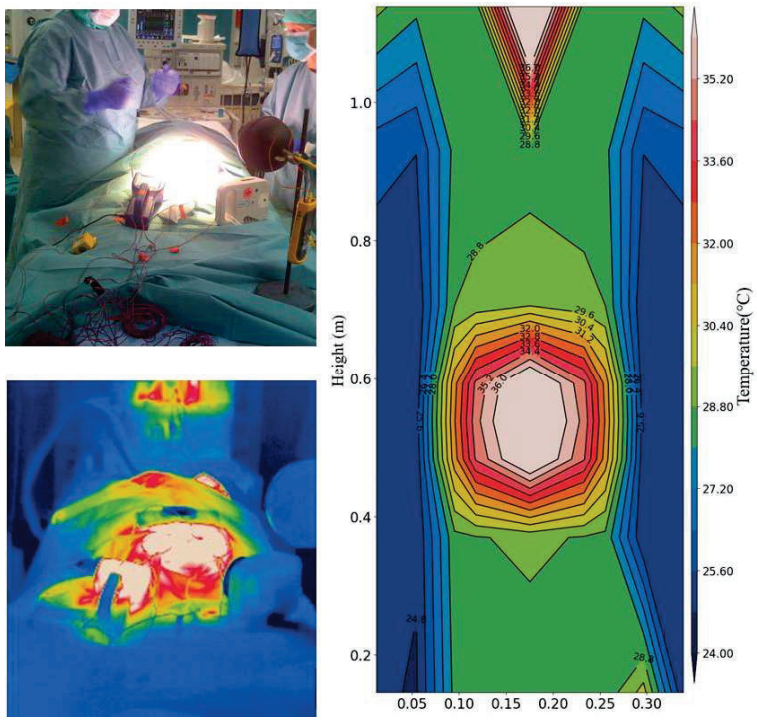

Figure 4.8 Comparation of the experimental and simulated results of the patient's body surface temperature

4.2.4 Prediction of human patient core body temperature

Some patient data during some real operations was collected to verify the accuracy of the model. From human patients, the heat transfer coefficients were modified, and the simulation process was the same as in Figure 4.9. The temperature thresholds were set at 36°C and 38°C for all human cases. As can be seen from Figure 4.9, the simulation accurately may predict the trend of temperature change. Within one hour, the temperature difference between simulation and measurement patient core body temperature is less than 0.2°C. For Case 3, the patient was measured using a heating pad, and the heating pad used a constant temperature of 39 °C. This condition was incorporated into the model, and the calculated data was accurately matched by measurement data within 180 minutes. However, for patient 2, the simulation results were 0.3°C different from the experiment at 90 minutes.

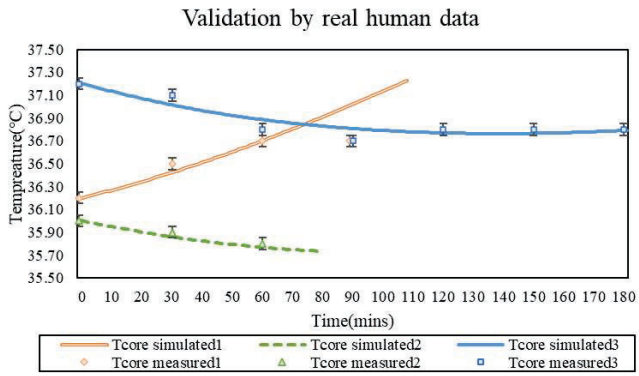

Figure 4.9 Real operative patient measurements versus simulated data

4.2.5 The performance of the prediction model

The model of human heat balance has undergone extensive development over the years. However, this model distinguishes itself from previous ones by disregarding the intricate details of the model and instead focusing on accurate heat transfer calculations. A simplified approach was introduced to convective heat transfer in blood vessels, known as the effective thermal conductivity method. To determine the corresponding coefficient, experimental data obtained from the real human body were used.

Skin blood flow is influenced by vasoconstriction and vasodilation. Under normal body temperature conditions, the average skin blood flow accounts for 5% of the cardiac output. However, during cold stress, it is distributed nearly evenly between 0% and the maximum vasodilation period, which corresponds to 60% of the cardiac output on the body surface [156]. The reaction of blood vessels was simplified, which typically involves an initial

response followed by a slower response. The initial response is often triggered by the stimulation of receptors on neurons and muscle cells, resulting in a sudden increase in calcium ion levels within vascular smooth muscle cells and subsequently leading to rapid vasoconstriction. Since the simulated time is much longer than the duration of the initial response (which usually lasts only a few seconds to a minute). Therefore, the change in thermal conductivity caused by vasoconstriction as a segmented process was considered.

Regarding the calculation of metabolic heat, Severens et al. [99] proposed an equation that accounts for the variation of metabolism with different tissue temperatures. However, changes in metabolism can cause fluctuations in tissue temperature, which may differ from the equation. Accurately predicting the heat generated by metabolism is crucial for maintaining the thermal balance of the human body. To improve this model in this thesis, the indirect calorimetry method was applied to calculate the metabolic rate, achieving an accuracy of up to 95%.

By comparing the final simulation results at various room air temperatures with actual measurement results, the results demonstrate the accurate prediction of the heat transfer processes within the human body. These processes include heat generation from metabolism, heat transfer from the interior to the exterior of body, and radiation heat exchange from surgical wounds. Figure 4.9 shows the similarity between the simulated temperature range, and the comparative simulation results.

To ensure the simulation efficiency, certain factors were neglected such as clothing wrinkles. Despite these simplifications, this model still effectively describes the phenomenon of heat transfer. Within two hours, the majority of the simulation data agreed with measurement results and fell within the margin of error, with temperature differences within an hour remaining within 0.2℃.

It is worth noting that in the temperature may change with real individuals, the core temperature of patient No. 2 in Figure 4.9 deviated by 0.3℃ from the experimental value after 90 minutes. This discrepancy may be attributed to the assumption that the metabolic rate would not change based on the current measurements. Predicting the changing trend and magnitude of the metabolic rate can aid in improving the model.

4.3 Research question three: Study on the effect of room air temperature on CFU level at surgical site

4.3.1 Measured CFU results.

The measured CFU level of every mockup surgery at different room air temperatures of nine measurements is shown in Figure 4.10. For the measurement of CFU level with the active sampling method, with the increase in the temperature, a decrease in CFU level was observed in all measurements, except for the first mockup surgery. All the measured CFU is less than 10 CFU/m^3, except for one case of 21°C in surgery 2. The results of the measured CFU showed similar patterns. However, the values of the passive sampled CFU were slightly lower than 3 CFU/h. The two CFU results are even 0.

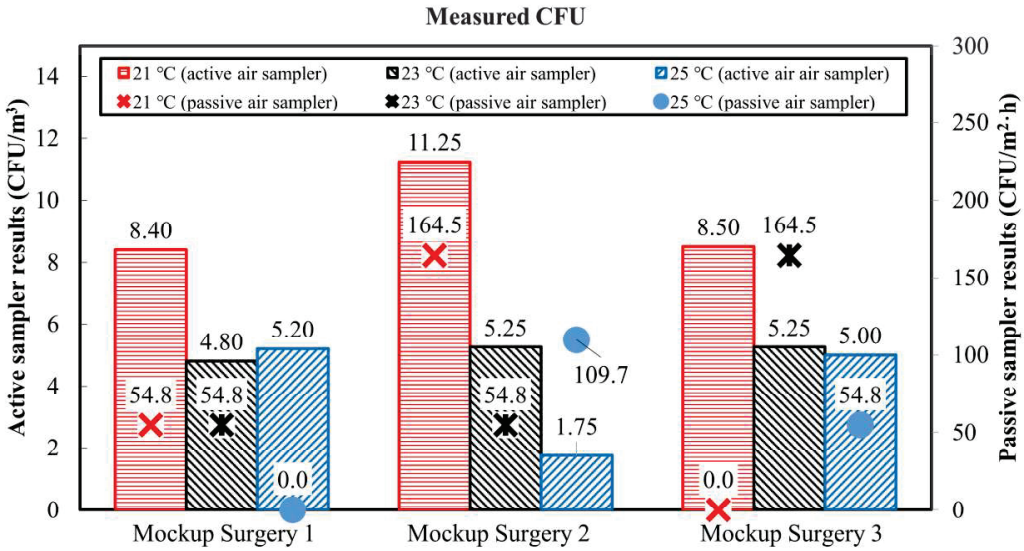

Figure 4.10 CFU results (active sampler and passive sampler)

4.3.2 Measured particle concentration

Table 4.2 shows the correlation coefficient between particle concentration during the surgeon's activities and the room air temperature which indicates that the thermal plume may reduce the exposure risk of the wound area. The particle (diameter < 3 μm) has a strong relationship with room air temperature. However, the larger particles, especially the particles with diameters between 5 μm and 10 μm, seem not always correlate with room air temperature.

Table 4.2 The correlation coefficient between particle concentration and room air temperature.

Particle size	Mock-up surgery 1		Mock-up surgery 2		Mock-up surgery 3	
	correlation coefficient	P-value	correlation coefficient	P-value	correlation coefficient	P-value
0.3	0.306	<0.001	0.586	<0.001	0.574	<0.001
0.5	0.236	0.001	0.410	<0.001	0.6	<0.001
1	0.334	<0.001	0.247	<0.001	0.309	<0.001
3	0.372	<0.001	0.067	0.358	0.146	0.041
5	0.313	<0.001	-0.147	0.042	-0.272	<0.001
10	0.173	0.019	0.027	0.711	-0.249	<0.001

4.3.3 The effect of room air temperature on CFU level and particle concentration.

The increase in the room air temperature leads to a higher particle concentration but a lower CFU level. The size of the bacteria that may cause SSI is between 0.2 and 5 micron, such as staphylococcus aureus, which may form aggregates of greater size (can be larger than 5 μm) after adhering to particles [157, 158]. However, these particles can originate from cloth, skin, resuspend, or ventilation system. Whereas desquamation from the skin of the surgical team and the patient can be the main source of the bacteria [67, 159]. Among them, the increased concentration of fine particles confirmed the previous hypothesis that the thermal plume at the wound site may prevent the deposition of particles on the surgical site. This thesis may suggest that as the room air temperature increases, the impact of air temperature on deposition becomes weaker. This viewpoint can be explained by the fact that higher temperatures lead to a reduced temperature difference between the human body and the environment, resulting in a weaker thermal plume generated by the body. The thermal plume tends to inhibit the deposition of particles as its direction is upward. Therefore, higher temperatures are associated with a reduced deposition effect, especially for smaller-sized particles, due to the weakened influence of the thermal plume. For CFU, a reduction in the rate at which the surgical team releases bacteria may be the main cause of its decline as room air temperature increases.

Skin scales are dead keratinocytes, which form the outermost layer of the skin. Normal people shed 3×10^8 cells every day [160], producing 21.6 million particles [161]. The main cause of cell droppings is desmosomal degradation, which induces the physiological desquamation process [160]. Desmosome decomposition is almost unaffected by temperature and only by hydrolase. But skin scales can contain different cells, causing smaller scales to be more numerous. In addition, previous studies have suggested that the rate of particulate matter release is related to human activity level, clothing, and lipids on the skin surface [162].

Under high temperatures, more sweat and sebum are secreted [163], which will also stick the cells that should be shed to the skin and prevent them from shedding normally. A previous study also observed that with the increase in temperature, the rate of microbial particulate matter produced by the human body decreased [164]. It is worth noting that the distribution of microorganisms on the skin is not uniform, with more on the head and chest than on the limbs [162], while the forehead and cheeks have the most oil secretion. Wearing clean scrubs can reduce the spread of BCP, however, some particles can still be released from the foreheads of surgical team members and the gaps in their clothing. Also, note that the skin on the forehead of the surgical team was exposed to air during the operation. There may be many other distant causes of increased CFU, such as indoor relative humidity, which are beyond the scope of this thesis.

Human activity is believed to increase the level of CFU at the surgical site [161, 165-169], and the amount of increase is related to human activity level [68]. When people are active, the physical friction between skin and clothing accelerates the shedding of skin scales [161]. Instead, the cells are released in smaller forms, which are easier to penetrate through and out of clothing spaces, leading to increased levels of CFU. Some previous studies have concluded that the upper body releases BCP at 2-3 times the rate of the lower body. Addition, detailed values and the relationship between the increase factor and temperature are discovered. In this thesis, the low-intensity activities performed by surgeons, such as cutting wounds, bending, and suturing, also increase CFU level, which are 1-5 times at 21-23℃, and 9-11 times at 25℃ comparing with no activities.

4.4 Research question four: Study on the performance of PLAF

4.4.1 CFU level at wound

Figure 4.11 shows the results of CFU detected at the surgical site under 12 simulated experimental conditions. The figure that the highest CFU level appeared in Cases 11-12. When the air supply velocity in the LAF region is 0.25 m/s, the CFU level Case 7 with PLAF is lower than that in the case of LAF. When the air supply velocity was 0.30 m/s, CFU levels were lower in all PLAF cases than in LAF cases except Case 12. The line between the two gas supply speeds indicates the efficiency, and the lower the line, the higher the ventilation efficiency. As you can see, the efficiency of Cases 7,8 is higher than that of LAF.

Based on the CFU results, it was indicated that the BCP in the wound was generated by the activities of two surgeons. It can be inferred that the most favorable condition is when the

surgeons' thermal plumes are disrupted, and the LAF dominates the whole protected zone. This scenario may facilitate the direct one-way removal of BCP generated from the surgeons' upper body. In cases where the supply airflow is insufficient or disturbed, the non-unidirectional flow may increase the probability of BCP settling on the wound. However, the PLAF, under suitable conditions (Case 7), allows the airflow to converge effectively without overly disrupting the LAF's unidirectional flow (as observed in Case 9), resulting in a more stable yet dynamic airflow pattern.

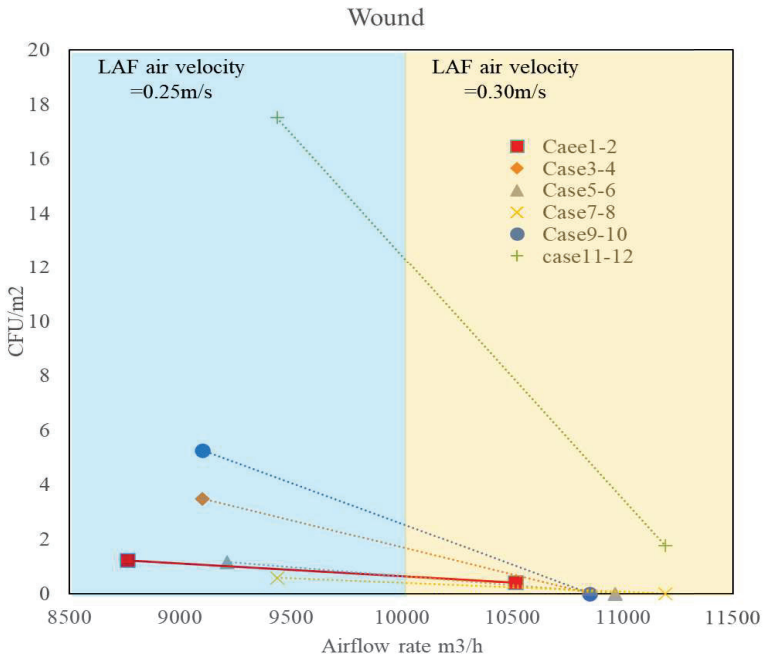

Figure 4.11 Simulated CFU level at the wound

4.4.2 CFU level at instrument tables

Figure 4.12 shows the CFU level at instrument table three and four. When the air supply velocity in the LAF area rises from 0.25 to 0.30 m/s, the CFU level of the instrument station increases in all cases. At 0.30 m/s, the CFU level of Cases 4 and 6 of PLAF is lower than that of LAF. Cases 9 and 14 are similar to LAF, and it can be seen that changing the outward angle of the downward plate jet does not make a lot of difference in the result. In contrast to the results at the surgical site, CFU levels on the instrument table were lower at higher air supply rates under all conditions.

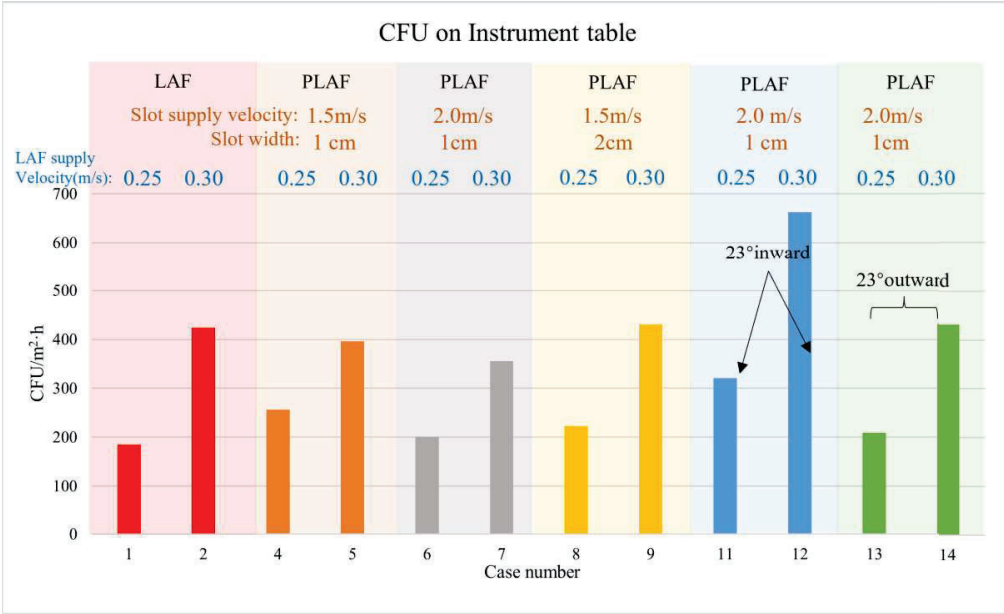

Figure 4.12 Measured CFU level on the instrument table

4.4.4 Simulated velocity vector results

Figure 4.13 shows the velocity vector at the instrument table's side for two different scenarios in an LAF environment and two scenarios in a PLAF environment, all corresponding to the highest CFU level at the instrument table. As can be seen, the air passes between the two surgical lamps, and eventually sweeps diagonally over the surgical site.

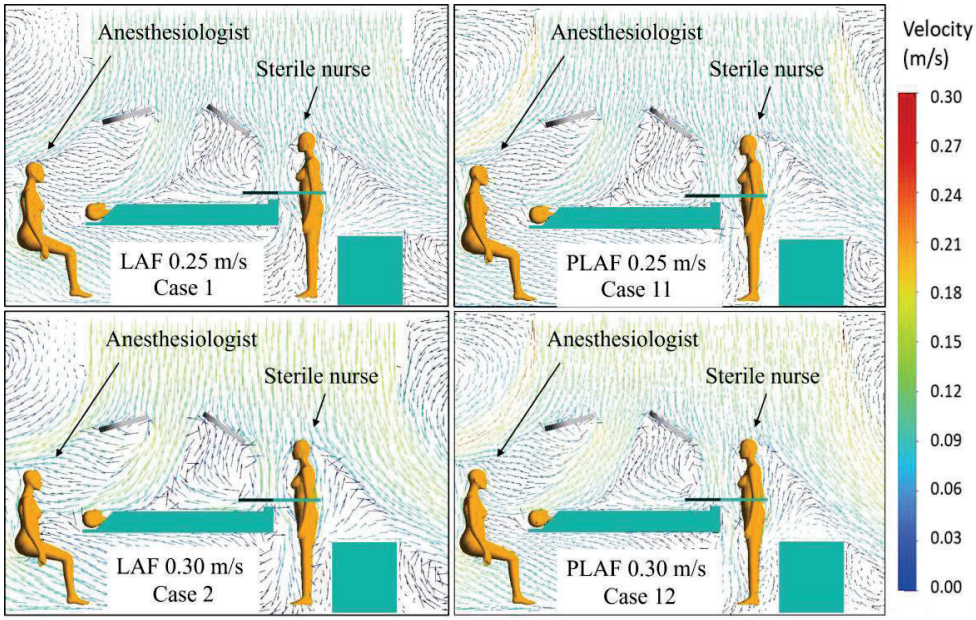

Figure 4.13 CFD velocity vector result for Case 1, Case 2, Case 11 and Case 12 from the side view

The airflow under the surgical lamp is disturbed and no longer unidirectional. The airflow behind the sterile nurse was also turbulent. The thermal plume of the sterile nurse mixed with the outgoing air supply stream is swept through the instrument table. After the air supply speed increases, the airflow falls faster near the instrument table.

Figure 4.14 shows the airflow distribution of the area between the two surgeons. Only the case of LAF Case 1 is shown. Case 7 is the case of PLAF with the lowest CFU level, and Case 11 is the case of PLAF CFU with the highest level of CFU. As can be seen from the figure, the air supply in different situations interacts with the surgeon's thermal plume.

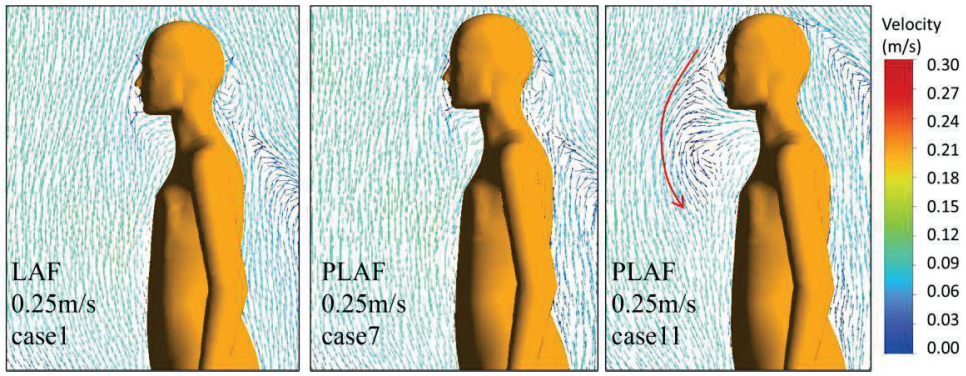

Figure 4.14 CFD velocity vector result in front of the surgeon on the left for Case 1, Case 7 and Case 11

In Case 11, the supply airflow is dominant, and the thermal plumes are almost invisible. Case 1, a thermal plume creates some backflow in the face, creating a partial area of upward airflow in front of the face. This region is the largest in Case 13, and the surgeon's thermal plume affects the downward unidirectional airflow in the LAF region to a certain extent.

4.4.3 Particle track and velocity distribution above the instrument table

The trajectories of 1/30000 of all of the particles, that originated from the sterile nurse in the LAF OR, is shown in Figure 4.15(a-c). Figure 4.15(d) shows the velocity distribution above the instrument table behind the sterile nurse. It can be seen in the Figure 4.15(a) that under Case 1, most of the large-size BCP drops on the ground behind the instrument table. While the large size of the BCP in Case 2 settles on the table. The velocity distribution shows the air velocity starts to decrease at the height of the head of the sterile nurse, because the thermal plume of the sterile nurse weakens the air velocity. The airflow velocity at this height is a major contributor to reducing the BCP produced by sterile nurses on the instrument table. Therefore, the earlier the airflow above the instrument table changes direction, the lower the

CFU level at the instrument table. The lowest velocity appeared at 1.4 m, 1.1 m, and 1.0 m for Case 1, Case 2, and Case 12, respectively. It is worth noting that the air velocity increased near the table. It seems that a higher air velocity may result in a higher CFU level.

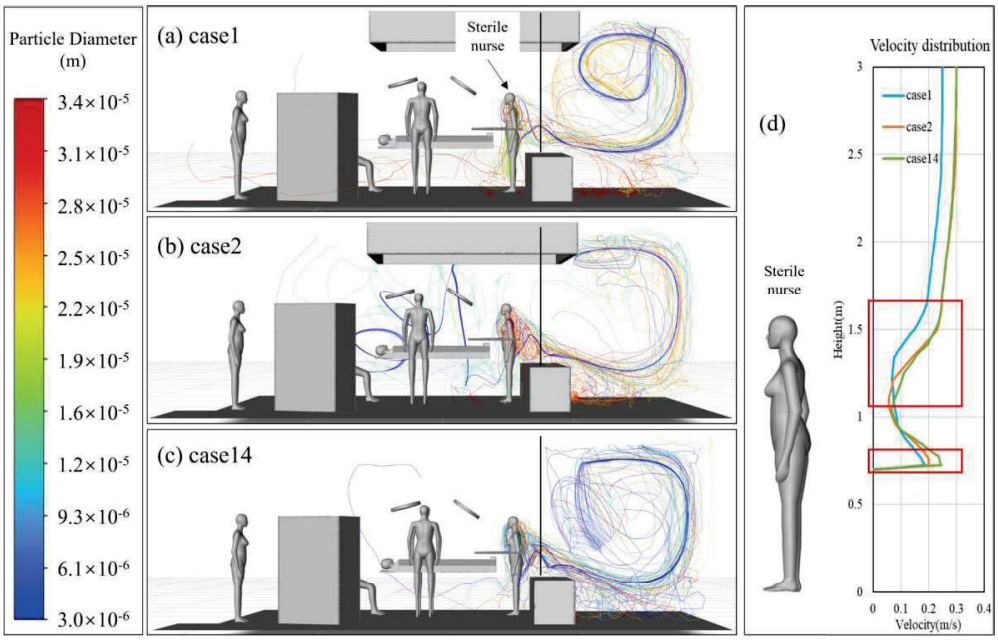

Figure 4.15 CFD particle track result and velocity distribution on the instrument table (a) particle trajectories in Case 1(b) particle trajectories in Case 2 (c) particle trajectories in Case 14 (d) Velocity distribution behind the sterile nurse above instrument tables

The Figure 4.15(d) shows velocity distribution behind the sterile nurse. The results indicate that a higher airflow velocity is not necessarily advantageous for the instrument table regarding CFU level. This is because the instrument table is located at the edge of the LAF zone, where the upper airflow is already disturbed and no longer unidirectional. As the non-unidirectional airflow velocity increases, the thermal plumes from the sterile nurse's activities tend to merge and will alter the overall airflow direction towards the outside of the instrument table area. The lower airflow velocity may allow these plumes to rise higher, leading to their early traveling away from the instrument table rather than directly settling on it.

4.4.4 Energy Consumption

The ventilation system in use at St. Olavs Hospital is the same as Case 2, so the results of Case 2 are used as a baseline. It is shown that adopting the conditions of Case 7 (slot width: 0.02 m; air velocity of plate jet: 1.5 m/s; air velocity of LAF region supply: 0.25 m/s) slightly increases the CFU level in the surgical site by approximately 0.17. However, the CFU level

on the instrument table decreases by more than 200. Moreover, the ventilation rate is reduced by 1076 m^3/h. Simple calculations show that if this amount of ventilation rate reduction is fresh air, the energy consumption related to the fresh air supply will decrease by over 10%, and the fan energy consumption will be reduced by approximately 28%. Overall, under the condition of Case 7, overall energy consumption by at least 10% will be reduced while maintaining a slightly higher CFU level at the surgical wound and a substantially lower CFU level at the instrument table.

Chapter 5: Conclusion and outlook

This chapter concludes the main findings of the thesis in Section 5.1, and limitations and recommendations for future studies in Section 5.2.

5.1 Main conclusion and contributions

The main aim of this doctoral work is to investigate how ventilation techniques can be used to create a safe and effective surgical microenvironment in the operating room. The following studies has been performed: conduct tracer gas experiments and a corresponding CFD study to investigate the exposure level of the surgical team to airborne microbes in the NPOR; perform mockup surgeries with animal and simulated human patient in the real TMV OR to investigate the influence of ambient temperature on the CFU level within the surgical microenvironment; developing a core temperature prediction model to calculate patient body temperature; and performing a series of CFD simulations to characterize different ventilation parameters of the PLAF. The main conclusions in the thesis are presented below,

- In NPOR, the exposure level to airborne microbes for assistant surgeons can be significantly higher, up to 12 times, compared to other surgical team members outside the sterile area. This discrepancy arises because assistant surgeons and anesthesiologists are expected to be in closer proximity to the contamination source (the patient) compared to other members of the surgical team who are positioned farther away.
- Increasing the pressure difference between the OR and the external environment effectively reduces the exposure levels of the surgical team, especially for surgeons near the patient, in the NPOR. However, for team members positioned farther from the contamination source, such as the distribution nurse and anesthesiologist, the impact of pressure difference on their exposure levels is relatively minimal. This is because the air in their vicinity has already thoroughly mixed with contaminants.
- The core temperature prediction model can precisely predict the heat transfer processes of the human body including heat generation, heat transfer and heat exchange with the surrounding indoor environment.
- By incorporating the principles of numerical heat transfer and integrating equivalent heat transfer and indirect calorimetry methods, the model demonstrates enhanced accuracy in predicting temporal changes in a patient's core temperature over the course of one hour. The prediction error within this one-hour timeframe is less than 0.2 °C.

- In ORs with TMV, the CFU level at the surgical site is lower when the room air temperature is higher. This can be explained by the fact that BCP are primarily influenced by the intensity of the contamination source release, rather than the thermal plume intensity above the patient's incision.
- In general, this thesis did not find a significant correlation between the level of colony-forming units (CFU) at the surgical site and particulate matter concentration. This lack of correlation can be attributed to the distinct particle size range of released particles and bacteria-carrying particles (BCP). Particulate matter originates from various sources such as clothing friction, skin flaking, and ventilation, while BCP solely arises from the shedding of skin scales.
- The surgeon's activity increases the concentration of particulate matter at the surgical site by 1 to 9 times compared to situations with no surgeon activities. This is attributed to the increased shedding of skin scales resulting from the surgeon's movements or spontaneous activities.
- The CFU level increased 10 minutes after the start of surgeon activities instead of immediately because the contamination from the body of the surgical teams is at some distance from the surgical site, and it takes time for the BCP to arrive.
- The performance of the PLAF system with a surrounding downward plane jet is superior to that of the Laminar Airflow (LAF) system in terms of controlling the CFU level in the surgical microenvironment. This is because the vertical downward air curtain impedes the diffusion of the LAF stream, thereby enhancing the effectiveness of unidirectional flow in sweeping away bacteria-carrying particles (BCP).
- Changing the direction of the surrounding downward plane jet does not contribute to the improvement of the Perioperative Laminar Airflow (PLAF) system's performance. This is because inward jet flow affects the mainstream flow, while outward jet flow increases the diffusion of Laminar Airflow (LAF) in the region, leading to a reduction in flow velocity reaching the surgeon and the incision site.
- Using PLAF has theoretical potential for energy saving at least 10%. Thus, PLAF can be considered as a candidate of future ventilation solutions for ORs.

5.2 Practical limitations and future work

Because the tracer gas sampling instrument took samples at intervals of six minutes, it is impossible to capture concentration fluctuations over shorter periods. In addition, the temperature of the inner walls inevitably increases 1-2 °C with the experiments, and such

subtle changes may have different degrees of influence on the simulation results. Moreover, there is much surgical equipment in the OR, so the airflow distribution will be significantly affected. The formation of the thermal plume in this complex surgical microenvironment therefore needs further research. Research on human thermal plumes in the surgical microenvironment may face several challenges: the influence of ventilation airflow [170], the modeling of thermal plumes [171], human body movement [172], and the effect of environmental temperature [82]. These studies also suggest that the human thermal plume is sensitive to environmental parameters. Therefore, the formation of the thermal plume in a more complex environment needs more in-depth research through CFD studies, experimental or theoretical studies.

For the patient core temperature prediction model, future research should determine the effect of different anesthetics on body temperature regulation, identify appropriate procedures for different surgical sites and wound sizes, and investigate temperature changes because of different heating methods. Additionally, it is crucial to consider the variations in vasoconstriction levels across different body regions when regulating body temperature. Infants have a higher surface area-to-volume ratio compared to adults, while the thermoregulation mechanisms in elderly individuals are less effective. These factors necessitate careful consideration in future research. In this thesis, a limited number of patients were involved. Having data from more people helps to understand more of the factors that influence the model and improve it.

In a real OR with operational conditions, it is extremely difficult to control various sources of the BCP, which may result in a certain degree of uncertainty of the data analysis. Future work could focus on more laboratory studies to explain the rate of BCP release from humans.

This thesis has compared a set of parameters and demonstrated the feasibility of the new PLAF ventilation solutions, but there are also many other solutions and procedures for future research. Firstly, the exploration of ventilation parameters in this study was limited to a specific range (downward plate jet supply velocity ranges from 1.5 m/s to 2.0 m/s; the LAF region supply air velocity range from 0.25 m/s to 0.30 m/s). Further investigations should optimize these parameters comprehensively. Optimizing the ventilation parameters, such as flow rates, temperature differences, and airflow distribution, is essential to achieve the highest level of performance and energy efficiency. Moreover, it is crucial to address the system's stability as a part of future work. Understanding the system's robustness in real-

operation scenarios and its ability to adapt to varying conditions will be essential for its practical implementation. Furthermore, future research should also study the integration of advanced control algorithms and sensor technologies to enhance autonomous operation and adaptability. This would enable the ventilation system to respond dynamically to changing environmental conditions and occupancy patterns and improving indoor air quality and energy efficiency. In summary, while this thesis provides a foundational understanding of a novel ventilation solution, future investigations should focus on optimizing ventilation parameters, assessing system stability under realistic conditions, and explore advanced control strategies to realize the full potential of this innovative approach.

BIBLIOGRAPHY

[1] Weiser TG, Regenbogen SE, Thompson KD, Haynes AB, Lipsitz SR, Berry WR, et al. An estimation of the global volume of surgery: a modelling strategy based on available data. The Lancet. 2008;372:139-44.
[2] Weiser TG, Haynes AB, Molina G, Lipsitz SR, Esquivel MM, Uribe-Leitz T, et al. Estimate of the global volume of surgery in 2012: an assessment supporting improved health outcomes. The Lancet. 2015;385:S11.
[3] Rose J, Weiser TG, Hider P, Wilson L, Gruen RL, Bickler SW. Estimated need for surgery worldwide based on prevalence of diseases: a modelling strategy for the WHO Global Health Estimate. The Lancet Global Health. 2015;3:S13-S20.
[4] Holmer H, Bekele A, Hagander L, Harrison EM, Kamali P, Ng-Kamstra JS, et al. Evaluating the collection, comparability and findings of six global surgery indicators. British Journal of Surgery. 2019;106:e138-e50.
[5] Meara JG, Leather AJM, Hagander L, Alkire BC, Alonso N, Ameh EA, et al. Global Surgery 2030: evidence and solutions for achieving health, welfare, and economic development. The Lancet. 2015;386:569-624.
[6] Organizations WH. Global guidelines for the prevention of surgical site infection, 2nd ed. 2018.
[7] Yi J, Xiang Z, Deng X, Fan T, Fu R, Geng W, et al. Incidence of Inadvertent Intraoperative Hypothermia and Its Risk Factors in Patients Undergoing General Anesthesia in Beijing: A Prospective Regional Survey. PLoS One. 2015;10:e0136136.
[8] Burns SM, Piotrowski K, Caraffa G, Wojnakowski M. Incidence of Postoperative Hypothermia and the Relationship to Clinical Variables. Journal of PeriAnesthesia Nursing. 2010;25:286-9.
[9] Long KC, Tanner EJ, Frey M, Leitao MM, Levine DA, Gardner GJ, et al. Intraoperative hypothermia during primary surgical cytoreduction for advanced ovarian cancer: Risk factors and associations with postoperative morbidity. Gynecologic Oncology. 2013;131:525-30.
[10] Sari S, Aksoy SM, But A. The incidence of inadvertent perioperative hypothermia in patients undergoing general anesthesia and an examination of risk factors. International Journal of Clinical Practice. 2021;75:e14103.
[11] Yi J, Zhan L, Lei Y, Xu S, Si Y, Li S, et al. Establishment and Validation of a Prediction Equation to Estimate Risk of Intraoperative Hypothermia in Patients Receiving General Anesthesia. Scientific reports. 2017;7:13927.
[12] McHugh SM, Hill ADK, Humphreys H. Laminar airflow and the prevention of surgical site infection. More harm than good? The Surgeon. 2015;13:52-8.
[13] Evans RP. Current Concepts for Clean Air and Total Joint Arthroplasty: Laminar Airflow and Ultraviolet Radiation: A Systematic Review. Clinical Orthopaedics and Related Research®. 2011;469:945-53.
[14] Cacciari P, Giannoni R, Marcelli E, Cercenelli L. [Cost evaluation of a ventilation system for operating theatre: an ultraclean design versus a conventional one]. Annali di igiene : medicina preventiva e di comunita. 2004;16:803-9.
[15] Bi Y, Heggebø FJ, Harsem TT, Mathisen HM, Aganovic A, Cao G. Experimental Study on the Surgical Microenvironment in an Operating Room with Mixing Ventilation under Positive and Negative Pressure. Healthy Buildings 2021–Europe Proceedings of the 17th International Healthy Buildings Conference 21-23 June 2021: SINTEF Academic Press; 2021.
[16] Roy CJ, Milton DK. Airborne transmission of communicable infection-the elusive pathway. New England Journal of Medicine. 2004;350:1710-2.
[17] Milton D. What was the primary mode of smallpox transmission? Implications for biodefense. Frontiers in Cellular and Infection Microbiology. 2012;2.

[18] Jiang Y, Wang H, Chen Y, He J, Chen L, Liu Y, et al. Clinical Data on Hospital Environmental Hygiene Monitoring and Medical Staff Protection during the Coronavirus Disease 2019 Outbreak. medRxiv. 2020:2020.02.25.20028043.
[19] Liu Y, Ning Z, Chen Y, Guo M, Liu Y, Gali NK, et al. Aerodynamic Characteristics and RNA Concentration of SARS-CoV-2 Aerosol in Wuhan Hospitals during COVID-19 Outbreak. BioRxiv. 2020:2020.03.08.982637.
[20] Tellier R. Review of aerosol transmission of influenza A virus. Emerg Infect Dis. 2006;12:1657-62.
[21] Jurelionis A, Gagytė L, Prasauskas T, Čiužas D, Krugly E, Šeduikytė L, et al. The impact of the air distribution method in ventilated rooms on the aerosol particle dispersion and removal: The experimental approach. Energy and Buildings. 2015;86:305-13.
[22] Jiang N, Yao S-y, Feng L-y, Sun H-j, Liu J-j. Experimental study on flow behavior of breathing activity produced by a thermal manikin. Building and Environment. 2017;123:200-10.
[23] Lai MYY, Cheng PKC, Lim WWL. Survival of Severe Acute Respiratory Syndrome Coronavirus. Clinical Infectious Diseases. 2005;41:e67-e71.
[24] Koullapis PG, Kassinos SC, Bivolarova MP, Melikov AK. Particle deposition in a realistic geometry of the human conducting airways: Effects of inlet velocity profile, inhalation flowrate and electrostatic charge. Journal of Biomechanics. 2016;49:2201-12.
[25] Hesaraki A, Myhren JA, Holmberg S. Influence of different ventilation levels on indoor air quality and energy savings: A case study of a single-family house. Sustainable Cities and Society. 2015;19:165-72.
[26] Al Maskari Z, Al Blushi A, Khamis F, Al Tai A, Al Salmi I, Al Harthi H, et al. Characteristics of healthcare workers infected with COVID-19: A cross-sectional observational study. International Journal of Infectious Diseases. 2021;102:32-6.
[27] Zheng L, Wang X, Zhou C, Liu Q, Li S, Sun Q, et al. Analysis of the Infection Status of Healthcare Workers in Wuhan During the COVID-19 Outbreak: A Cross-sectional Study. Clinical Infectious Diseases. 2020;71:2109-13.
[28] Wong J, Goh QY, Tan Z, Lie SA, Tay YC, Ng SY, et al. Preparing for a COVID-19 pandemic: a review of operating room outbreak response measures in a large tertiary hospital in Singapore. Canadian Journal of Anesthesia/Journal canadien d'anesthésie. 2020;67:732-45.
[29] Sikkema RS, Pas SD, Nieuwenhuijse DF, O'Toole Á, Verweij J, van der Linden A, et al. COVID-19 in health-care workers in three hospitals in the south of the Netherlands: a cross-sectional study. The Lancet Infectious Diseases. 2020;20:1273-80.
[30] Cheng H, Clymer JW, Po-Han Chen B, Sadeghirad B, Ferko NC, Cameron CG, et al. Prolonged operative duration is associated with complications: a systematic review and meta-analysis. Journal of Surgical Research. 2018;229:134-44.
[31] Ti LK, Ang LS, Foong TW, Ng BSW. What we do when a COVID-19 patient needs an operation: operating room preparation and guidance. Canadian Journal of Anesthesia/Journal canadien d'anesthésie. 2020;67:756-8.
[32] Forrester JD, Nassar AK, Maggio PM, Hawn MT. Precautions for Operating Room Team Members During the COVID-19 Pandemic. Journal of the American College of Surgeons. 2020;230:1098-101.
[33] Awad ME, Rumley JCL, Vazquez JA, Devine JG. Perioperative Considerations in Urgent Surgical Care of Suspected and Confirmed COVID-19 Orthopaedic Patients: Operating Room Protocols and Recommendations in the Current COVID-19 Pandemic. JAAOS - Journal of the American Academy of Orthopaedic Surgeons. 2020;28.
[34] Leyva Moraga FA, Leyva Moraga E, Leyva Moraga F, Juanz González A, Ibarra Celaya JM, Ocejo Gallegos JA, et al. Aerosol box, An Operating Room Security Measure in COVID-19 Pandemic. World journal of surgery. 2020;44:2049-50.
[35] Collaborative WSRI. Surgery during the COVID-19 pandemic: operating room suggestions from an international Delphi process. British Journal of Surgery. 2020;107:1450-8.
[36] Luo Y, Zhong M. [Standardized diagnosis and treatment of colorectal cancer during the outbreak of novel coronavirus pneumonia in Renji hospital]. Zhonghua wei chang wai ke za zhi = Chinese journal of gastrointestinal surgery. 2020;23:E003.

[37] Li Y, Qin JJ, Wang Z, Yu Y, Wen YY, Chen XK, et al. [Surgical treatment for esophageal cancer during the outbreak of COVID-19]. Zhonghua zhong liu za zhi [Chinese journal of oncology]. 2020;42:296-300.
[38] Chen R, Zhang Y, Huang L, Cheng B-h, Xia Z-y, Meng Q-t. Safety and efficacy of different anesthetic regimens for parturients with COVID-19 undergoing Cesarean delivery: a case series of 17 patients. Canadian Journal of Anesthesia/Journal canadien d'anesthésie. 2020;67:655-63.
[39] Arora V, Evans C, Langdale L, Lee A. You Need a Plan: A Stepwise Protocol for Operating Room Preparedness During an Infectious Pandemic. Federal practitioner : for the health care professionals of the VA, DoD, and PHS. 2020;37:212-8.
[40] Al-Benna S. Negative pressure rooms and COVID-19. Journal of Perioperative Practice. 2020;31:18-23.
[41] Chow T, Kwan A, Lin Z, Bai W. Conversion of operating theatre from positive to negative pressure environment. Journal of Hospital Infection. 2006;64:371-8.
[42] Chow T-t, Kwan A, Lin Z, Bai W. A computer evaluation of ventilation performance in a negative-pressure operating theater. Anesthesia & Analgesia. 2006;103:913-8.
[43] China MoHaU-RDotPsRo. Architectural technical code for hospital clean operating department. 2013.
[44] National Health Service U. Health Technical Memorandum 03-01 Specialised ventilation for healthcare premises
Part A: The concept, design, specification, installation and acceptance testing of healthcare ventilation systems. 2021. p. 64.
[45] Prevention CfDCa. Guidelines for Preventing the Transmission of Mycobacterium tuberculosis in Health-Care Settings, 2005. 2005. p. 64.
[46] Canada PHAo. Canadian Tuberculosis Standards 7th Edition. Chapter 15: Prevention and Control of Tuberculosis Transmission in Health Care and Other Settings. p. 23.
[47] Barranco R, Ventura F. Covid-19 and infection in health-care workers: An emerging problem. Medico-Legal Journal. 2020;88:65-6.
[48] Yánez Benítez C, Güemes A, Aranda J, Ribeiro M, Ottolino P, Di Saverio S, et al. Impact of Personal Protective Equipment on Surgical Performance During the COVID-19 Pandemic. World Journal of Surgery. 2020;44:2842-7.
[49] Lee HP, Wang DY. Objective Assessment of Increase in Breathing Resistance of N95 Respirators on Human Subjects. The Annals of Occupational Hygiene. 2011;55:917-21.
[50] Visentin LM, Bondy SJ, Schwartz B, Morrison LJ. Use of personal protective equipment during infectious disease outbreak and nonoutbreak conditions: a survey of emergency medical technicians. Canadian Journal of Emergency Medicine. 2009;11:44-56.
[51] Castle N, Owen R, Hann M, Clark S, Reeves D, Gurney I. Impact of Chemical, Biological, Radiation, and Nuclear Personal Protective Equipment on the performance of low- and high-dexterity airway and vascular access skills. Resuscitation. 2009;80:1290-5.
[52] Loth AG, Guderian DB, Haake B, Zacharowski K, Stöver T, Leinung M. Aerosol exposure during surgical tracheotomy in SARS-CoV-2 positive patients. Shock. 2021;55:472-8.
[53] Murr A, Lenze NR, Brown WC, Gelpi MW, Ebert CS, Senior BA, et al. Quantification of Aerosol Particle Concentrations During Endoscopic Sinonasal Surgery in the Operating Room. American Journal of Rhinology & Allergy. 2020;35:426-31.
[54] Tsui BCH, Pan S. Are aerosol-generating procedures safer in an airborne infection isolation room or operating room? British Journal of Anaesthesia. 2020;125:e485-e7.
[55] Garbey M, Joerger G, Furr S. A Systems Approach to Assess Transport and Diffusion of Hazardous Airborne Particles in a Large Surgical Suite: Potential Impacts on Viral Airborne Transmission. International Journal of Environmental Research and Public Health. 2020;17:5404.
[56] Wilson J. Surgical site infection: the principles and practice of surveillance. Part 1: Key concepts in the methodology of SSI surveillance. Journal of Infection Prevention. 2013;14:6-12.
[57] Barie PS, Eachempati SR. Surgical Site Infections. Surgical Clinics. 2005;85:1115-35.
[58] Cao G, Storås MC, Aganovic A, Stenstad L-I, Skogås JG. Do surgeons and surgical facilities disturb the clean air distribution close to a surgical patient in an orthopedic operating room with laminar airflow? American journal of infection control. 2018;46:1115-22.
[59] Friberg B. Ultraclean laminar airflow ORs. AORN journal. 1998;67:841-51.

[60] Mangram AJ, Horan TC, Pearson ML, Silver LC, Jarvis WR, Committee HICPA. Guideline for prevention of surgical site infection, 1999. American journal of infection control. 1999;27:97-134.
[61] Singh R, Singla P, Chaudhary U. Surgical site infections: classification, risk factors, pathogenesis and preventive management. Int J Pharm Res Health Sci. 2014;2:203-14.
[62] Salkind AR, Rao KC. Antiobiotic prophylaxis to prevent surgical site infections. American family physician. 2011;83:585-90.
[63] Mawalla B, Mshana SE, Chalya PL, Imirzalioglu C, Mahalu W. Predictors of surgical site infections among patients undergoing major surgery at Bugando Medical Centre in Northwestern Tanzania. BMC surgery. 2011;11:1-7.
[64] Suetens C, Hopkins S, Kolman J, Hogberg L. European Centre for Disease Prevention and Control: point prevalence survey of healthcare-associated infections and antimicrobial use in European acute care hospitals. Stockholm: European Centre for Disease Prevention and Control. 2013.
[65] Chinn RY, Sehulster L. Guidelines for environmental infection control in health-care facilities; recommendations of CDC and Healthcare Infection Control Practices Advisory Committee (HICPAC). 2003.
[66] Society JTCotBT. Control and prevention of tuberculosis in the United Kingdom: code of practice 2000. Thorax. 2000;55:887-901.
[67] Hoffman PN, Williams J, Stacey A, Bennett AM, Ridgway GL, Dobson C, et al. Microbiological commissioning and monitoring of operating theatre suites. Journal of Hospital Infection. 2002;52:1-28.
[68] Cao G, Pedersen C, Zhang Y, Drangsholt F, Radtke A, Langvatn H, et al. Can clothing systems and human activity in operating rooms with mixed flow ventilation systems help achieve the ultraclean air requirement (≤10 CFU/m3) during orthopaedic surgeries? Journal of Hospital Infection. 2022;120:110-6.
[69] Aganovic A, Cao G, Stenstad L-I, Skogås JG, MATHISEN HM. Experimental study of the effect of operation lamps on downward airflow distribution in an operating theatre in St. Olavs Hospital in Norway. Healthy Buildings 2017 Europe. 2017.
[70] Cao G, Nilssen AM, Cheng Z, Stenstad L-I, Radtke A, Skogås JG. Laminar airflow and mixing ventilation: Which is better for operating room airflow distribution near an orthopedic surgical patient? American journal of infection control. 2019;47:737-43.
[71] Cao G, Kvammen I, Hatten TAS, Zhang Y, Stenstad L-I, Kiss G, et al. Experimental measurements of surgical microenvironments in two operating rooms with laminar airflow and mixing ventilation systems. Energy and Built Environment. 2021;2:149-56.
[72] Zhang Y, Cao G, Feng G, Xue K, Pedersen C, Mathisen HM, et al. The impact of air change rate on the air quality of surgical microenvironment in an operating room with mixing ventilation. Journal of Building Engineering. 2020;32:101770.
[73] Aganovic A, Cao G, Fecer T, Ljungqvist B, Lytsy B, Radtke A, et al. Ventilation design conditions associated with airborne bacteria levels within the wound area during surgical procedures: a systematic review. Journal of Hospital Infection. 2021;113:85-95.
[74] Bi Y, Aganovic A, Mathisen HM, Cao G. Experimental study on the exposure level of surgical staff to SARS-CoV-2 in operating rooms with mixing ventilation under negative pressure. Building and Environment. 2022;217:109091.
[75] Cao G, Storås MCA, Aganovic A, Stenstad L-I, Skogås JG. Do surgeons and surgical facilities disturb the clean air distribution close to a surgical patient in an orthopedic operating room with laminar airflow? American journal of infection control. 2018;46:1115-22.
[76] Aganovic A, Cao G, Stenstad L-I, Skogås JG. Impact of surgical lights on the velocity distribution and airborne contamination level in an operating room with laminar airflow system. Building and Environment. 2017;126:42-53.
[77] Duryea EL, Nelson DB, Wyckoff MH, Grant EN, Tao W, Sadana N, et al. The impact of ambient operating room temperature on neonatal and maternal hypothermia and associated morbidities: a randomized controlled trial. American Journal of Obstetrics and Gynecology. 2016;214:505.e1-.e7.
[78] Dunn JC, Kusnezov N, Koehler LR, Orr JD. The Sweaty Surgeon: Raising Ambient Operating Room Temperature Benefits Neither Patient nor Surgeon. JBJS. 2017;99.
[79] Liu Z, Zhang M, Cao G, Tang S, Liu H, Wang L. Influence of air supply velocity and room temperature conditions on bioaerosols distribution in a class I operating room. Building and Environment. 2021;204:108116.

[80] Liu Z, Yin D, Niu Y, Cao G, Liu H, Wang L. Effect of human thermal plume and ventilation interaction on bacteria-carrying particles diffusion in operating room microenvironment. Energy and Buildings. 2022;254:111573.
[81] Bi Y, Heggebø FJ, Harsem TT, Mathisen HM, Aganovic A, Cao G. Experimental Study on the Surgical Microenvironment in an Operating Room with Mixing Ventilation under Positive and Negative Pressure. Healthy Buildings 2021–Europe Proceedings of the 17th International Healthy Buildings Conference 21–23 June 2021: SINTEF Academic Press; 2021.
[82] Feng G, Bi Y, Zhang Y, Cai Y, Huang K. Study on the motion law of aerosols produced by human respiration under the action of thermal plume of different intensities. Sustainable Cities and Society. 2020;54:101935.
[83] Voelker C, Maempel S, Kornadt O. Measuring the human body's microclimate using a thermal manikin. Indoor Air. 2014;24:567-79.
[84] Zhou J, Fang W, Cao Q, Yang L, Chang VW-C, Nazaroff WW. Influence of moisturizer and relative humidity on human emissions of fluorescent biological aerosol particles. Indoor Air. 2017;27:587-98.
[85] Leslie K, Sessler DI, Bjorksten AR, Moayeri A. Mild Hypothermia Alters Propofol Pharmacokinetics and Increases the Duration of Action of Atracurium. Anesthesia & Analgesia. 1995;80.
[86] Mason SE, Kinross JM, Hendricks J, Arulampalam TH. Postoperative hypothermia and surgical site infection following peritoneal insufflation with warm, humidified carbon dioxide during laparoscopic colorectal surgery: a cohort study with cost-effectiveness analysis. Surgical Endoscopy. 2017;31:1923-9.
[87] Reynolds L, Beckmann J, Kurz A. Perioperative complications of hypothermia. Best Practice & Research Clinical Anaesthesiology. 2008;22:645-57.
[88] Choi J-W, Kim D-K, Kim J-K, Lee E-J, Kim J-Y. A retrospective analysis on the relationship between intraoperative hypothermia and postoperative ileus after laparoscopic colorectal surgery. PLoS One. 2018;13:e0190711.
[89] Ruetzler K, Kurz A. Chapter 41 - Consequences of perioperative hypothermia. In: Romanovsky AA, editor. Handbook of Clinical Neurology: Elsevier; 2018. p. 687-97.
[90] Yi J, Lei Y, Xu S, Si Y, Li S, Xia Z, et al. Intraoperative hypothermia and its clinical outcomes in patients undergoing general anesthesia: National study in China. PLoS One. 2017;12:e0177221.
[91] Sessler Daniel I, Todd Michael M. Perioperative Heat Balance. Anesthesiology. 2000;92:578-.
[92] Rincón DA, Valero JF, Eslava-Schmalbach J. Construcción y validación de un modelo predictivo de hipotermia intraoperatoria*. Revista Española de Anestesiología y Reanimación. 2008;55:401-6.
[93] Kim EJ, Yoon H. Preoperative Factors Affecting the Intraoperative Core Body Temperature in Abdominal Surgery Under General Anesthesia: An Observational Cohort. Clinical Nurse Specialist. 2014;28:268-76.
[94] Chalari E, Intas G, Zyga S, Fildissis G, Tolia M, Tsoukalas N, et al. Preoperative factors affecting the intraoperative core body temperature in elective hysterectomy under general anesthesia. CEOG. 2019;46:560-4.
[95] Wallisch C, Zeiner S, Scholten P, Dibiasi C, Kimberger O. Development and internal validation of an algorithm to predict intraoperative risk of inadvertent hypothermia based on preoperative data. Scientific reports. 2021;11:22296.
[96] Stolwijk JA. A mathematical model of physiological temperature regulation in man. NASA; 1971.
[97] Fiala D, Lomas KJ, Stohrer M. A computer model of human thermoregulation for a wide range of environmental conditions: the passive system. Journal of Applied Physiology. 1999.
[98] Romadhon R, Rinata AD, Suprijanto, Bindar Y, Soelami FXN. Development of Thermoregulation Model of Surgical Patient and Heat Exchange with Air Condition in the Operating Room. Procedia Engineering. 2017;170:547-51.
[99] Severens NMW, Lichtenbelt WDvM, Frijns AJH, Steenhoven AAV, Mol BAJMd, Sessler DI. A model to predict patient temperature during cardiac surgery. Physics in Medicine and Biology. 2007;52:5131-45.
[100] Severens NMW. Modelling hypothermia in patients undergoing surgery [Phd Thesis 1 (Research TU/e / Graduation TU/e)]. Eindhoven: Technische Universiteit Eindhoven; 2008.

[101] Tindall MJ, Peletier MA, Severens NMW, Veldman DJ, Mol BAJMd. Understanding post-operative temperature drop in cardiac surgery: a mathematical model. Mathematical Medicine and Biology: A Journal of the IMA. 2008;25:323-35.
[102] Duh M, Skok K, Perc M, Markota A, Gosak M. Computational modeling of targeted temperature management in post-cardiac arrest patients. Biomechanics and Modeling in Mechanobiology. 2022.
[103] Bräuer A, Gassner S, Koch J, Heise D, Quintel M. Retrospective Validation of New Simulation Software to Prevent Perioperative Hypothermia in Major Urologic Abdominal Surgery. ISRN Anesthesiology. 2011;2011:620905.
[104] Dai R, Liu S, Li Q, Wu H, Wu L, Ji C. A systematic review and meta-analysis of indoor bioaerosols in hospitals: The influence of heating, ventilation, and air conditioning. PLoS One. 2021;16:e0259996.
[105] Salvati EA, Robinson RP, Zeno SM, Koslin BL, Brause BD, Wilson PD, Jr. Infection rates after 3175 total hip and total knee replacements performed with and without a horizontal unidirectional filtered air-flow system. JBJS. 1982;64.
[106] Yang B, Melikov AK, Kabanshi A, Zhang C, Bauman FS, Cao G, et al. A review of advanced air distribution methods - theory, practice, limitations and solutions. Energy and Buildings. 2019;202:109359.
[107] Xue K, Cao GY, Liu M, Zhang YX, Pedersen C, Mathisen HM, et al. Experimental study on the effect of exhaust airflows on the surgical environment in an operating room with mixing ventilation. Journal of Building Engineering. 2020;32:101837.
[108] Air treatment in health care facilities - Requirements for design and construction of facilities. 2022.
[109] G. Management Specification of Air Cleaning Technique in Hospitals 2013.
[110] Kovalenko M. Comparative analysis of European and Russian standards for ventilation of operating rooms in hospitals. 2013.
[111] DIN. Ventilation and air conditioning - Part 4: Ventilation in buildings and rooms of health care. 2018.
[112] 森本 正, 湯 懷, 滝沢 英, 田辺 新, 堤 仁, 堀 賢. D-37 医療・福祉施設における感染制御に関する研究 : (第 11 報) 多床室の病原体濃度低減の検討. 空気調和・衛生工学会大会　学術講演論文集. 2012;2012.2:1455-8.
[113] Agency NHC. Commissioning and Testing of Operating Theatre & Isolation Room in Norway. 2014.
[114] Purity of air in medical institutions. General requirements. 2006.
[115] Nastase I, Croitoru C, Vartires A, Tataranu L. Indoor Environmental Quality in Operating Rooms: An European Standards Review with Regard to Romanian Guidelines. Energy Procedia. 2016;85:375-82.
[116] Mikrobiologisk renhet i operationsrum - Förebyggande av luftburen smitta - Vägledning och grundläggande krav. 2015.
[117] Health Do. Heating and Ventilation System -specialized Ventilation for Healthcare Premises. 2007.
[118] American National Standards Institute. American Society of Heating R, Engineers AC. ANSI/ASHRAE Standard 170–2017: Ventilation of Health Care Facilities. 2017.
[119] Sadeghian P, Wang C, Duwig C, Sadrizadeh S. Impact of surgical lamp design on the risk of surgical site infections in operating rooms with mixing and unidirectional airflow ventilation: A numerical study. Journal of Building Engineering. 2020;31:101423.
[120] Ouyang X, Wang Q, Li X, Zhang T, Rastogi S. Laminar airflow ventilation systems in orthopaedic operating room do not prevent surgical site infections: a systematic review and meta-analysis. Journal of Orthopaedic Surgery and Research. 2023;18:572.
[121] Alsved M, Civilis A, Ekolind P, Tammelin A, Andersson AE, Jakobsson J, et al. Temperature-controlled airflow ventilation in operating rooms compared with laminar airflow and turbulent mixed airflow. Journal of Hospital Infection. 2018;98:181-90.

[122] Wang C, Holmberg S, Sadrizadeh S. Numerical study of temperature-controlled airflow in comparison with turbulent mixing and laminar airflow for operating room ventilation. Building and Environment. 2018;144:45-56.
[123] Sadrizadeh S, Ekolind P. A new principle of ventilation system for operating rooms: Temperature-Controlled Air Flow. CLIMA 20162016.
[124] Liu Z, Liu H, Yin H, Rong R, Cao G, Deng Q. Prevention of surgical site infection under different ventilation systems in operating room environment. Frontiers of Environmental Science & Engineering. 2020;15:36.
[125] Bulitta C, Vasiuk S, Vasylchyshyn Y, Vasyuk V, Guttenberger R, Buhl S. Clinical validation and efficacy of a temperature-controlled ventilation system (TcAF) in the OR to reduce surgical site infections. Current Directions in Biomedical Engineering. 2020;6:301-3.
[126] Li Y, Nielsen PV, Sandberg M. Displacement ventilation in hospital environments. Ashrae Journal. 2011;53:86-9.
[127] Gao N, He Q, Niu J. Numerical study of the lock-up phenomenon of human exhaled droplets under a displacement ventilated room. Building Simulation. 2012;5:51-60.
[128] Erichsen Andersson A, Petzold M, Bergh I, Karlsson J, Eriksson BI, Nilsson K. Comparison between mixed and laminar airflow systems in operating rooms and the influence of human factors: Experiences from a Swedish orthopedic center. American journal of infection control. 2014;42:665-9.
[129] Bivolarova M, Ondráček J, Melikov A, Ždímal V. A comparison between tracer gas and aerosol particles distribution indoors: The impact of ventilation rate, interaction of airflows, and presence of objects. Indoor Air. 2017;27:1201-12.
[130] Laporthe S, Virgone J, Castanet S. A comparative study of two tracer gases: SF6 and N2O. Building and Environment. 2001;36:313-20.
[131] Englehardt RK, Nowak BM, Seger MV, Duperier FD. Contamination resulting from aerosolized fluid during laparoscopic surgery. JSLS : Journal of the Society of Laparoendoscopic Surgeons. 2014;18:e2014.00361.
[132] ANSI/ASHRAE. Standard-170 (2017). Ventilation of Healthcare Facilities. ANSI/ASHRAE Atlanta, GA; 2017.
[133] Control CfD, Prevention. Guidelines for environmental infection control in health-care facilities. Centers for Disease Control and Prevention (US): Centers for Disease Control and Prevention (US); 2017.
[134] Health Do. Health technical memorandum HTM 03-01: Specialised ventilation for healthcare premises, Part A: Design and validation. 2007.
[135] Mundt E, Mathisen HM, Nielsen PV, Moser A. Ventilation effectiveness: Rehva; 2004.
[136] Novoselac A, Srebric J. Comparison of air exchange efficiency and contaminant removal effectiveness as IAQ indices. Transactions-American Society of Heating Refrigerating and Air Conditioning Engineers. 2003;109:339-49.
[137] Bushby K, Cole T, Matthews J, Goodship J. Centiles for adult head circumference. Archives of disease in childhood. 1992;67:1286-7.
[138] Henneberg M, Ulijaszek SJ. Body frame dimensions are related to obesity and fatness: Lean trunk size, skinfolds, and body mass index. American Journal of Human Biology. 2010;22:83-91.
[139] Tao W. Numerical heat transfer. 2001.
[140] McLean J, Tobin G. Animal and human calorimetry: Cambridge University Press; 2007.
[141] Qingqing W, Jianhua L, Liang Z, Jiawen Z, Linlin J. Effect of temperature and clothing thermal resistance on human sweat at low activity levels. Building and Environment. 2020;183:107117.
[142] Sadrizadeh S, Afshari A, Karimipanah T, Håkansson U, Nielsen PV. Numerical simulation of the impact of surgeon posture on airborne particle distribution in a turbulent mixing operating theatre. Building and Environment. 2016;110:140-7.
[143] Srebric J, Vukovic V, He G, Yang X. CFD boundary conditions for contaminant dispersion, heat transfer and airflow simulations around human occupants in indoor environments. Building and Environment. 2008;43:294-303.
[144] Darwish M, Moukalled F. The finite volume method in computational fluid dynamics: an advanced introduction with OpenFOAM® and Matlab®: Springer; 2016.

[145] Chow TT, Lin Z, Bai W. The Integrated Effect of Medical Lamp Position and Diffuser Discharge Velocity on Ultra-clean Ventilation Performance in an Operating Theatre. Indoor and Built Environment. 2006;15:315-31.
[146] Zhao B, Zhang Y, Li X, Yang X, Huang D. Comparison of indoor aerosol particle concentration and deposition in different ventilated rooms by numerical method. Building and Environment. 2004;39:1-8.
[147] Hinds WC, Zhu Y. Aerosol technology: properties, behavior, and measurement of airborne particles: John Wiley & Sons; 2022.
[148] Matida EA, Nishino K, Torii K. Statistical simulation of particle deposition on the wall from turbulent dispersed pipe flow. International Journal of Heat and Fluid Flow. 2000;21:389-402.
[149] Lai ACK, Chen FZ. Comparison of a new Eulerian model with a modified Lagrangian approach for particle distribution and deposition indoors. Atmospheric Environment. 2007;41:5249-56.
[150] Sadrizadeh S, Tammelin A, Ekolind P, Holmberg S. Influence of staff number and internal constellation on surgical site infection in an operating room. Particuology. 2014;13:42-51.
[151] Noakes C, Fletcher L, Sleigh P, Booth W, Beato-Arribas B, Tomlinson N. Comparison of tracer techniques for evaluating the behaviour of bioaerosols in hospital isolation rooms. Proceedings of healthy buildings: Syracuse USA; 2009. p. 13-7.
[152] Zhang Z, Chen X, Mazumdar S, Zhang T, Chen Q. Experimental and numerical investigation of airflow and contaminant transport in an airliner cabin mockup. Building and Environment. 2009;44:85-94.
[153] Georgopoulos PG, Seinfeld JH. Statistical Distributions of Air Pollutant Concentrations. Environmental Science & Technology. 1982;16:A401-&.
[154] Ott WR. Environmental statistics and data analysis: Routledge; 2018.
[155] Ott WR. A physical explanation of the lognormality of pollutant concentrations. J Air Waste Manage Assoc. 1990;40:1378-83.
[156] Kellogg Jr DL. In vivo mechanisms of cutaneous vasodilation and vasoconstriction in humans during thermoregulatory challenges. Journal of Applied Physiology. 2006;100:1709-18.
[157] Memarzadeh F, Manning AP. Comparison of operating room ventilation systems in the protection of the surgical site / Discussion. ASHRAE transactions. 2002;108:3.
[158] Hansen D, Krabs C, Benner D, Brauksiepe A, Popp W. Laminar air flow provides high air quality in the operating field even during real operating conditions, but personal protection seems to be necessary in operations with tissue combustion. International Journal of Hygiene and Environmental Health. 2005;208:455-60.
[159] Dankert J, Zijlstra JB, Lubberding H. A garment for use in the operating theatre: the effect upon bacterial shedding. Journal of Hygiene. 1979;82:7-14.
[160] Milstone LM. Epidermal desquamation. Journal of Dermatological Science. 2004;36:131-40.
[161] Bhangar S, Adams RI, Pasut W, Huffman JA, Arens EA, Taylor JW, et al. Chamber bioaerosol study: human emissions of size-resolved fluorescent biological aerosol particles. Indoor Air. 2016;26:193-206.
[162] Noble WC. Dispersal of skin microorganisms*. British Journal of Dermatology. 1975;93:477-85.
[163] Kim S, Park JW, Yeon Y, Han JY, Kim E. Influence of exposure to summer environments on skin properties. Journal of the European Academy of Dermatology and Venereology. 2019;33:2192-6.
[164] Tham KW, Zuraimi MS. Size relationship between airborne viable bacteria and particles in a controlled indoor environment study. Indoor Air. 2005;15 Suppl 9:48-57.
[165] You R, Cui W, Chen C, Zhao B. Measuring the Short-Term Emission Rates of Particles in the "Personal Cloud" with Different Clothes and Activity Intensities in a Sealed Chamber. Aerosol and Air Quality Research. 2013;13:911-21.
[166] Hambraeus A. Aerobiology in the operating room—a review. Journal of Hospital Infection. 1988;11:68-76.
[167] Taaffe K, Lee B, Ferrand Y, Fredendall L, San D, Salgado C, et al. The Influence of Traffic, Area Location, and Other Factors on Operating Room Microbial Load. Infection Control & Hospital Epidemiology. 2018;39:391-7.

[168] Annaqeeb MK, Zhang Y, Dziedzic JW, Xue K, Pedersen C, Stenstad LI, et al. Influence of surgical team activity on airborne bacterial distribution in the operating room with a mixing ventilation system: a case study at St. Olavs Hospital. Journal of Hospital Infection. 2021;116:91-8.
[169] Liu Z, Liu H, Rong R, Cao G. Effect of a circulating nurse walking on airflow and bacteria-carrying particles in the operating room: An experimental and numerical study. Building and Environment. 2020;186:107315.
[170] Ma JC, Qian H, Nielsen PV, Liu L, Li YG, Zheng XH. What dominates personal exposure? Ambient airflow pattern or local human thermal plume. Building and Environment. 2021;196:107790.
[171] Dokka TH, Tjelflaat PO. A SIMPLIFIED MODEL FOR HUMAN INDUCED CONVECTIVE AIR FLOWS-MODEL PREDICTONS COMPARED TO EXPERIMENTAL DATA. Proceeding of Room Vent 2002 (8th International Conference on Air Distribution in Rooms): Citeseer; 2002.
[172] Tao Y, Inthavong M, Tu JY. A numerical investigation of wind environment around a walking human body. Journal of Wind Engineering and Industrial Aerodynamics. 2017;168:9-19.

Appendix-papers

Article I **Y. Bi,** A. Aganovic, H.M. Mathisen, G. Cao, Experimental study on the exposure level of surgical staff to SARS-CoV-2 in operating rooms with mixing ventilation under negative pressure, Building and Environment 217 (2022) 109091.

Article II Sadeghian, P., **Bi, Y**., Cao, G. et al. Reducing the risk of viral contamination during the coronavirus pandemic by using a protective curtain in the operating room. Patient Saf Surg 16, 26 (2022).

Article III **Yang Bi,** Tomáš Fečer, Hans Martin Mathisen; Liv Inger Stenstad, Jan Gunnar Skogås, Gabriel Kiss, Guangyu Cao. Modeling of body temperature for perioperative patients in the operating room. (Submitted to *Building and Environment)*

Article IV **Yang Bi**, Tomas Facer, Hans Martin Mathisen; Sara Edvardsen, Liv Inger Stenstad, Jan Gunnar Skogås, Guangyu Cao. Influence of the room air temperature on the airborne particles of the surgical microenvironment in an operating room with mixing ventilation (Submitted to *BMC Infectious Diseases*)

Article V **Yang Bi,** Nan Hu, Parastoo Sadeghian, Sasan Sadrizadeh, Marina Asuero Von Munthe Af Morgenstierne, Hans Martin Mathisen, Elyas Larkermani, Laurent Georges1, Guangyu Cao. Numerical study on an improved protective operating room laminar flow ventilation system. (Submitted to *Energy and Buildings*)

Article I **Y. Bi,** A. Aganovic, H.M. Mathisen, G. Cao, Experimental study on the exposure level of surgical staff to SARS-CoV-2 in operating rooms with mixing ventilation under negative pressure, Building and Environment 217 (2022) 109091.

Building and Environment 217 (2022) 109091

Contents lists available at ScienceDirect

Building and Environment

journal homepage: www.elsevier.com/locate/buildenv

Experimental study on the exposure level of surgical staff to SARS-CoV-2 in operating rooms with mixing ventilation under negative pressure

Yang Bi [a,*], Amar Aganovic [b], Hans Martin Mathisen [a], Guangyu Cao [a]

[a] Norwegian University of Science and Technology, Trondheim, Norway
[b] The Arctic University of Norway, Tromsø, Norway

ARTICLE INFO

Keywords:
Ventilation
Airflow distribution
Negative pressure operating room
Airborne transmission
COVID-19
Surgical microenvironment

ABSTRACT

The purpose of this study was to reveal the exposure level of surgical staff to severe acute respiratory syndrome coronavirus 2 (SARS-CoV-2) from the patient's nose and wound during operations on COVID-19 patients. The tracer gas N_2O is used to simulate SARS-CoV-2 from the patient's nose and wound. In this study, concentration levels of tracer gas were measured in the breathing zones of these surgical staff in the operating room under three pressure difference conditions: −5 pa–15 pa and −25 pa compared to the adjunction room. These influencing factors on exposure level are analyzed in terms of ventilation efficiency and the thermal plume distribution characteristics of the patient. The results show that the assistant surgeon faces 4 to 12 times higher levels of exposure to SARS-CoV-2 than other surgical staff. Increasing the pressure difference between the OR lab and adjunction room can reduce the level of exposure for the main surgeon and assistant surgeon. Turning on the cooling fan of the endoscope imager may result in a higher exposure level for the assistant surgeon. Surgical nurses outside of the surgical microenvironment are exposed to similar contaminant concentration levels in the breathing zone as in the exhaust. However, the ventilation efficiency is not constant near the surgical patient or in the rest of the room and will vary with a change in pressure difference. This may suggest that the air may not be fully mixed in the surgical microenvironment.

1. Introduction

Since the outbreak of the coronavirus disease 2019 (COVID-19) pandemic, health care workers in hospitals have been at high risk of being infected by severe acute respiratory syndrome coronavirus 2 (SARS-CoV-2) [1–4]. The operating room (OR) is a setting where both patients and surgical staff may stay for a long time, which increases the infection risk of surgical staff. The average duration of the majority of operation types is beyond 2 h [5]. Therefore, ORs have also received great attention, and researchers have continuously proposed measures to prevent surgical staff from being infected, including the utilization of personal protective equipment (PPE) [6–8], aerosol boxes [9], and stricter infection control methods [8]. In addition, some hospitals shared their experience in the prevention of infection control in ORs [3,10].

Whether airborne transmission is one of the main modes of transmission for SARS-CoV-2 has been intensively debated since the beginning of the pandemic [11–13]. However, with more research conducted, airborne transmission has been widely recognized as one of the main modes of transmission for SARS-CoV-2. For instance, some studies have found viral ribonucleic acid (RNA) in air samples taken from rooms where COVID-19 patients have stayed [14–16]; other studies have found evidence of aerosol transmission by reviewing past outbreak events [17–20]. Ventilation is then considered to be an effective means of avoiding infection to prevent the spread of airborne transmission virus [21].

Based on the consensus that airborne transmission is one of the main modes of transmission of COVID-19, several measures around the operating room to prevent cross-infection are proposed. Many studies have suggested transforming ventilation in ORs from positive to negative pressure to treat COVID-19 patients [3,22–26]. Compared with positive pressure ventilation, the air outside ORs flows into ORs by penetrating through the cracks of doors and windows of the negative pressure operating room (NPOR), which prevents SARS-CoV-2 from spreading out of the OR.

In contrast, the pressure difference of positive pressure ventilation has no significant effect because there is little air penetrating the room to disturb the airflow distribution in a positive pressure room. At present, there is very little experimental research on the exposure risk of airborne

* Corresponding author.
E-mail address: yang.bi@ntnu.no (Y. Bi).

https://doi.org/10.1016/j.buildenv.2022.109091
Received 17 January 2022; Received in revised form 6 March 2022; Accepted 10 April 2022
Available online 21 April 2022

transmission of COVID-19 in NPOR, except in a few studies using simulation [27,28]. Different countries have different recommendations and requirements regarding the value of the pressure difference of NPORs. For example, the technical specification of surgical cleaning units in China clearly states that patients infected with airborne diseases should be operated on in a negative pressure operating room, but the specification does not indicate a specific pressure value [29]. British ventilation guidelines suggest that the pressure in a negative pressure operating room should be at least - 5 Pa [30]. Both Canadian and CDC guidelines suggest a differential pressure of −2.5 Pa in a negative pressure operating room [31,32].

Equipping PPE has been recommended since the COVID-19 pandemic to prevent surgical staff from being infected in the OR by aerosol viruses released by patients [6,33]. PPE, including respirators, can effectively reduce the wearer's exposure to pollutants. In some cases, nurses, who usually stay far from the patient during operations, should also wear PPE during surgery. However, more than half of OR surgical staff reported a decrease in overall comfort with PPE, and more than 80% of respondents reported increased surgical fatigue. In addition, this combination of PPE can lead to increased respiratory work, reduced vision, reduced touch, and heat stress [34–36]. However, the air change rate in the OR is generally higher than 20 air changes per hour (ACH), and surgical staff away from the operating table may not be exposed to high concentrations of contaminants. This makes it difficult for surgical staff to choose protection equipment that may result in different safety and comfort levels. Therefore, revealing the contaminated exposure level of the breathing zone of surgical staff in the OR is an important indicator to help the medical staff determine whether PPE should be worn.

To date, there have been few studies on the exposure levels of surgical staff to SARS-CoV-2 in ORs. Some of these studies statistically analyze the existing infection cases of surgical staff. In addition to some investigation studies, some experimental and simulation studies were also carried out. Loth Andreas G et al. [37], conducted an experimental study of aerosol exposure levels in patients during tracheotomy and found that 4.8 ± 3.4% of aerosols were removed from surgeons in laminar ORs, compared with ten times as much in nonlaminar ORs. Alex Murr et al. [38]. used optical granulometry to measure aerosol concentrations during endoscopic nasal surgery. Aerosol concentrations at the surgeon's position were significantly increased with the republic bit, a miniature defibrillator. Ban C.H. Sui et al. [39] used a nebulizer to simulate aerosol exposure during intubation and compared aerosol concentrations in the operating room and isolation room, and the results showed that aerosol exposure levels in both rooms were similar. Marc Garbey et al. [40] conducted experimental and simulated studies on the diffusion of surgical smoke in the operating room. The results suggest that opening doors during surgery and inefficient actions by medical personnel can increase indoor pollutant concentrations. However, none of the earlier studies have investigated the effect of different negative pressure conditions on the exposure level of surgical staff to SARS-CoV-2 in ORs with mixing ventilation.

The purpose of this study is to quantify the exposure level of different surgical staff to SARS-CoV-2, which is simulated by tracer gas, under different negative pressure conditions in one OR with mixing ventilation. The findings of this study could be used to assess the infectious risk of surgical staff in ORs and help surgical staff select proper personal protection equipment under the COVID-19 pandemic and other scenarios of airborne transmission diseases.

2. Methodology

2.1. Experimental setup and the OR lab

All measurements for this study were performed in the full-scale OR lab (OR lab) in the Department of Energy and Process Engineering, Norwegian University of Science and Technology (NTNU). The dimensions of the OR Lab are 8.73 m × 7.05 m × 3.25 m (length × width × height), and the volume of the OR lab is 200 m^3. The OR lab has a similar layout and design to an actual OR equipped with a mixing ventilation system in St. Olavs Hospital [41]. Fig. 1 shows the layout of the OR lab and medical equipment.

2.1.1. Ventilation system

The OR lab is equipped with a mixing ventilation system with four supply air diffusers (0.55 m × 0.55 m), as shown in Fig. 1(c), four lower-level exhaust outlets (0.175 m × 0.575 m), and four higher-level exhaust outlets (0.55 m × 0.55 m), as shown in Fig. 1(b). Each lower exhaust grill is connected to a 0.6 m × 0.2 m × 0.315 m plenum box, and each upper exhaust is connected to a 0.315 m × 0.4 m plenum box. The plenum box is equipped with a balancing damper and pressure outlets so that the airflow rate can be measured and controlled. The TSI VelociCalc 9565-P (accuracy of ±1 Pa) was used for pressure measurements in the plenum boxes attached to the exhaust grills and air diffusers to calculate airflow rates. Accordingly, the measuring uncertainty with this method is ±5%. The distribution of exhausted air between the higher and lower exhaust grills for each of the vertical exhaust modules is approximately 1/3 and 2/3, respectively.

2.1.2. OR lab facilities and thermal manikins

The OR lab is equipped with several real medical equipment for ORs, including an anesthesia machine (Fig. 1(a)), an ultrasonic imager (Fig. 1(b)), two endoscope imagers (Fig. 1(d)), two surgical lamps, and an operating table. For some of the other medical devices that do not produce heat, we use manufactured models instead, for instance, two medical ceiling pendants, an instrument table, and some storage cabinets.

Six thermal manikins were used to mimic surgical staff in an OR, including one patient, two surgeons, two nurses, and an anesthesiologist. The specific locations of these manikins can be found in Fig. 1. The surface temperature of the anesthesiologist and the patient can be controlled by the temperature control device. The patient's head, arms, and body were set at 33 °C, 30 °C, and 31 °C, respectively. The head, arms, body, and legs of the anesthesiologist were set at 33 °C, 30 °C, 31 °C and 30 °C, respectively. The heat power of all other manikins is constant power whose value is set according to ASHRAE 55–2020 [42], which can be found in Table 1.

2.2. Experiment set up

A study by Bivolarova et al. [43] found a strong linear relation ($r^2 >$ 0.9) between the mean concentrations of microparticles sized 0.7 and 3.5 μm and the tracer gas nitrous oxide (N_2O) in an indoor ventilated environment. The same study also showed that N_2O, 0.7 μm, and 3.5 μm particles follow almost identical patterns with only a 2%–9% difference in the normalized concentrations. Noakes et al. [44] showed good agreement between the behavior of N_2O tracer gas and 3–5 μm particles in a hospital isolation room. Furthermore, tracer gas has been extensively used in health care-specific studies to assess ventilation system efficiency in removing contaminants [45–47]. In this study, N_2O tracer gas was used to simulate coronaviruses released from the breath and wound of a surgical patient. Studies have shown that aerosolized blood droplets may carry airborne viruses during laparoscopic surgery to release intra-abdominal pressure [48]. Surgical lights will be used at this time, so this study will use two surgical lights throughout all measurements. The sources were released from the nose and wound of the patient separately in each case.

The standards of most countries only set a minimum air change frequency, which is between 18 and 22 ACH [49–52]. The influence of ACH change on air distribution in the operating room has also been studied, so a constant air supply volume of 20 ACHs was used in all these cases. Most standards specify the temperature range, from 18°C to 24 °C [49–52]. In this study, the air temperature was 22 ± 1 °C in the OR lab

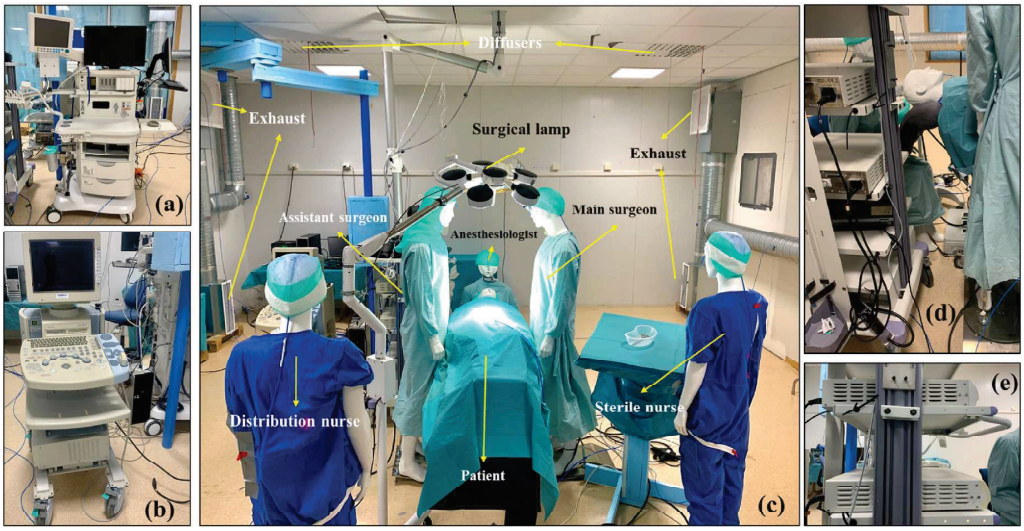

Fig. 1. Medical equipment and layout in the operating room. (a) Anesthesia machine; (b) Ultrasonic imager; (c) the layout of the OR laboratory; (d) Endoscope imager; (e) The cooling fan of the endoscope imager.

Table 1
The heat power of all heat sources in the OR laboratory.

Equipment	Heating power (W)
Surgical lamp 1	61
Surgical lamp 2	74
Supersonic cleaner	45
Endoscope imager	232
Anesthesia machine	136
Main surgeon	150
Assistant surgeon	150
Sterile nurse	140

during measurements. As there is little information on recommended values for negative pressurized ORs, three negative values were used in this study: −5 Pa, −15 Pa, and −25 Pa. The change in pressure difference in the OR lab was achieved by regulating the air extract rate. In total, nine cases were investigated with tracer gas under conditions with or without a ventilation system, different heights of surgical lamps, and different indoor heat intensities. The measurement conditions for each case can be found in Table 2. The air supply volume of all cases is 4000 m^3/h.

2.3. Measurement procedure and instrument

The tracer gas N_2O, which was placed outside of the OR lab, was continually released through a plastic tube (φ33 mm). The flow rate of N_2O is controlled by a gas rotameter connected to the tank. The N_2O flow rate was kept at 0.18 m^3/h (3 L/min) in all cases.

The sampled tracer gas was then sent continuously to a precalibrated Innova 1303 multigas sampler and doser (Brüel & Kjær, Ballerup, Denmark) coupled to an Innova 1302 photoacoustic monitor, which is shown in Fig. 2(a). According to the manufacturer, the repeatability of the Innova 1302 measurements is ±1% under standard conditions. All standard deviations of the measured results performed under conditions without medical equipment were calculated to be under 5% of the mean value. There were six tracer gas measurement points, including exhaust (Point 1), breathing zone of distribution nurse (Point 2), anesthetist (Point 3), sterile nurse (Point 4), main surgeon (Point 5), and assistant surgeon (Point 6).

AirDistSys5000 anemometers were used to measure air temperature and airspeed at 5 × 7 = 35 points in the OR lab, as shown in Fig. 2(b). The lowest measurement points were 10 cm higher than those of the patient. These anemometers measure airspeed and temperature with an accuracy of ±0.02 m/s (accuracy of ±0.2 °C, respectively. The measurement plane is shown in Fig. 2(b). Each measurement lasted for 3 min with a sampling rate of 0.5 Hz and the average values of 90 data were used.

Before each experiment, the OR lab was ventilated for 2 h in advance, the tracer gas was turned on after the indoor temperature was stable and the wall temperature remained unchanged. The sampling time of the Innova 1302 photoacoustic monitor was approximately 60 s/channel, and six channels were measured in sequence, giving 6 min between each measurement at the same location. The total sampling time for one case with two repeated measurements was between 300 and

Table 2
Measurement conditions.

Case	Tracer gas source	Pressure difference	Heat source	Ventilation	Surgical lamp	Air extract rate
1.	Nose	−5 Pa	All on	On	1.95 m	4140 (m^3/h)
2.	Nose	−15 Pa	All on	On	1.95 m	4242 (m^3/h)
3.	Nose	−25 Pa	All on	On	1.95 m	4316 (m^3/h)
4.	Wound	−5 Pa	All on	On	1.95 m	4140 (m^3/h)
5.	Wound	−15 Pa	All on	On	1.95 m	4242 (m^3/h)
6.	Wound	−25 Pa	All on	On	1.95 m	4316 (m^3/h)
7.	Wound	−5 Pa	Endoscope off	On	1.95 m	4140 (m^3/h)
8.	Wound	−5 Pa	All off	On	1.95 m	4140 (m^3/h)
9.	Wound	−5 Pa	All on	On	2.05 m	4140 (m^3/h)

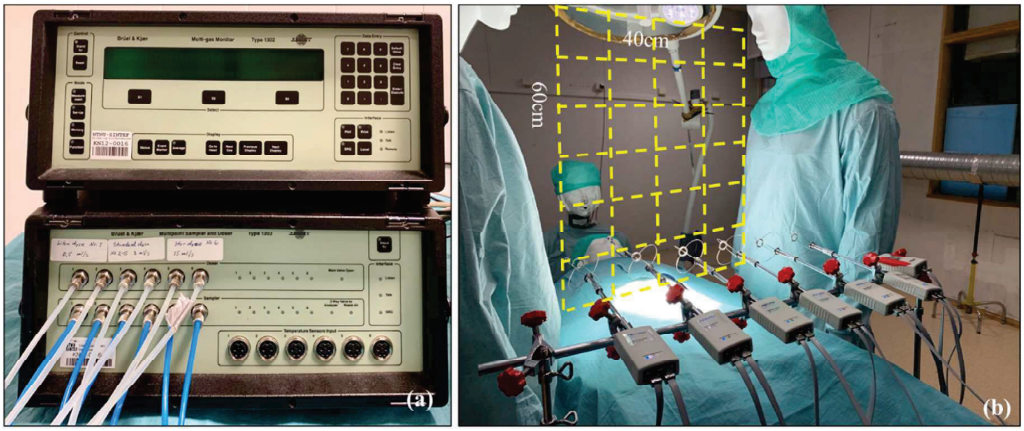

Fig. 2. Experimental equipment and measuring plane. (a) Tracer gas measuring equipment (b) Hot-wire anemometer and the measuring grid.

350 min. The clean-up procedure was performed between two cases to keep the level of N_2O rate below 0.5 ppm, which should be extracted from the measurement value.

2.4. Statistics analysis

Descriptive statistics were used for the analysis of the sampled N_2O levels at six measurement points. Skewness and kurtosis statistics were used to test the assumption of normality for the N_2O levels. Levene's test for equality of variances was used to test the assumption of homogeneity of the variance. Given that the statistical assumptions were met, a 1-way analysis of variance (ANOVA) assessed whether the mean N_2O levels were significantly different between the same measurement points for different cases. If the statistical assumptions were violated, nonparametric Kruskal-Wallis tests were used as an alternative for ANOVA. Kruskal-Wallis tests the stochastic dominance between groups, i.e., whether any randomly measured concentration of N_2O (ppm) from one case is higher or lower than any random concentration from another group. As both ANOVA and Kruskal-Wallis methods do not specify which specific cases were significantly different, significant differences between every two cases for one position were examined using Mann-Whitney U tests in a post hoc fashion. The significance was defined as $p < 0.05$. All analyses were conducted using SPSS version 27. (IBM, Armonk, NY).

2.5. Ventilation effectiveness

Air change efficiency and local air change index category indicators were used to interpret the measured results in this study [53,54]. The air change efficiency, ε, is defined as the ratio between the shortest possible air change time for the air in the room, the nominal time constant, τ_n, and the actual air change time,$\overline{\tau}_e$.

3. Results

3.1. Measurement results of pollutant concentration when tracer gas is released from the nose of a patient (Cases 1–3)

Fig. 3 shows a boxplot of the measured concentration results in Cases 1 to 3 when the tracer gas is released through the patient's nose under three different pressure values. The figure contains information on mean values, medium values, 1.5 interquartile range (IQR), and outliers at different measurement points. Due to the large difference in data at different points, the y axis is displayed as a logarithmic axis. This figure shows that the highest concentration appears at point 6, the breathing zone of the assistant surgeon, which is 333.1 ppm, 284.7 ppm, and 186.0 ppm under three different pressure conditions: −5 Pa, - 15 Pa, and −25 Pa, respectively. This was followed by point 5, at the breathing zone of the main surgeon, whose mean concentration at the breathing zone was 74.3 ppm 48.7 ppm, and 40.0 ppm. The lowest concentration results

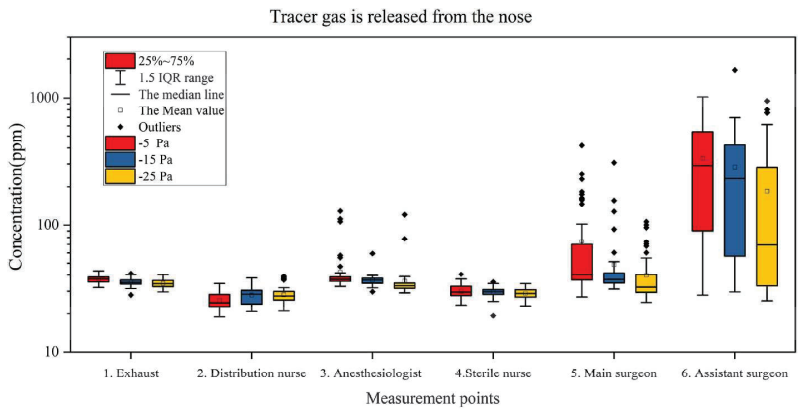

Fig. 3. Boxplot of concentration results when tracer gas is released from patient's nose.

were found at point 2, the breathing zone of the distribution nurse, at 25.5 ppm. 28.0 ppm and 28.1 ppm, which are lower than the exhaust concentration. The concentration at point 3, the breathing zone of the anesthesiologist, was slightly higher than that in the exhaust at between 103% (35.8 ppm) and 114% (42.5 ppm). The concentration results at point 4, the breathing zone of the sterile nurse, showed a value of 29.0 ppm and slightly changed with the change in pressure difference. Considering the effect of pressure change on concentration, except for the distribution nurse, the mean value of concentration at all points decreases with increasing pressure. Despite this, except for two surgeons, the concentrations in the breathing zone of other surgical staff were not significantly different from those of the exhaust. This may indicate that the supply air is fully mixed with room air outside the surgical microenvironment.

3.2. Measurement results of pollutant concentration when tracer gas is released from the surgical wound (Cases 4–6)

Fig. 4 shows the boxplot of concentration results at each point in Case 4-Case 6 as tracer gas is released from the wound of the patient.

The highest mean concentrations were found at point 6, reaching 443.0 ppm, 412.0 ppm, and 446.0 ppm at −5 pa, −15 Pa, and −25 Pa, respectively, all of which were more than 12 times the mean value of the concentration at point 1, the exhaust. This was followed by concentration point 5, whose mean concentration reached 102.0 ppm, 61.0 ppm, and 62.0 ppm at −5 Pa, −15 Pa, and −25 Pa, respectively, which were 293%, 185%, and 190% of the exhaust concentration. The mean concentrations of other measurement points were close to the mean concentration at the exhaust, among which the lowest concentrations were 38.4 ppm, 33.2 ppm, and 28.3 ppm at −5 Pa, −15 Pa, and −25 Pa, respectively, at point 4. Considering the influence of the pressure difference on the concentration, we found that with increasing pressure difference, the concentration of all the measuring points decreased except the concentration at point 2, which shows a similar trend as Case 1 to Case 3. The difference comparing the first three cases is that the concentration at point 6 does not change drastically with the change in the pressure difference.

3.3. Measurement results of reference experimental settings (Cases 7–9)

Cases 7–9 changed some experimental settings based on Case 4 and compared the differences in different influencing factors. In Case 7, the endoscopic equipment was turned off, and all heat sources in Case 8 were turned off, while in Case 9, the operating lamp was moved up 10 cm. The results of the 4 cases of Case 4 and Case 7–9 are shown in Fig. 5. After the endoscope was turned off (Case 7), the concentration result of Point 5 (185.5 ppm) showed little difference from point 6 (199.1 ppm). However, when the endoscope was turned on, the concentration at point 6 (443.3 ppm) was much higher than that at point 5 (102.4 ppm) because points 1, 2, and 4 are similar in these two cases, both in terms of the mean and the degree of dispersion of the data. The average at Point 3 shows a decrease from 41.1 ppm to 35.6 ppm.

When we turned off all the heat sources (Case 8) in the room, including all manikins, the concentrations at points 5 and 6 dropped dramatically, while the concentration at points 2 and 3 increased. This suggests that in the absence of a thermal plume, pollutants may spread horizontally rather than vertically. In Case 9, the surgical lamp was raised by 10 cm, and the results showed that the concentration at point 2 and point 4 decreased compared with those in Case 4, while the concentration at point 6 increased. Original data for of all measurements can be found in Appendix 1 and Appendix 2.

3.4. Air change efficiency and local air change index

The air change efficiency and local air change index were used to evaluate the performance of airflow distribution at these measurement points. Air change efficiency represents the performance of the air distribution of the ventilation system in the room. The calculated value of the air change efficiency of the OR is 49.24%, 49.91%, and 50.18% at −5 Pa, −15 Pa, and −25 Pa, respectively. For a mixing ventilated room, the ideal air change efficiency is 50%, and it may be lower due to air recirculation and higher due to a better air distribution method.

Fig. 6 shows the local air change index by using the measurement results. As explained in Section 2.5, the local air change index indicates the ratio of the time it takes for air to reach the exhaust to the time it takes to reach a specific position in the room. The ideal value in a mixing ventilation room is 100%. If the index at a point is less than 100%, it means that the air reaches this point more slowly than the air reaches the exhaust, and vice versa. Fig. 6 shows the local air change index from point 2 to point 6. From the figure, we can see that the local air change index of points 2, 3, and 4 is similar to the trend of pressure; that is, the increase in pressure will increase the local air change index of these points. Among them, point 3 has the largest variation range, which increases from 75.26%, which is the lowest value, at −5 Pa to 108.56% at −25 Pa. However, this value is the lowest among the three points at −5 Pa and −15 Pa. Among the three points, the index of point 4 is the highest in each pressure difference condition, which are 104.47%, 111.94%, and 119.94% at −5 Pa, −15 Pa, and −25 Pa, respectively. The index value of point 2 also increased steadily from 92.38% at −5 Pa to 105.45% at −25 Pa.

The local air change index at point 5 and point 6 is greater than 100% under all pressure conditions, but it does not show the same change

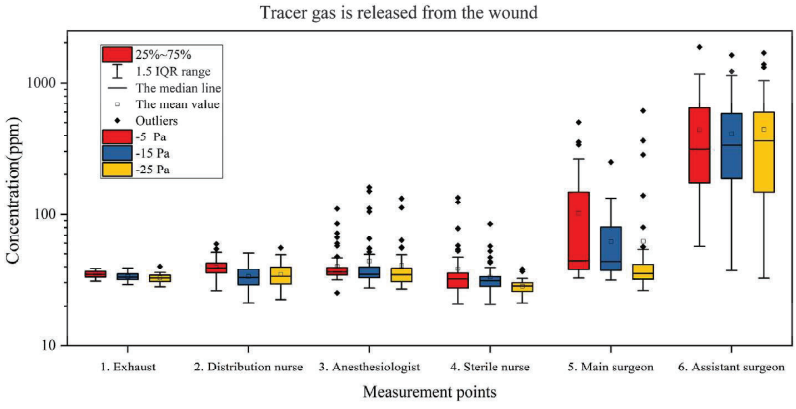

Fig. 4. Boxplot of concentration results when tracer gas is released from patient's wound.

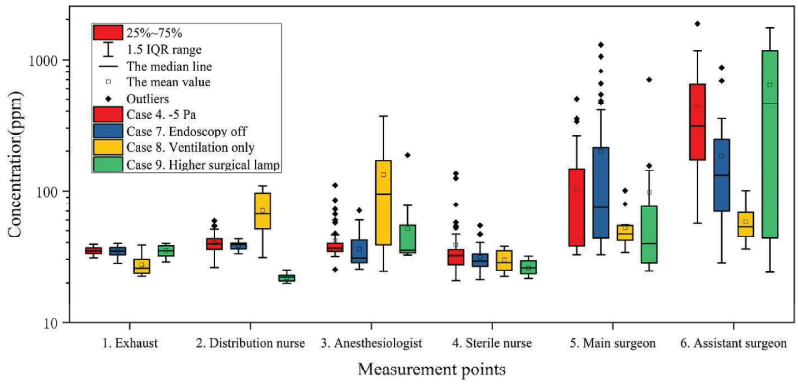

Fig. 5. Comparison of the concentration distribution of closed endoscopy in Case 4.

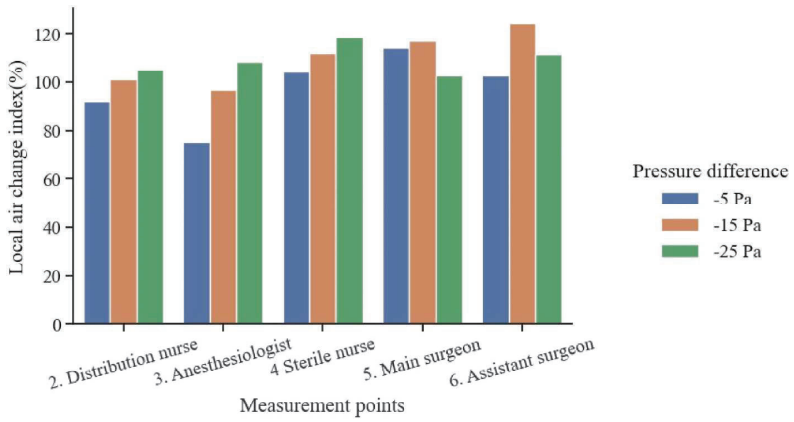

Fig. 6. Local air change index of each surgical staff breathing zone.

pattern as the first three points. As the pressure increased, the local air change index at point 5 increased slightly from 114.28% (-5 Pa) to 117.11% (-15 Pa) but decreased to 102.69% (-25 Pa). The local air change index at point 6 also experienced an increase, from 102.59% (-5 Pa) to 124.49 (-15 Pa), and then decreased to 111.73% at −25 Pa.

The original measured data and the calculated value of λ can be

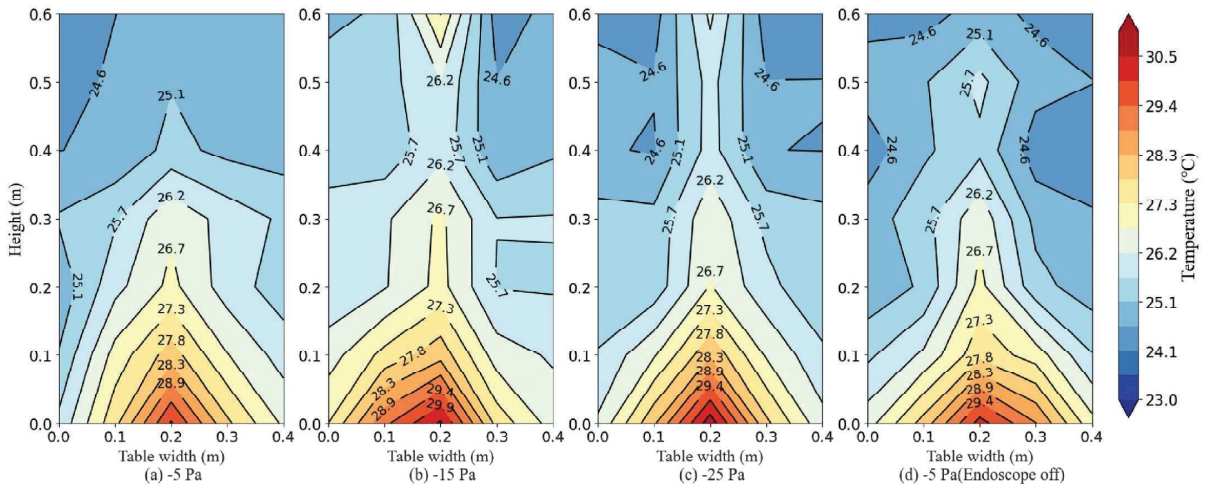

Fig. 7. Contour plot of the temperature distribution of the patient's thermal plume (a) −5 Pa (b) −15 Pa (c) −25 Pa.

found in Appendix 3 and Appendix 4.

3.5. Temperature and velocity distribution of the thermal plume above the wound (Case 4)

Fig. 7 shows the temperature distribution of the thermal plume above the wound. The distribution of the thermal plume presents some similar characteristics under different pressures as well as when the endoscope is turned off. First, the maximum temperature, which was approximately 31 °C, was found at the bottom middle of the measurement area, which was directly above the wound area. Second, as height increases, the temperature decreases, which is a typical feature of the thermal plume. At the initial part of the thermal plume, the temperature gradient is similar. In the height range of 0–0.3 m at three pressure difference conditions, the temperature of the centerline of the thermal plume decreases by approximately 3.7 °C. In addition, the temperature distribution of the thermal plume is symmetric in all cases. However, when the height is greater than 0.3 m, the temperature gradient attenuation varies greatly under different working conditions. At −5 Pa, the temperature is 26.6 °C at 0.3 m and 24.5 °C at 0.6 m, which decreases by 2.1 °C. At a pressure difference of −15 Pa, the centerline temperature of the thermal plume decreases from 26.8 °C (0.3 m) to 26.0 °C (0.4 m) and then increases to 27.3 °C (0.6 m). Similarly, at −25 Pa, the centerline temperature of the thermal plume decreased from 26.6 °C (0.3 m) to 25.8 °C (0.4 m) and then increased to 26.3 °C (0.6 m). When the endoscope was closed, similar characteristics of the patient thermal plume with other cases were observed.

Fig. 8 shows the measured velocity distribution of the thermal plume. Under the three pressure difference conditions, the maximum velocities of the thermal plume are 0.20 m/s, 0.20 m/s, and 0.19 m/s. These maximum values of the velocity of the thermal plume occur at a similar height of 0.4 m but not a similar width. The point with the highest velocity at the −5 Pa condition is at 0.0 m of table width, while under −15 Pa, it occurs at 0.1 m of table width and occurs in the middle of the table width, that is, 0.2 m under −25 Pa. A significant shift toward the center as the differential pressure increases can be seen. In addition, the thermal plume has shifted toward the assistant surgeon at height = 0 m (10 cm above the patient) in the figure. The velocity profile is different from the typical thermal plume velocity distribution, in which the velocity reaches the maximum at the centerline and decreases with increasing height. As the thermal plume deflects toward the assistant surgeon, a slow zone appears in front of the main surgeon's abdomen, where the velocity is less than 0.13 m/s. The airflow velocities in front of the assistant surgeon's nose were 0.18 m/s, 0.18 m/s, and 0.17 m/s under the three working conditions. The airflow velocity in front of the nose of the main surgeon was 0.132 m/s in all three differential pressure situations. The thermal plume velocity distribution was more symmetrical when the endoscope was closed than when the endoscope was turned on at −5 Pa. The maximum velocity of the plume was 0.19 m/s in both cases, but with the endoscope closed it appeared at the highest point along the centerline. In addition, a lower minimum velocity of 0.05 m/s was observed with the endoscope is turned off.

4. Discussion

4.1. Distribution characteristics of tracer gas concentration

From Figs. 3–5, we noticed that many outliers were observed at all test points except the exhaust and distribution nurse breathing zones in all working conditions. In addition, the results of the respiratory zone concentration of the assistant surgeon and the main surgeon showed that the data were skewed, so we could confirm that the data did not follow a normal distribution. Some previous studies measuring air pollutant concentrations have yielded similar results and provided explanations. Air pollutant concentrations are inherently random variables because of their dependence on the fluctuations of a variety of meteorological and emission variables [55]. . It depends on the position, the flow state. The distribution of air pollution is generally a two-parameter lognormal distribution [56]. This phenomenon is very common in contaminant detection, which is explained by the theory of continuous random dilution. According to theory, pollutants are still in the process of being diluted rather than completely mixed [57]. In this study, we observed this phenomenon in the breathing zones of surgical staff near the surgical microenvironment, including an anesthesiologist, assistant surgeon, and main surgeon, which suggests that tracer gas is still in the intermediate stage of dilution when moving to these areas rather than being completely mixed with air. This may indicate that surgical staff who work in proximity to a COVID-19-infected patient may be exposed to a higher coronavirus concentration than those who work further from the patient in ORs with mixing ventilation under negative pressure.

4.2. Influence of pressure difference on exposure level

Table 3 shows the results of the intergroup posttest, indicating whether there was a statistically significant difference between the two groups. Points 1 and 2, regardless of whether the pollutant is released

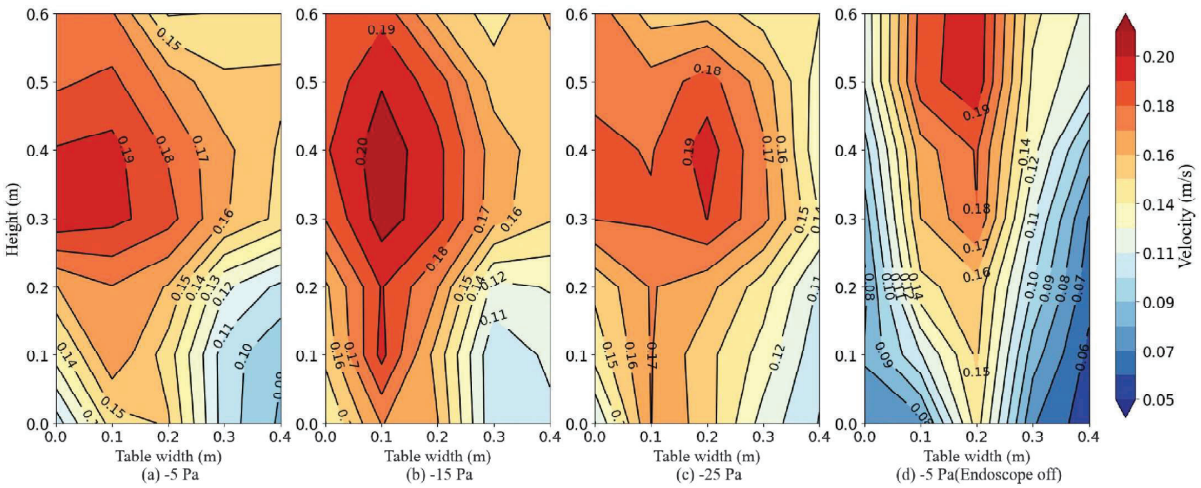

Fig. 8. Contour plot of the velocity distribution of the patient's thermal plume.

Table 3
Data analysis of whether the variation of pressure difference in different positions has a significant effect on the concentration data.

Measurement point	Case #-#					
	1–2	2–3	1–3	4–5	5–6	4–6
1. Exhaust	$p = 0.001$	$p = 0.180$	$p < 0.001$	$p = 0.001$	$p = 0.371$	$p < 0.001$
2. Distribution nurse	$p = 0.003$	$p = 1.000$	$p = 0.006$	$p < 0.001$	$p = 0.823$	$p < 0.001$
3. Anesthesiologist	$p = 0.126$	$p < 0.001$	$p < 0.001$	$p = 0.758$	$p = 0.848$	$p = 0.998$
4. Sterile nurse	$p = 0.807$	$p = 0.098$	$p = 0.127$	$p = 0.538$	$p = 0.001$	$p < 0.001$
5. Main surgeon	$p = 0.039$	$p = 0.008$	$p < 0.001$	$p = 0.301$	$p < 0.001$	$p < 0.001$
6. Assistant surgeon	$p = 0.268$	$p = 0.005$	$p < 0.001$	$P = 0.767$	$p = 0.649$	$p = 0.989$

from the nose or the wound, show similar characteristics. This is easy to understand since both sites are far away from the patient. When the pressure difference changes from −5 Pa to −15 Pa, there is a significant difference between the two groups of data, but when the pressure difference changes from −15 Pa to −25 Pa, there is no significant difference between the two groups of data. According to the actual measured exhaust air volume, we know that there is a small difference in the actual ventilation volume with different pressure differences. The ventilation volume differences between −5 Pa and −15 Pa and between −15 Pa and −25 Pa are 102 m^3/h and 74 m^3/h, respectively. This difference is due to the relationship between the pressure difference and ventilation volume determined by the following equation:

$$\Delta p^{0.5}\delta = Q \tag{1}$$

where Δp is the pressure difference, Pa; Q is the flow rate, m^3/h; and δ is a coefficient. For this experiment, the relationship between the flow rate and pressure difference can be fitted as $63.58\ \Delta p^{0.5} = Q$ ($R = 0.99$). The characteristics of the results at points 1 and 2 may be because the concentration discharge is more sensitive to changes in large ventilation volumes and less sensitive to changes in small ventilation rates.

At point 3, there is a significant difference only between the Case 2 and Case 3 data, while at point 4, there is a significant difference only between the Case 5 and Case 6 data. From the concentration results, such a difference is very small and may be caused by changes in ventilation volume.

On the other hand, according to the results of the local air change index at each point combined with the results of the concentration, with the increase of the pressure difference, the local air change index at point 2 to point 4 increases, and the concentration at each point decreases accordingly. The concentration data can be related to the local air change index. That is, the greater the local air index is, the smaller the concentration. This can explain the influencing factors of indoor concentration at each point, including the actual ventilation volume and air distribution. However, for points 5 and 6, this conclusion does not apply. We did not observe the relationship between the local air change index and concentration data.

When the differential pressure changes from −15 Pa to −25 Pa, the concentration data at point 5 differ significantly regardless of where the tracer gas is released. It can be seen from the thermal plume results that the change of pressure difference can significantly change the characteristics of the patient's thermal plume, which may be due to the influence of airflow infiltration into the gap of the room envelope, and this influence is more intense for point 5 than the change of ventilation rate and the change of the same fraction efficiency. When tracer gas was released from the wound, the concentration data of point 6 did not differ significantly under different pressure differences. This may be due to the Coanda effect on the chest of the assistant surgeon after the thermal plume from the patient's wound is diverted to the assistant surgeon. This effect will not be affected by external airflow.

4.3. Other factors affecting exposure levels

In this study, we observed that pollutant exposure levels of the assistant surgeon were much higher than those of other medical staff, despite the proximity of the assistant surgeon to the main surgeon. Previous studies of smoke from laparoscopic surgery have also pointed to high levels of assistant surgeon exposure to smoke from patients' wounds [58]. Field measurements by et al. at St. Olavs Hospital also found that assistant surgeons were significantly more sensitive to par-ticulate matter of various sizes during certain surgeries than other medical staff [59].

A hypothesis was proposed to explain this characteristic based on the concentration comparison results and the thermal plume velocity distribution results under the switching endoscope imager. Due to the operation of the cooling fan of the endoscope imager, the airflow generated by the endoscope imager affects the patient's thermal plume, diverting it to the surgeon at the early stage of development. This deflection directly entrains contaminants from the patient's wound, or the patient's breath, toward the assistant surgeon. The pollutant exposure concentration of the assistant surgeon was much higher than that of other surgical staff.

4.4. Practical limitations

Due to the tracer gas sampling instrument taking samples at intervals of 6 min, it is impossible to capture concentration fluctuations over shorter periods. In addition, the temperature of the indoor wall inevitably increases by 1–2 °C with the ventilation time, and such subtle changes may have different degrees of influence on the results.

In addition, some hypotheses about the influence of the cooling fan on thermal plume formation are proposed based on the experimental results. Moreover, there is much surgical equipment in the operating room, so the airflow distribution will be significantly affected. The formation of the thermal plume in this complex surgical microenvironment needs further research. Research on human thermal plumes in the surgical microenvironment may face several challenges: the influence of ventilation airflow [60], the modeling of thermal plumes [61], human body movement [62], and the effect of environmental temperature [63]. These studies also suggest that the human thermal plume is sensitive to environmental parameters. Therefore, the formation of the thermal plume in a more complex environment needs more in-depth research through computational fluid dynamic (CFD) studies or theoretical studies.

This study only analyzed the distribution tracer gas in the operating room by mixing ventilation with thermal manikins. However, the movement of surgical staff in the operating room is very normal, and it is not clear whether personnel movement will have a great impact on coronavirus distribution in ORs.

The results of this study provide the concentration of tracer gas in the surgical staff breathing zone in the operating room, and the corresponding concentration attenuation can be obtained. Therefore, the infection risk of the surgical staff can be calculated by using an accurate risk assessment model and virus source intensity. Based on the risk of infection, recommendations can be made to the surgical staff on how to choose PPE equipment. However, it is difficult to calculate the precise risk of infection as there is no clear dose-response relationship for inhalation of the SARS-CoV-2. Therefore, risk assessment was not considered in this study.

5. Conclusion

In this paper, the distribution of airborne contamination released by COVID-19 patients in the OR was studied using tracer gas. The contamination sources were the noses and the wound area of the patients, and the concentrations in the breathing zone of surgical staff in the OR were measured. In addition, the velocity distribution and temperature distribution of the patient's thermal plume were measured, and the airflow interference was compared and analyzed. The following conclusion can be drawn.

- Contaminant exposure levels of the sterile nurse and the distribution nurse outside the surgical microenvironment are affected mainly by the ventilation airflow rate. The exposure levels of surgical nurses are sensitive to the ventilation rate. Due to the difference in the local air change index, there are slight differences in the measured concentration of contaminants between each measured nurse, but they are all around the average exhaust concentration.
- The main surgeon, assistant surgeon, and anesthesiologist in the surgical microenvironment had higher exposure levels to the contamination concentrations in their breathing zones, regardless of whether the source was the nose or a wound. The highest exposure concentration may occur for the assistant surgeon, which can be 12 times higher than the exposure level of other surgical staff outside the surgical microenvironment.
- The cooling fan of the endoscope image, which is located nearby, may have a great effect on the exposure level of the assistant surgeon. This may result in asymmetry in the patient's thermal plume, which in turn results in higher concentrations of contaminants in the assistant surgeon's breathing zone than in that of the main surgeon.
- Increasing the differential pressure resulted in lower concentration levels in the breathing zone of the main surgeon and the assistant surgeon. When the contaminant emission source was the nose, the exposure concentration of both the main surgeon and assistant surgeon decreased. When the contaminant emission source is the wound, the concentration level of the assistant surgeon will not be affected by the pressure difference because the thermal plume is biased toward the assistant surgeon.
- It is recommended that patients with COVID-19 should be operated in a negative-pressure ventilated operating room with a large differential pressure during the COVID-19 epidemic to reduce the risk of infection on surgical staff.

CRediT authorship contribution statement

Yang Bi: Investigation, Methodology, Writing – original draft, Conceptualization. **Amar Aganovic:** Formal analysis, Methodology. **Hans Martin Mathisen:** Supervision. **Guangyu Cao:** Conceptualization, Project administration, Supervision, Writing – review & editing.

Declaration of competing interest

The authors declare that they have no known competing financial interests or personal relationships that could have appeared to influence the work reported in this paper.

Acknowledgment

The authors are grateful to the China Scholarship Council for the financial support to Yang Bi (CSC student ID: 202009210006). We greatly appreciate the collaboration with the Operating Room of the Future (FOR) at St. Olavs hospital in Norway.

Appendix A. Supplementary data

Supplementary data to this article can be found online at https://doi.org/10.1016/j.buildenv.2022.109091.

References

[1] Z. Al Maskari, A. Al Blushi, F. Khamis, A. Al Tai, I. Al Salmi, H. Al Harthi, M. Al Saadi, A. Al Mughairy, R. Gutierrez, Z. Al Blushi, Characteristics of healthcare workers infected with COVID-19: a cross-sectional observational study, Int. J. Infect. Dis. 102 (2021) 32–36.

[2] L. Zheng, X. Wang, C. Zhou, Q. Liu, S. Li, Q. Sun, M. Wang, Q. Zhou, W. Wang, Analysis of the infection status of healthcare workers in Wuhan during the COVID-19 outbreak: a cross-sectional study, Clin. Infect. Dis. 71 (16) (2020) 2109–2113.

[3] J. Wong, Q.Y. Goh, Z. Tan, S.A. Lie, Y.C. Tay, S.Y. Ng, C.R. Soh, Preparing for a COVID-19 pandemic: a review of operating room outbreak response measures in a large tertiary hospital in Singapore, Can. J. Anesthesia/J. Can. Anesthésie 67 (6) (2020) 732–745.

[4] R.S. Sikkema, S.D. Pas, D.F. Nieuwenhuijse, Á. O'Toole, J. Verweij, A. van der Linden, I. Chestakova, C. Schapendonk, M. Pronk, P. Lexmond, T. Bestebroer, R. J. Overmars, S. van Nieuwkoop, W. van den Bijllaardt, R.G. Bentvelsen, M.M.L. van Rijen, A.G.M. Buiting, A.J.G. van Oudheusden, B.M. Diederen, A.M.C. Bergmans, A. van der Eijk, R. Molenkamp, A. Rambaut, A. Timen, J.A.J.W. Kluytmans, B. B. Oude Munnink, M.F.Q. Kluytmans van den Bergh, M.P.G. Koopmans, COVID-19 in health-care workers in three hospitals in the south of The Netherlands: a cross-sectional study, Lancet Infect. Dis. 20 (11) (2020) 1273–1280.

[5] H. Cheng, J.W. Clymer, B. Po-Han Chen, B. Sadeghirad, N.C. Ferko, C.G. Cameron, P. Hinoul, Prolonged operative duration is associated with complications: a systematic review and meta-analysis, J. Surg. Res. 229 (2018) 134–144.

[6] L.K. Ti, L.S. Ang, T.W. Foong, B.S.W. Ng, What we do when a COVID-19 patient needs an operation: operating room preparation and guidance, Can. J. Anesthesia/J. Can. Anesthésie 67 (6) (2020) 756–758.

[7] J.D. Forrester, A.K. Nassar, P.M. Maggio, M.T. Hawn, Precautions for operating room team members during the COVID-19 pandemic, J. Am. Coll. Surg. 230 (6) (2020) 1098–1101.

[8] M.E. Awad, J.C.L. Rumley, J.A. Vazquez, J.G. Devine, Perioperative considerations in urgent surgical care of suspected and confirmed COVID-19 orthopaedic patients: operating room protocols and recommendations in the current COVID-19 pandemic, JAAOS - J. Am. Acad. Orthopaed. Surg. 28 (11) (2020).

[9] F.A. Leyva Moraga, E. Leyva Moraga, F. Leyva Moraga, A. Juanz González, J. M. Ibarra Celaya, J.A. Ocejo Gallegos, J.A. Barreras Espinoza, Aerosol box, an operating room security measure in COVID-19 pandemic, World J. Surg. 44 (7) (2020) 2049–2050.

[10] W.S.R.I. Collaborative, Surgery during the COVID-19 pandemic: operating room suggestions from an international Delphi process, Br. J. Surg. 107 (11) (2020) 1450–1458.

[11] T. Greenhalgh, J.L. Jimenez, K.A. Prather, Z. Tufekci, D. Fisman, R. Schooley, Ten scientific reasons in support of airborne transmission of SARS-CoV-2, Lancet 397 (10285) (2021) 1603–1605.

[12] D. Lewis, Is the coronavirus airborne? Experts can't agree, Nature 580 (7802) (2020) 175.

[13] C. Heneghan, E. Spencer, J. Brassey, A. Plüddemann, I. Onakpoya, D. Evans, J. Conly, T. Jefferson, SARS-CoV-2 and the role of airborne transmission: a systematic review [version 1; peer review: 1 approved with reservations, 2 not approved], F1000Research 10 (232) (2021).

[14] J.L. Santarpia, D.N. Rivera, V.L. Herrera, M.J. Morwitzer, H.M. Creager, G. W. Santarpia, K.K. Crown, D.M. Brett-Major, E.R. Schnaubelt, M.J. Broadhurst, J. V. Lawler, S.P. Reid, J.J. Lowe, Aerosol and surface contamination of SARS-CoV-2 observed in quarantine and isolation care, Sci. Rep. 10 (1) (2020), 12732.

[15] Y. Liu, Z. Ning, Y. Chen, M. Guo, Y. Liu, N.K. Gali, L. Sun, Y. Duan, J. Cai, D. Westerdahl, X. Liu, K.-f. Ho, H. Kan, Q. Fu, K. Lan, Aerodynamic Characteristics and RNA Concentration of SARS-CoV-2 Aerosol in Wuhan Hospitals during COVID-19 Outbreak, bioRxiv, 2020, 2020.03.08.982637.

[16] Y. Jiang, H. Wang, Y. Chen, J. He, L. Chen, Y. Liu, X. Hu, A. Li, S. Liu, P. Zhang, H. Zou, S. Hua, Clinical Data on Hospital Environmental Hygiene Monitoring and Medical Staff Protection during the Coronavirus Disease 2019 Outbreak, medRxiv, 2020, 2020.02.25.20028043.

[17] S.L. Miller, W.W. Nazaroff, J.L. Jimenez, A. Boerstra, G. Buonanno, S.J. Dancer, J. Kurnitski, L.C. Marr, L. Morawska, C. Noakes, Transmission of SARS-CoV-2 by inhalation of respiratory aerosol in the Skagit Valley Chorale superspreading event, Indoor Air 31 (2) (2021) 314–323.

[18] Y. Li, H. Qian, J. Hang, X. Chen, P. Cheng, H. Ling, S. Wang, P. Liang, J. Li, S. Xiao, J. Wei, L. Liu, B.J. Cowling, M. Kang, Probable airborne transmission of SARS-CoV-2 in a poorly ventilated restaurant, Build. Environ. 196 (2021), 107788.

[19] P. Azimi, Z. Keshavarz, J.G. Cedeno Laurent, B. Stephens, J.G. Allen, Mechanistic transmission modeling of COVID-19 on the Diamond Princess cruise ship demonstrates the importance of aerosol transmission, Proc. Natl. Acad. Sci. Unit. States Am. 118 (8) (2021), e2015482118.

[20] A.C. Fears, W.B. Klimstra, P. Duprex, A. Hartman, S.C. Weaver, K.C. Plante, D. Mirchandani, J.A. Plante, P.V. Aguilar, D. Fernández, A. Nalca, A. Totura, D. Dyer, B. Kearney, M. Lackemeyer, J.K. Bohannon, R. Johnson, R.F. Garry, D. S. Reed, C.J. Roy, Comparative Dynamic Aerosol Efficiencies of Three Emergent Coronaviruses and the Unusual Persistence of SARS-CoV-2 in Aerosol Suspensions, medRxiv, 2020, 2020.04.13.20063784.

[21] L. Morawska, D.K. Milton, It is time to address airborne transmission of coronavirus disease 2019 (COVID-19), Clin. Infect. Dis. 71 (9) (2020) 2311–2313.

[22] Y. Luo, M. Zhong, [Standardized diagnosis and treatment of colorectal cancer during the outbreak of novel coronavirus pneumonia in Renji hospital], Zhonghua Wei Chang Wai ke Za Zhi = Chin. J. Gastrointestin. Surg. 23 (3) (2020) E003.
[23] Y. Li, J.J. Qin, Z. Wang, Y. Yu, Y.Y. Wen, X.K. Chen, W.X. Liu, Y. Li, [Surgical treatment for esophageal cancer during the outbreak of COVID-19], Zhonghua Zhong liu Za Zhi [Chin. J. Oncol.] 42 (4) (2020) 296–300.
[24] R. Chen, Y. Zhang, L. Huang, B.-h. Cheng, Z.-y. Xia, Q.-t. Meng, Safety and efficacy of different anesthetic regimens for parturients with COVID-19 undergoing Cesarean delivery: a case series of 17 patients, Can. J. Anesthesia/J. Can. Anesthésie 67 (6) (2020) 655–663.
[25] V. Arora, C. Evans, L. Langdale, A. Lee, You need a plan: a stepwise protocol for operating room preparedness during an infectious pandemic, federal practitioner : for the health care professionals of the VA, DoD, and PHS, Perioperat. Care Operat. Room Manag. 37 (5) (2020) 212–218.
[26] S. Al-Benna, Negative pressure rooms and COVID-19, J. Perioperat. Pract. 31 (1–2) (2020) 18–23.
[27] T. Chow, A. Kwan, Z. Lin, W. Bai, Conversion of operating theatre from positive to negative pressure environment, J. Hosp. Infect. 64 (4) (2006) 371–378.
[28] T.-t. Chow, A. Kwan, Z. Lin, W. Bai, A computer evaluation of ventilation performance in a negative-pressure operating theater, Anesth. Analg. 103 (4) (2006) 913–918.
[29] M.o.H.a.U.-R.D.o.t.P.s.R.o. China, Architectural Technical Code for Hospital Clean Operating Department, 2013.
[30] U. National Health Service, Health Technical Memorandum 03-01 Specialised Ventilation for Healthcare Premises Part A: the Concept, Design, Specification, Installation and Acceptance Testing of Healthcare Ventilation Systems, 2021, p. 64.
[31] C.f.D.C.a. Prevention, Guidelines for Preventing the Transmission of Mycobacterium tuberculosis in Health-Care Settings, vol. 2005, 2005, p. 64.
[32] P.H.A.o. Canada, Canadian Tuberculosis Standards 7th Edition, Chapter 15: Prevention and Control of Tuberculosis Transmission in Health Care and Other Settings, p. 23.
[33] R. Barranco, F. Ventura, Covid-19 and infection in health-care workers: an emerging problem, Med. Leg. J. 88 (2) (2020) 65–66.
[34] H.P. Lee, D.Y. Wang, Objective assessment of increase in breathing resistance of N95 respirators on human subjects, Ann. Occup. Hyg. 55 (8) (2011) 917–921.
[35] L.M. Visentin, S.J. Bondy, B. Schwartz, L.J. Morrison, Use of personal protective equipment during infectious disease outbreak and nonoutbreak conditions: a survey of emergency medical technicians, Can. J. Emerg. Med. 11 (1) (2009) 44–56.
[36] N. Castle, R. Owen, M. Hann, S. Clark, D. Reeves, I. Gurney, Impact of chemical, biological, radiation, and nuclear personal protective equipment on the performance of low- and high-dexterity airway and vascular access skills, Resuscitation 80 (11) (2009) 1290–1295.
[37] A.G. Loth, D.B. Guderian, B. Haake, K. Zacharowski, T. Stöver, M. Leinung, Aerosol exposure during surgical tracheotomy in SARS-CoV-2 positive patients, Shock 55 (4) (2021) 472–478.
[38] A. Murr, N.R. Lenze, W.C. Brown, M.W. Gelpi, C.S. Ebert, B.A. Senior, B.D. Thorp, A.M. Zanation, A.J. Kimple, Quantification of aerosol particle concentrations during endoscopic sinonasal surgery in the operating room, Am. J. Rhinol. Allergy 35 (4) (2020) 426–431.
[39] B.C.H. Tsui, S. Pan, Are aerosol-generating procedures safer in an airborne infection isolation room or operating room? Br. J. Anaesth. 125 (6) (2020) e485–e487.
[40] M. Garbey, G. Joerger, S. Furr, A systems approach to assess transport and diffusion of hazardous airborne particles in a large surgical suite: potential impacts on viral airborne transmission, Int. J. Environ. Res. Publ. Health 17 (15) (2020) 5404.
[41] G. Cao, A.M. Nilssen, Z. Cheng, L.-I. Stenstad, A. Radtke, J.G. Skogås, Laminar airflow and mixing ventilation: which is better for operating room airflow distribution near an orthopedic surgical patient? Am. J. Infect. Control 47 (7) (2019) 737–743.
[42] ASHRAE, Standard 55-2020 – Thermal Environmental Conditions for Human Occupancy (ANSI Approved), American Society of Heating, Refrigerating and Air-Conditioning Engineers, 2021.
[43] M. Bivolarova, J. Ondráček, A. Melikov, V. Ždímal, A comparison between tracer gas and aerosol particles distribution indoors: the impact of ventilation rate, interaction of airflows, and presence of objects, Indoor Air 27 (6) (2017) 1201–1212.
[44] C. Noakes, L. Fletcher, P. Sleigh, W. Booth, B. Beato-Arribas, N. Tomlinson, Comparison of tracer techniques for evaluating the behaviour of bioaerosols in hospital isolation rooms, in: Proceedings of Healthy Buildings, Syracuse, 2009, pp. 13–17.
[45] J.W. Tang, C.J. Noakes, P.V. Nielsen, I. Eames, A. Nicolle, Y. Li, G.S. Settles, Observing and quantifying airflows in the infection control of aerosol- and airborne-transmitted diseases: an overview of approaches, J. Hosp. Infect. 77 (3) (2011) 213–222.
[46] A. Aganovic, G. Cao, L.-I. Stenstad, J.G. Skogås, An experimental study on the effects of positioning medical equipment on contaminant exposure of a patient in an operating room with unidirectional downflow, Build. Environ. 165 (2019), 106096.
[47] Y. Zhang, G. Cao, G. Feng, K. Xue, C. Pedersen, H.M. Mathisen, L.-I. Stenstad, J. G. Skogås, The impact of air change rate on the air quality of surgical microenvironment in an operating room with mixing ventilation, J. Build. Eng. 32 (2020), 101770.
[48] R.K. Englehardt, B.M. Nowak, M.V. Seger, F.D. Duperier, Contamination resulting from aerosolized fluid during laparoscopic surgery, J. Soc. Laparoendosc. Surg. 18 (3) (2014) e2014.00361.
[49] ANSI ASHRAE, Standard-170 2017, Ventilation of Healthcare Facilities, ANSI/ASHRAE Atlanta, GA, 2017.
[50] C.f.D. Control, Prevention, Guidelines for Environmental Infection Control in Health-Care Facilities, Centers for Disease Control and Prevention (US), Centers for Disease Control and Prevention (US), 2017.
[51] D.o. Health, Health Technical Memorandum HTM 03-01: Specialised Ventilation for Healthcare Premises, Part A: Design and Validation, 2007.
[52] G, Management Specification of Air Cleaning Technique in Hospitals, 2013.
[53] E. Mundt, H.M. Mathisen, P.V. Nielsen, A. Moser, Ventilation Effectiveness, Rehva, 2004.
[54] A. Novoselac, J. Srebric, Comparison of air exchange efficiency and contaminant removal effectiveness as IAQ indices, Trans.-Am. Soc. Heat. Refrigerat. Air Condit. Eng. 109 (2) (2003) 339–349.
[55] P.G. Georgopoulos, J.H. Seinfeld, Statistical distributions of air pollutant concentrations, Environ. Sci. Technol. 16 (7) (1982) 401A–416A.
[56] W.R. Ott, Environmental Statistics and Data Analysis, Routledge, 2018.
[57] W.R. Ott, A physical explanation of the lognormality of pollutant concentrations, J. Air Waste Manag. Assoc. 40 (10) (1990) 1378–1383.
[58] E.A.F. Van Gestel, E.S. Linssen, M. Creta, K. Poels, L. Godderis, J.J. Weyler, A. De Schryver, J.A.J. Vanoirbeek, Assessment of the absorbed dose after exposure to surgical smoke in an operating room, Toxicol. Lett. 328 (2020) 45–51.
[59] S.F. Ragde, R.B. Jørgensen, S. Føreland, Characterisation of exposure to ultrafine particles from surgical smoke by use of a fast mobility particle sizer, Ann. Occup. Hyg. 60 (7) (2016) 860–874.
[60] J. Ma, H. Qian, P.V. Nielsen, L. Liu, Y. Li, X. Zheng, What dominates personal exposure? Ambient airflow pattern or local human thermal plume, Build. Environ. 196 (2021), 107790.
[61] T.H. Dokka, P.O. Tjelflaat, A simplified model for human induced convective air flows-model PREDICTONS compared to experimental data, in: Proceeding of Room Vent 2002 (8th International Conference on Air Distribution in Rooms), Citeseer, 2002.
[62] Y. Tao, K. Inthavong, J. Tu, A numerical investigation of wind environment around a walking human body, J. Wind Eng. Ind. Aerod. 168 (2017) 9–19.
[63] G. Feng, Y. Bi, Y. Zhang, Y. Cai, K. Huang, Study on the motion law of aerosols produced by human respiration under the action of thermal plume of different intensities, Sustain. Cities Soc. 54 (2020), 101935.

Article II Sadeghian, P., **Bi, Y**., Cao, G. et al. Reducing the risk of viral contamination during the coronavirus pandemic by using a protective curtain in the operating room. Patient Saf Surg 16, 26 (2022).

Patient Safety in Surgery

RESEARCH

Open Access

Reducing the risk of viral contamination during the coronavirus pandemic by using a protective curtain in the operating room

Parastoo Sadeghian[1*], Yang Bi[2], Guangyu Cao[2] and Sasan Sadrizadeh[1]

Abstract

Background: Airborne transmission diseases can transfer long and short distances via sneezing, coughing, and breathing. These airborne repertory particles can convert to aerosol particles and travel with airflow. During the Coronavirus disease 2019 (COVID-19) pandemic, many surgeries have been delayed, increasing the demand for establishing a clean environment for both patient and surgical team in the operating room.

Methods: This study aims to investigate the hypothesis of implementing a protective curtain to reduce the transmission of infectious contamination in the surgical microenvironment of an operating room. In this regard, the spread of an airborne transmission disease from the patient was evaluated, consequently, the exposure level of the surgical team. In the first part of this study, a mock surgical experiment was established in the operating room of an academic medical center in Norway. In the second part, the computational fluid dynamic technique was performed to investigate the spread of airborne infectious diseases. Furthermore, the field measurement was used to validate the numerical model and guarantee the accuracy of the applied numerical models.

Results: The results showed that the airborne infectious agents reached the breathing zone of the surgeons. However, using a protective curtain to separate the microenvironment between the head and lower body of the patient resulted in a 75% reduction in the spread of the virus to the breathing zone of the surgeons. The experimental results showed a surface temperature of 40 ˚C, which was about a 20 ˚C increase in temperature, at the wound area using a high intensity of the LED surgical lamps. Consequently, this temperature increase can raise the patient's thermal injury risk.

Conclusion: The novel method of using a protective curtain can increase the safety of the surgical team during the surgery with a COVID-19 patient in the operating room.

Keywords: COVID-19, Operating room, Computational fluid dynamics, Airborne infectious disease, Thermal injury, Protective curtain

Background

Airborne transmission diseases can spread via released droplets from the human respiratory system. These droplets transfer during speaking, breathing, sneezing, and coughing [1, 2]. Due to evaporation, these water droplets can have various size distributions [3]. Moreover, these airborne particles can be contaminated with agents of infectious diseases, including tuberculosis, SARS-CoV, and measles [4–6]. These airborne infectious diseases are

*Correspondence: parsad@kth.se

[1] Department of Civil and Architectural Engineering, KTH Royal Institute of Technology, Brinellvägen 23, 10044 Stockholm, Sweden
Full list of author information is available at the end of the article

highly contagious since they can transmit through short and long distances, besides transferring from a contaminated person due to direct contact [7, 8].

During the outbreak of Coronavirus disease 2019 (COVID-19), most surgeries have been postponed in spring 2020 [9]; consequently, surgical patients have received delayed treatments [10]. On the other hand, these delays caused patients to suffer for a longer time till delivering surgical treatments. The pandemic has brought new challenges to the operating room's (OR) performance. As a result, a clean environment in the OR has not been important only for patient safety. Protection of the healthcare workers (HCW) has also been considered to avoid the surgical team's infection from a COVID-19 patient.

An increasing number of studies indicate that airborne transmission is the main method of the SARS-CoV-2 virus spread among the populations [6, 11, 12]. These studies showed that the SARS-CoV-2 virus could not only spread over short distances through behaviours such as sneezing, coughing, and talking that produce large aerosol particles, but also through breathing that generates small aerosols. Some studies have proposed performing the surgery for COVID-19 patients in the negative pressure OR. In this regard, the spread of the SARS-CoV-2 virus has been controlled from penetrating adjacent rooms by gaps in doors and windows [13–15]. Hill et al. [16] introduced a novel method called "Corona Curtain" to guarantee the safety of the emergency department staff during intubations of a COVID-19 patient. This novel concept used a plastic drape role to make the walls of an intubation tent. Although their proposed concept had successful results in the early stages, they lacked scientific data to evaluate the system's effectiveness. Some research works have suggested using personal protective equipment (PPE) [17, 18] and aerosol boxes [19] to protect the surgical team. However, Yánez Benítez et al. [20] reported that using PPE significantly reduced the attendance of HCWs, and more than 80% of respondents reported an increase in surgical fatigue. Therefore, there is a high demand to propose new approaches to protect health care workers without compromising their performance.

The previous literature mainly proposed protective methods for HCW during the treatment of COVID-19 patients in the hospital wards. In contrast, this study investigated the safety of the medical team during the surgery with an infected patient in the OR. In this regard, the spread of airborne infectious diseases like COVID-19 from the surgical patient was studied. A new method was proposed to improve the safety of the surgical team. Moreover, the effect of various surgical lamps' radiation intensity on temperature distribution in the wound area was experimentally and numerically evaluated.

Methods

Experimental study

Operating room laboratory

All experimental measurements were finished in a full-scale OR laboratory of the Department of Energy and Process Engineering at Norwegian University of Science and Technology, Norway. The dimension of the laboratory is 8.73 m × 7.05 m × 3.25 m (length × width × height), and the total volume is 200m^3. The OR was equipped with a mixing ventilation system with an air change rate of 20 ACH, as presented in Fig. 1. A variety of medical equipment was located in the OR, including an ultrasonic cleaner, two endoscope imagers, an anaesthesia machine, and two surgical ceiling pendants. All the equipment had a similar setup to a real OR at St. Olavs hospital, Norway. The clean air supply rate was about 4000 m^3/h, and the air extract rate was about 4242 m^3/h, consequently resulting in a negative pressure condition of -5 Pa. The air temperature was 20℃ in the laboratory room. Two LED surgical lights were used; in which the first lamp was a Z 500 M lamp (made by the Meditech (India) company), and the second one was a STARLED3 NX lamp (manufactured by the ACEM Medical Company). The surgical lamps had a calorific value, and their heating power at the maximum brightness is shown in Table 1.

There were six thermal manikins in the laboratory room, including an anaesthesiologist nurse, a circulating nurse, a scrub nurse, a patient, a main, and an assistant surgeon. The skin surface temperature of the anaesthesiologist and patient was constant and regulated by a temperature control device. Their skin surfaces were set at 33℃ for the head, 30℃ for the arm, 31℃ for the chest, and 29℃ for the legs. Other thermal manikins generated a constant heat flux, as listed in Table 1. The heating power of each manikin was set according to the ASHRAE standard [21].

Experimental equipment and setup

AirDistSys5000 was used to measure the turbulence intensity, air velocity (with an accuracy of 0.2 m/s), and temperature (with an accuracy of 0.2℃) distributions. Overall, there were 66 measurement points, as presented in Fig. 1b. The applied instrument supported simultaneous measurements with up to eight instruments in series, of which six were used in this study. The instrument levels were placed according to the position shown in Fig. 1b, and the distance between the two instruments was 0.1 m, located 1.2 m in height above the floor. The whole measurement lasted for three minutes, and the data was recorded every two seconds, resulting in 90 data sets. The measurement was repeated after all devices were moved 20 cm horizontally along the operating table.

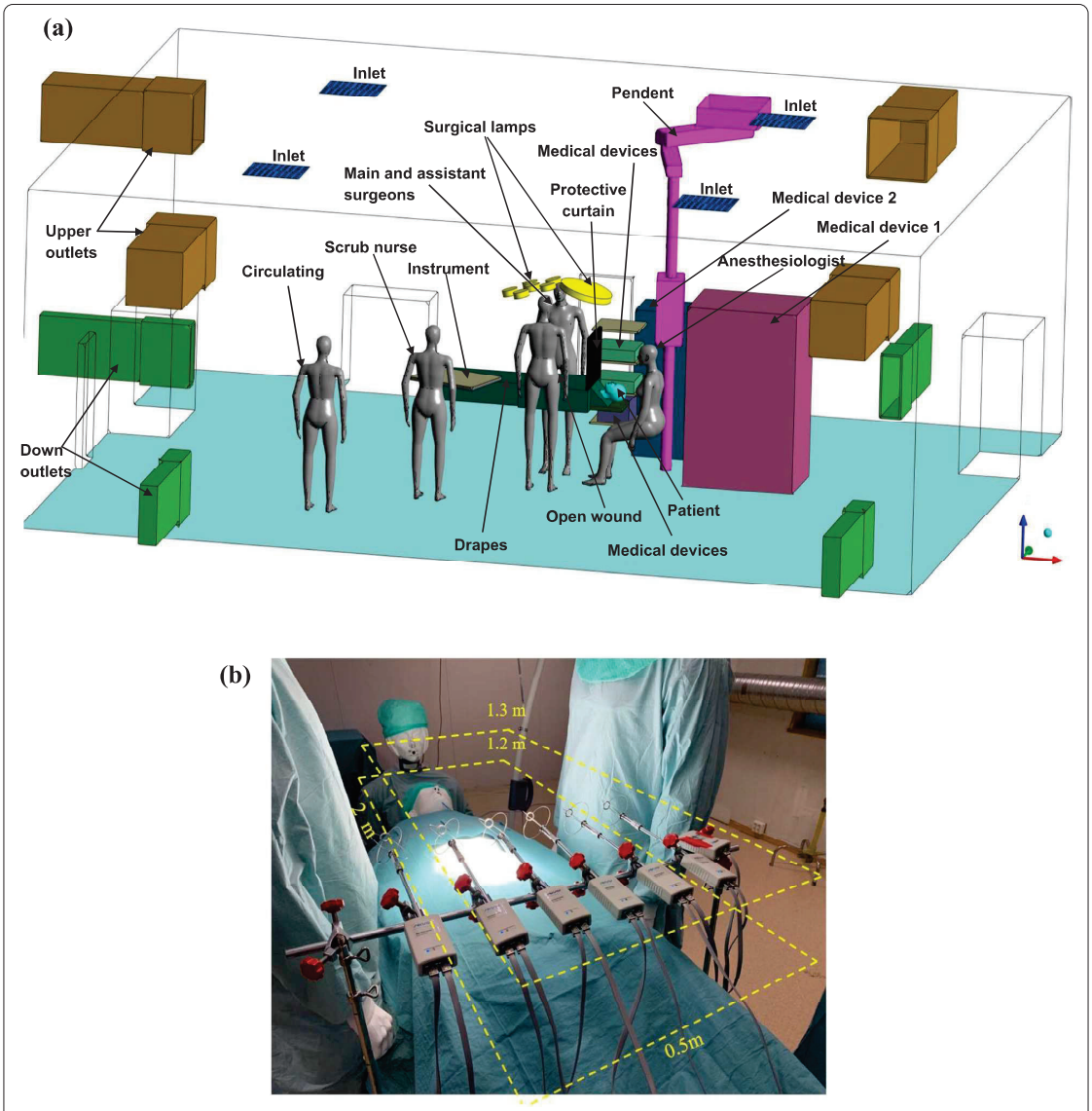

Fig. 1 OR configuration with **a**) an isometric view, and **b**) measurement plane and instrument

Moreover, the power of all heat sources was measured with COLTECH EMT707CTL.

Numerical study

Hospitals and operating room environments are complex, and conducting experimental studies to investigate the airflow field and contaminant levels might be difficult, expensive, and time-demanding.

Alternatively, the computational fluid dynamics (CFD) technique is powerful for predicting the airflow field and conducting high-quality parametric studies. In this regard, we prepared a replica model of the lab experiment to first validate our numerical model and then

Table 1 Heating power of heat sources

Heat source	Heating power (W)
Surgical lamp 1	**61**
Surgical lamp 2	**74**
Supersonic cleaner	**45**
Endoscope imager	**232**
Main surgeon	**150**
Assistant surgeon	**150**
Scrub nurse	**140**
Circulating nurse	**140**

perform comprehensive numerical modelling and data visualization.

Computational fluid dynamics technique

CFD is a part of fluid mechanics knowledge that has been mainly applied for visualization of the temperature and airborne particle distributions, air movement, the impact of different types of ventilation systems, and contamination level in the air in enclosed environments [22–27]. This technique adopts numerical methods and models to investigate the fluid flow. Due to the complicated behaviour of the indoor airflow and airborne particles movements, using CFD simulation has been a common approach to predict airflow fields. CFD simulations present highly accurate results for the case studies that controlling the background factors is challenging, like ORs. The below four steps are required to apply the CFD technique.

Geometry In the first step, the geometry of the laboratory room, including the configuration of the staff and medical equipment, was generated (Fig. 1a). Some degree of simplification was used for producing the geometry for the unimportant equipment located far from the operating table.

Mesh generation The second step in CFD technique application is subdividing the computational geometry into cells, called mesh. The mesh resolution needs to have optimal value to save calculation time and computation resources. Finer mesh increases the accuracy of the simulation results. Thus, it requires to be fine enough to provide an accurate solution. It is important that the obtained simulation results be independent of mesh resolution. This study accomplished a mesh independence study to assure the results were independent of the generated mesh. The grid resolution of 8 million cells was used in this study to guarantee high-quality CFD results.

Solving methods To compute airflow, airborne particle movement, and gas distribution in the physical model, it was necessary to define the required numerical models, equations, and boundary conditions. It was required to set up conditions to supply air diffusers, exhaust grills and gas release. The Navier–Stokes equation is the fundamental equation for the computation of the fluid momentum in most CFD simulations.

Since a large number of surgeries have been postponed during the COVID-19 pandemic, the spread of the SARS-CoV-2 virus from a COVID-19 patient was investigated. For modelling this spread, the SF6 gas was released from the patient's mouth and nose. This simulation was accomplished by solving the gas transport model and equations. All the equations for the simulation of BCPs and COVID -19 disperse were solved using commercial CFD code Fluent 19.2. Moreover, a novel approach, locating a protective shield curtain between the patient's head and lower body, was introduced to moderate the COVID-19 disperse (Fig. 1a).

Post-processing results The post-processing software was used to extract and visualize the CFD simulation results for the airflow field, particle, and gas distribution. This software improved the insight into the simulation results by generating velocity and velocity vector contour plots, airborne contamination, and gas dispersion contour plots, including the variation range of each studied variable.

Model validation

The simulation results were compared with the experimental data to guarantee the applied CFD code precisely predicted the airflow behaviour in the OR. In this regard, the temperature and velocity distribution were validated at 66 measured points in the surgical microenvironment (Fig. 1b). Figure 2a compares two common turbulence models, RNG and Realizable k-ε models, with experimental results predicting the velocity distribution. The relative error between experimental and CFD simulation results was less than 5%. Thus, both turbulence models could successfully predict the airflow field.

During the experimental step, the temperature values above the surgical patient were registered since the heat generation from the medical equipment and manikins has an impact on the airflow behaviour. Furthermore, the temperature distribution was compared between the experimental and CFD simulation results, as presented in Fig. 2b. The maximum relative error was 10% in this comparison (Fig. 2b). Thus, the CFD simulation accurately predicts the airflow field and temperature distribution.

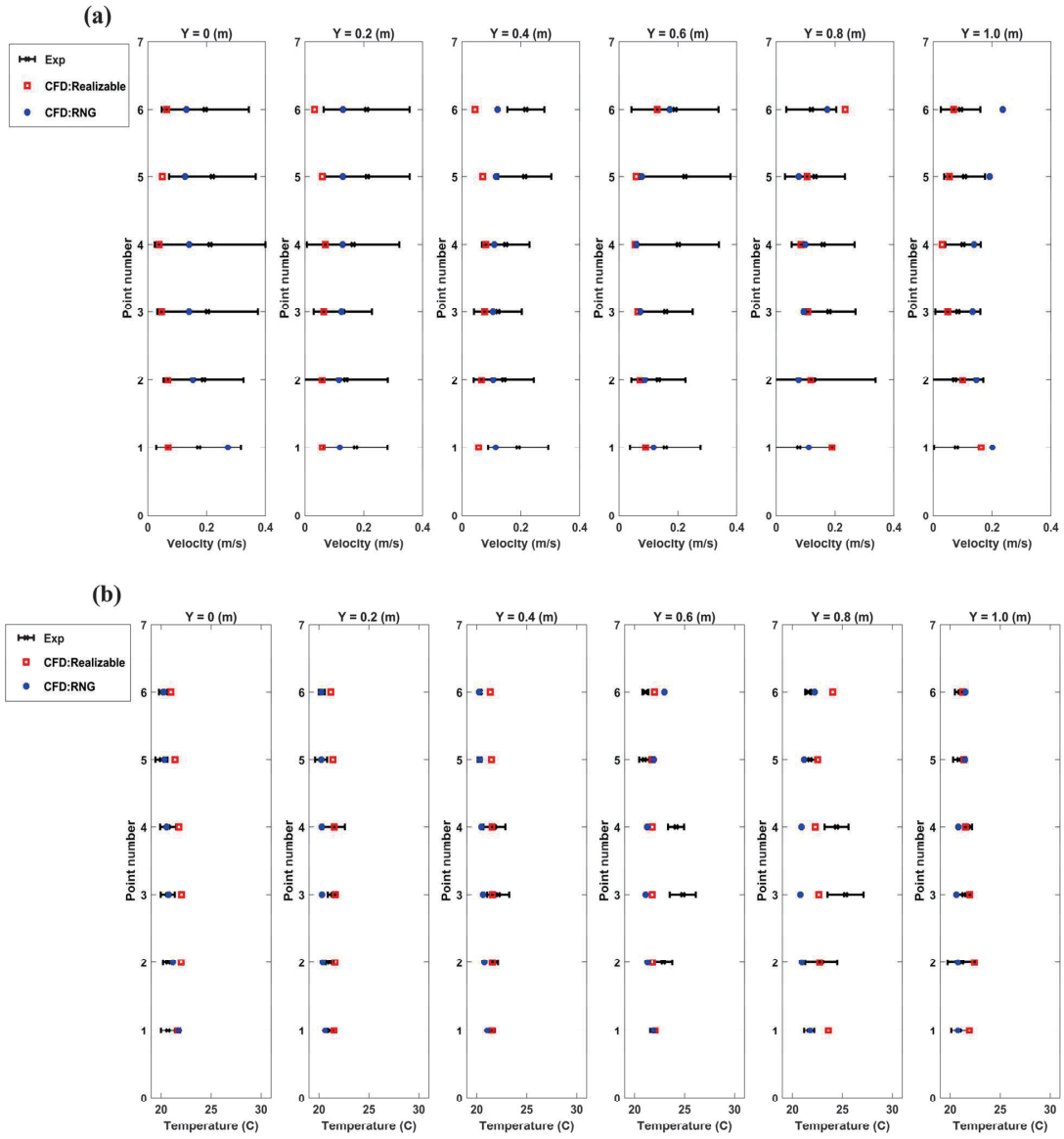

Fig. 2 Comparison of **a**) velocity; and **b**) temperature distribution between CFD simulation and experimental results

Result

Airflow behaviour

The CFD simulation results showed that the air temperature above the surgical site was higher than in other areas. The maximum air temperature was 25℃ above the surgical site at the height of 1.2 m and 23.5℃ at 1.3 m above the floor (Fig. 3). However, the air temperature was around 21℃, further from the wound in the surgical microenvironment. A careful analysis of the measurement data confirmed this temperature variation in the surgical microenvironment. Furthermore, the surface temperature of the wound area increased from 20℃ to 40℃ during the experimental study.

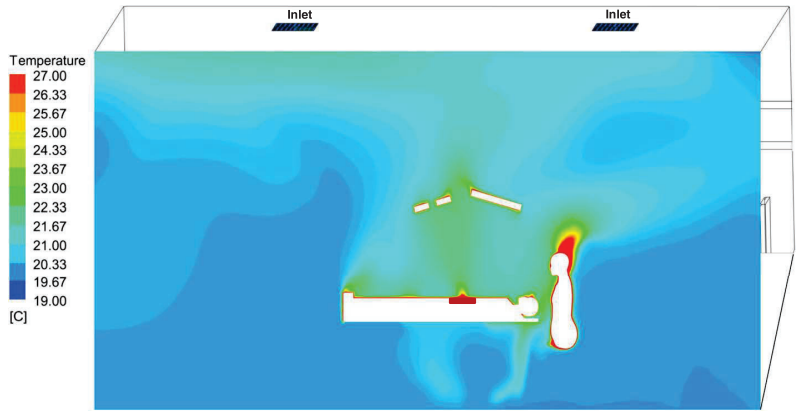

Fig. 3 Visualizing the temperature distribution in the surgical microenvironment

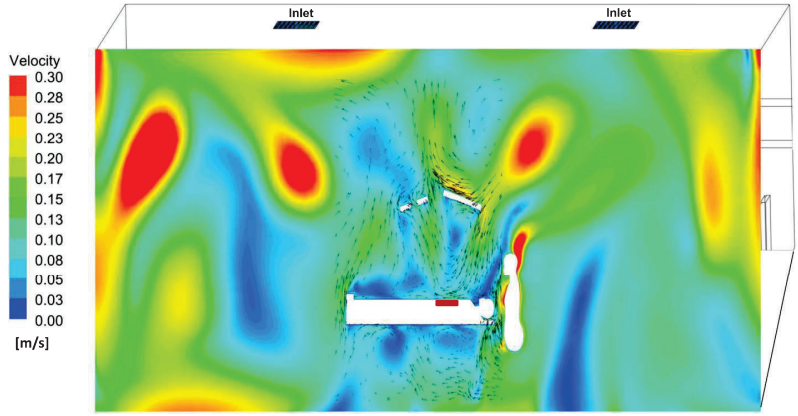

Fig. 4 Visualizing the airflow behaviour in the surgical microenvironment

Figure 4 shows the velocity distribution and airflow behaviour in the surgical microenvironment above the patient.

Contamination distribution

The SARS-CoV-2 virus was released from the patient during an ongoing surgery to evaluate the exposure level of the medical team. Overall, three different scenarios were numerically simulated to investigate the spread of airborne infectious diseases like the SARS-CoV-2 virus from the patient, as following:

OR equipped with

Case 1: high intensity of the LED surgical lamp,

Case 2: low intensity of the LED surgical lamp, and

Case 3: high intensity of the LED surgical lamp with a protective curtain.

The distribution of infectious airborne particles such as SARS-CoV-2 from the contaminated patient is presented for all cases in Fig. 5, in which SF6 tracer gas represents the airborne infectious particles. The results showed that in cases 1 and 2, the infectious airborne particles reached the maximum mass fraction of 0.18×10^{-3} at the breathing zone of the surgeon, and assistant surgeon, where located around the operating table (Fig. 5a, b). Using a protective curtain in Case 3 resulted in a 0.025×10^{-3}

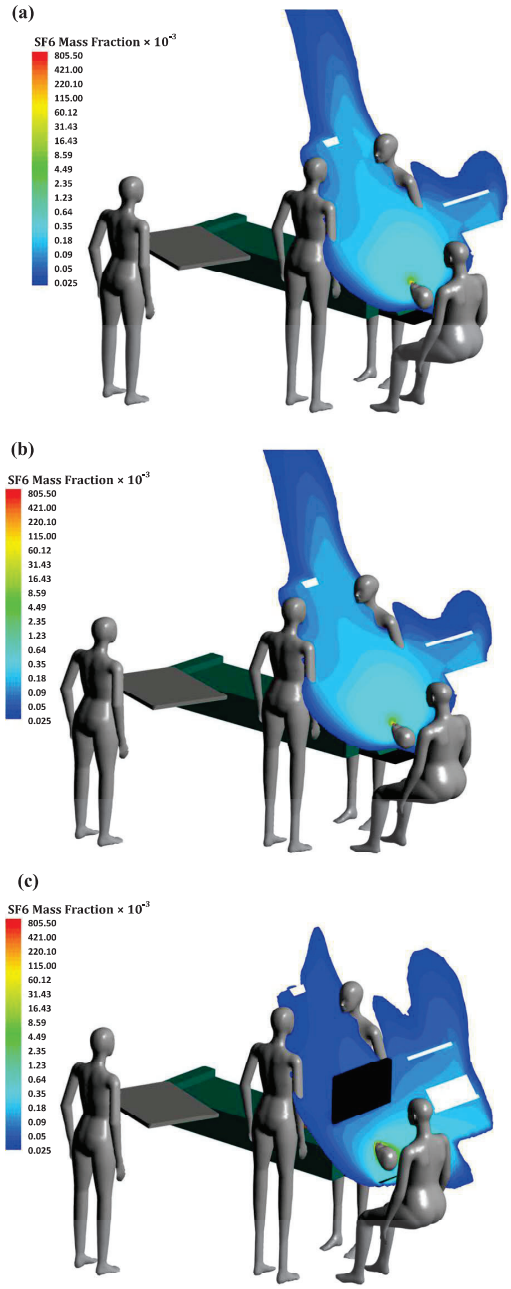

Fig. 5 The spread of tracer gas from the patient's mouth **a**) case 1: high intensity-LED surgical lamp; **b**) case 2: low intensity-LED surgical lamp; and case 3: high intensity-LED surgical lamp with a curtain

particle mass fraction in the surgeons' breathing zone (Fig. 5c). In both cases, with and without protecting curtain, the virus was not obtained in the breathing zone of scrub and circulating nurses. However, the virus contamination was detected close to the anaesthesiologist nurse in all studied cases.

Discussion

Several previous research studies reported burning damages in some patients' wound areas by xenon, halogen, and shadowless surgical lamps [28, 29]. LED surgical lamps have been recognized as the best replacement for halogen lamps. However, the impact of various intensities of LED surgical lamps on wound thermal injury has not been clear. In the current study, the experimental results showed the wound surface temperature increased from 20℃ up to 40 ℃ by using a high intensity of the LED surgical lamp. This phenomenon might be due to radiation from the LED lamp, consequently heating the surface temperature of the wound. Thus, the high intensity of this surgical lamp has the potential to raise the wound temperature to 100% and cause severe thermal injury to the surgical patient. To prevent such injuries to the wound site, it is recommended to use low-intensity of LED lamps for long operations. Maximizing the distance between the surgical lamp and the wound site can substantially reduce the thermal radiation, consequently decreasing the risk of wound thermal injuries.

Since the outbreak of COVID-19, the safety of the medical team has become on priority. Various strategies have been proposed to increase the protection level of HCWs in hospitals. Hill et al. [16] suggested a novel concept entitled "Corona Curtain" that implemented plastic drape roles for making an intubation tent for a COVID-19 patient. Although their proposed concept was successful, the Corona Curtain was designed for hospital wards. Thus, it could compromise the performance of the surgical team in ORs. In this regard, the current study evaluated the exposure level of the surgical team while using a protective curtain located between the upper and lower patient's body in the OR. The SF6 gas was released from the patient as representative of airborne infectious diseases spread like COVID-19. This contamination reached the breathing zone of surgeons in cases without the protective curtain (Cases 1 and 2). In this regard, the part of the surgical team close to the operating table needs a good protection level during surgery with COVID-19 patients. However, the CFD simulations showed that using this protective curtain reduced the exposure level up to 75% in the breathing area of the surgeons. Since using a protective curtain between the anaesthesiologist nurse and patient might affect the performance of this nurse, using a high protection mask rather than a surgical mask is highly

recommended. Thus, using the proposed protective curtain reduces the spread of airborne infectious diseases from the patient and improves the safety of the surgeons.

Conclusion

This study aimed to reduce the exposure level of the surgical team to airborne infectious contaminants during any future pandemic like COVID-19. In this regard, we proposed using a novel protective curtain to decrease the spread of SARS-CoV-2 from the patient to guarantee surgeons' safety. Thus, using the proposed protection method could increase the safety of surgeons without compromising their performance. The SARS-CoV-2 distribution results showed that using a proper facemask is highly recommended for the anaesthesiologist who is close to the patient. The experimental and CFD simulation results highlighted the importance of avoiding using the LED surgical lamp at its high intensity to prevent thermal injuries. There is a demand for future studies to define the optimum light intensity, time duration, and distance from the LED surgical lamps.

Abbreviations

CFD: Computational fluid dynamics; CFU: Colony-forming unit; COVID-19: Coronavirus disease 2019; HCW: Healthcare worker; OR: Operating room; PPE: Personal protective equipment; SSI: Surgical site infection.

Authors' contributions

PS: Writing - original draft, Methodology, Validation, Conceptualization. YB: Methodology, Experimental step, Writing - review & editing. GC: Writing - review & editing. SS: Supervision, Writing - review & editing. The author(s) read and approved the final manuscript.

Funding

Open access funding provided by Royal Institute of Technology. The Swedish Research Council Formas [2017–01088] supported the financial funding of the current study. The Swedish National Infrastructure provided the computation sources for computing (SNIC) at PDC [2018–05973].

Declarations

Ethics approval and consent to participate

Not applicable.

Consent for publication

Not applicable.

Competing interests

The authors declare to have no competing interests.

Author details

[1]Department of Civil and Architectural Engineering, KTH Royal Institute of Technology, Brinellvägen 23, 10044 Stockholm, Sweden. [2]Department of Energy and Process Engineering, Norwegian University of Science and Technology, Trondheim, Norway.

Received: 25 March 2022 Accepted: 22 June 2022
Published online: 06 August 2022

References

1. Duguid JP. The size and the duration of air-carriage of respiratory droplets and droplet-nuclei. J Hyg (Lond). 1946;44:471–9.
2. Naseri A, Emdad H, Mehrabi S, Sadrizadeh S, Abouali O. Inhalability of micro-particles through the human nose breathing at high free-stream airflow velocities. Build Environ. 2020;179:106948.
3. Hinds WC. Aerosol Technology : Properties, Behavior, and Measurement of Airborne Particles. 1999. p. 3.
4. Stadnytskyi V, Bax CE, Bax A, Anfinrud P. The airborne lifetime of small speech droplets and their potential importance in SARS-CoV-2 transmission. Proc Natl Acad Sci U S A. 2020;117:11875–7.
5. Edwards DA, Man JC, Brand P, Katstra JP, Sommerer K, Stone HA, et al. Inhaling to mitigate exhaled bioaerosols. Proc Natl Acad Sci U S A. 2004;101:17383–8.
6. Azimi P, Keshavarz Z, Cedeno Laurent JG, Stephens B, Allen JG. Mechanistic transmission modeling of COVID-19 on the Diamond Princess cruise ship demonstrates the importance of aerosol transmission. Proc Natl Acad Sci U S A. 2021;118(8):e2015482118.
7. Gupta JK, Lin CH, Chen Q. Characterizing exhaled airflow from breathing and talking. Indoor Air. 2010;20:31–9.
8. Gupta JK, Lin CH, Chen Q. Flow dynamics and characterization of a cough. Indoor Air. 2009;19:517–25.
9. Stahel PF. How to risk-stratify elective surgery during the COVID-19 pandemic? Patient Saf Surg. 2020;14:8.
10. Elizabeth Brindle M, Gawande A. Managing COVID-19 in Surgical Systems. Ann Surg. 2020;272:3–4.
11. Yuan L, Zhi N, Yu Ch, Ming G, Yingle L, Kumar G N, et al. Aerodynamic characteristics and RNA concentration of SARS-CoV-2 aerosol in Wuhan hospitals during COVID-19 outbreak. bioRxiv. 2020; 86:2020.03.08.982637.
12. Li Y, Qian H, Hang J, Chen X, Cheng P, Ling H, et al. Probable airborne transmission of SARS-CoV-2 in a poorly ventilated restaurant.Build Environ. 2021;196:107788.
13. Arora V, Evans C, Langdale L, Lee A. You Need a Plan: A Stepwise Protocol for Operating Room Preparedness During an Infectious Pandemic. Fed Pract. 2020;37:212–8.
14. Chen R, Zhang Y, Huang L, Cheng BH, Xia ZY, Meng QT. Safety and efficacy of different anesthetic regimens for parturients with COVID-19 undergoing Cesarean delivery: a case series of 17 patients. Can J Anesth. 2020;67:655–63.
15. Li H, Zhong K, Zhai ZJ. Investigating the influences of ventilation on the fate of particles generated by patient and medical staff in operating room. Build Environ. 2020;180:1–11.
16. Hill E, Crockett C, Circh RW, Lansville F, Stahel PF. Introducing the 'corona Curtain': An innovative technique to prevent airborne COVID-19 exposure during emergent intubations. Patient Saf Surg. 2020;14:1–9.
17. Ti LK, Ang LS, Foong TW, Ng BSW. What we do when a COVID-19 patient needs an operation: operating room preparation and guidance. Can J Anesth. 2020;67:756–8.
18. Douglas JDM, Mclean N, Horsley C, Higgins G, Douglas CM, Robertson E. COVID-19: Smoke testing of surgical mask and respirators. Occup Med (Chic Ill). 2020;70:556–63.
19. Leyva Moraga FA, Leyva Moraga E, Leyva Moraga F, Juanz González A, Ibarra Celaya JM, Ocejo Gallegos JA, et al. Aerosol box, An Operating Room Security Measure in COVID-19 Pandemic. World J Surg. 2020;44:2049–50.
20. Yánez Benítez C, Güemes A, Aranda J, Ribeiro M, Ottolino P, Di Saverio S, et al. Impact of Personal Protective Equipment on Surgical Performance During the COVID-19 Pandemic. World J Surg. 2020;44:2842–7.
21. ASHRAE. ASHRAE Standard 55-2010, Thermal Environmental Conditions for Human Occupancy. ASHRAE. 2010;227:2–36.
22. Chow TT, Yang XY. Ventilation performance in the operating theatre against airborne infection: Numerical study on an ultra-clean system. J Hosp Infect. 2005;59:138–47.
23. Tang JW, Noakes CJ, Nielsen PV, Eames I, Nicolle A, Li Y, et al. Observing and quantifying airflows in the infection control of aerosol- and airborne-transmitted diseases: An overview of approaches. J Hosp Infect. 2011;77:213–22.
24. Walker JT, Hoffman P, Bennett AM, Vos MC, Thomas M, Tomlinson N. Hospital and community acquired infection and the built environment - design and testing of infection control rooms. J Hosp Infect. 2007;65:43–9.

25. Yam R, Yuen PL, Yung R, Choy T. Rethinking hospital general ward ventilation design using computational fluid dynamics. J Hosp Infect. 2011;77:31–6.
26. Chow TT, Kwan A, Lin Z, Bai W. Conversion of operating theatre from positive to negative pressure environment. J Hosp Infect. 2006;64:371–8.
27. Yuen PL, Yam R, Yung R, Choy KL. Fast-track ventilation strategy to cater for pandemic patient isolation surges. J Hosp Infect. 2012;81:246–50.
28. Itagaki T, Doi M, Sato S, Kato S. Skin Burn Caused by Operating Light during a Long Operation after Photodynamic Therapy. Anesthesiology. 2003;98:1005–7.
29. Prasad N, Tavaluc R, Harley E. Thermal injury to common operating room materials by fiber optic light sources and endoscopes. Am J Otolaryngol - Head Neck Med Surg. 2019;40:631–5.

Publisher's Note

Article III **Yang Bi,** Hans Martin Mathisen, Guangyu Cao. Modeling of body temperature for perioperative patients in the operating room. (Submitted to *Building and Environment*)

This paper is submitted for publication and is therefore not included.

Article IV **Yang Bi,** Tomas Facer, Hans Martin Mathisen; Sara Edvardsen, Liv Inger Stenstad, Jan Gunnar Skogås, Guangyu Cao. Influence of the room air temperature on the airborne particles of surgical microenvironment in an operating room with mixing ventilation (submitted to *BMC Infectious Dieases*)

This paper is submitted for publication and is therefore not included.

Article V **Yang Bi**, Hans Martin Mathisen, Guangyu Cao. Numerical study on an improved protective operating room laminar flow ventilation system. (Submitted to *Energy and Building*)

This paper is submitted for publication and is therefore not included.